



Universiteit Utrecht

UTRECHT UNIVERSITY

INSTITUTE FOR THEORETICAL PHYSICS

MASTER'S THESIS

---

# Multi-Channel Kondo Model & Kitaev Quantum Quench

---

*Author:*  
Jurriaan WOUTERS, BSc.

*Supervisor:*  
Dr. Lars FRITZ

---

June 30, 2017



## Abstract

This thesis consists of two parts. In part one we discuss the Kondo model. First we point out the differences in physical properties between the one- and multi-channel Kondo model using a renormalization group analysis. We also point out the challenges in obtaining exact solutions. Then we give an overview of two approaches, bosonization and spin chain, for finding solutions for the one-, two- and four-channel Kondo model. Using bosonization we review a mapping from the one- and two-channel model to the exactly solvable resonant level model for a specific coupling strength. Following previous work, we derive the Kondo effect for a spin chain construction with XX and Ising coupling, showing the low energy behavior to be equivalent to the two- or four-channel Kondo model. We also discuss why one, two and four channels are special and we point out the difficulties in extending these approaches to other multi-channel Kondo models.

Then in part two we investigate survival of the topological edge effects of the Kitaev chain (Majorana edge modes) after a quantum quench. We determine a stability region for the edge modes after chemical potential and superconductivity quenches, by analyzing the wave functions using two measure: inverse participation ratio and overlap. We see that this region does not cover the full topological phase in parameter space. The Majoranas already disappear before the quenched system has reached the phase transition.



“You can’t bully the javelin!”  
*Keith Beard*



## Outline of the Thesis

This thesis consist of two parts. Part I contemplates the physics of the multi-channel Kondo model and Part II considers a quantum quench for the Kitaev model. Both topics consider strongly correlated quantum systems, but the approach and methods are distinct. The first part consist of analytic and technical methods to find solution for the multi-channel Kondo model. While the second part is a numerical lattice approach for quantum quenching the Kitaev chain.

The clear separation in the thesis is a reflection of my Master research. Initially, I focused on finding interesting new physical results for the multi-channel Kondo model. This topic has been thoroughly studied over the last fifty years by many of the physics brightest minds. It was therefore difficult to obtain any novel results.

We (my supervisor and I) decided to switch towards the second topic. The quantum quench for the Kitaev chain has not yet had as much attention by the physics community as the Kondo model.

We were able to find new interesting results for the Kitaev on quench survival of Majorana edge modes.

Both topics will be introduced extensively in the respective parts.





# Contents

|  |           |
|--|-----------|
| Outline of the Thesis                                  | v         |
| <b>I Kondo Problem</b>                                 | <b>1</b>  |
| <b>1 Introduction to the Kondo Model</b>               | <b>3</b>  |
| 1.1 Kondo Hamiltonian . . . . .                        | 5         |
| 1.2 Kondo Model from Anderson Impurity Model . . . . . | 5         |
| 1.3 Kondo Model from Three to One Dimension . . . . .  | 7         |
| <b>2 Kondo Renormalization Group</b>                   | <b>9</b>  |
| 2.1 One-Channel . . . . .                              | 10        |
| 2.2 Multi-Channel . . . . .                            | 15        |
| <b>3 Bosonization for the Kondo Model</b>              | <b>23</b> |
| 3.1 Bosonization Ingredients . . . . .                 | 24        |
| 3.1.1 Bosonized Kondo Hamiltonian . . . . .            | 25        |
| 3.2 Renormalization Group One-Channel . . . . .        | 26        |
| 3.3 One-Channel Kondo - Toulouse Limit . . . . .       | 27        |
| 3.4 Two-Channel - Emery-Kivelson Solution . . . . .    | 28        |
| 3.5 Beyond . . . . .                                   | 29        |
| <b>4 Spin Chains to Kondo Models</b>                   | <b>31</b> |
| 4.1 XX to Four-Channel Kondo . . . . .                 | 31        |
| 4.1.1 Star Junction . . . . .                          | 31        |
| 4.1.2 Jordan-Wigner Transformation . . . . .           | 32        |
| 4.1.3 Mapping . . . . .                                | 34        |
| 4.2 Ising Chain to Two-Channel Kondo . . . . .         | 35        |
| 4.3 In Between XX and Ising . . . . .                  | 36        |
| 4.4 Beyond . . . . .                                   | 37        |
| <b>5 Conclusion and Discussion - Kondo Model</b>       | <b>39</b> |

|           |  |           |
|-----------|--|-----------|
| <b>II</b> | <b>Quantum Quenching the Kitaev Chain</b>                      | <b>41</b> |
| <b>6</b>  | <b>Introduction to Kitaev Chain and Quantum Quench</b>         | <b>43</b> |
| 6.1       | Kitaev Chain . . . . .   | 43        |
| 6.2       | Kitaev Hamiltonian . . . . .                                   | 44        |
| 6.2.1     | Majorana Edge Modes . . . . .                                  | 46        |
| 6.3       | Disorder . . . . .   | 48        |
| <b>7</b>  | <b>Technical Details Quench</b>                                | <b>51</b> |
| 7.1       | Projected Overlap . . . . .                                    | 51        |
| 7.2       | Measures: Inverse Participation Ratio and Overlap . . . . .    | 53        |
| <b>8</b>  | <b>Results - Kitaev Chain Quantum Quench</b>                   | <b>57</b> |
| 8.1       | Examples Quench . . . . .                                      | 57        |
| 8.2       | Chemical Potential Quench . . . . .                            | 57        |
| 8.3       | Superconductivity Quench . . . . .                             | 61        |
| 8.4       | Adding Disorder . . . . .                                      | 62        |
| <b>9</b>  | <b>Conclusion and Discussion - Kitaev Chain Quantum Quench</b> | <b>65</b> |
|           | <b>Appendices</b>  | <b>69</b> |
| <b>A</b>  | <b>Kondo Model from Anderson Impurity Model</b>                | <b>69</b> |
| <b>B</b>  | <b>Matsubara</b>   | <b>73</b> |
| <b>C</b>  | <b>Bosonization</b>  | <b>75</b> |
| C.1       | Bosonization Conventions . . . . .                             | 75        |
| C.1.1     | Boson Representation . . . . .                                 | 76        |
| C.1.2     | Bosonization Identity . . . . .                                | 77        |
| C.2       | Free Hamiltonian . . . . .                                     | 78        |
| C.2.1     | Heisenberg Picture . . . . .                                   | 78        |
| C.3       | Some Useful Identities . . . . .                               | 79        |
| C.3.1     | Baker-Campbell-Hausdorff . . . . .                             | 79        |
| C.3.2     | Thermal Average of Exponent of Boson Operators . . . . .       | 80        |
| C.3.3     | Normal Ordering of Exponent $\phi$ . . . . .                   | 80        |
| C.4       | Commutation and Anti-Commutation Relations . . . . .           | 81        |
| C.5       | Useful Correlation Functions . . . . .                         | 82        |
| C.6       | Bosonization One-channel Renormalization Group . . . . .       | 83        |
| C.6.1     | First Order . . . . .  | 84        |
| C.6.2     | Second Order . . . . .   | 85        |

|   |               |
|---|---------------|
| <b>D Symmetries of the Kitaev Chain</b>               | <b>87</b>     |
| D.1 Particle-Hole Symmetry . . . . .                  | 87            |
| D.2 Inversion + Time Reversal Symmetry . . . . .      | 88            |
| D.3 Condition Majorana Edge Modes . . . . .           | 89            |
| D.3.1 Transfer Matrix . . . . .                       | 89            |
| D.4 Zero Energy Mode in Semi Infinite Chain . . . . . | 90            |
| <br><b>References</b>                                 | <br><b>92</b> |



**Part I**

**Kondo Problem**



# Chapter 1

## Introduction to the Kondo Model

In 1934 in the Kamerlingh Onnes Laboratory (Leiden, Netherlands) three Dutch physicists made an interesting discovery. When De Haas, De Boer and Van de Berg measured the low temperature resistivity of gold ( $Au$ ) they found a finite temperature minimum (see Figure 1.1).[1] At the time, it was impossible to explain resistivity minimum in a metal theoretically. Up to then, it was understood that the resistivity decreases as the temperature decreases. It turned out that this peculiar behavior was caused by magnetic impurities. However, until the 1960's the electrical properties due to magnetic impurities were calculated by considering effective Heisenberg coupling, which could not explain this low temperature minimum.

In 1964 Kondo presented a perturbative calculation that was a good step towards unraveling the low energy behavior around this minimum.[2] He calculated the resistivity up to third order perturbation using the s-d model.[3] Figure 1.2 shows the s-d system, consisting of a bath of itinerant electrons (gray) coupled to a spin impurity (arrow). Kondo was not able to get a full solution for the model. In his perturbative expansion he encountered terms that diverge for low temperature ( $\ln T$ ).

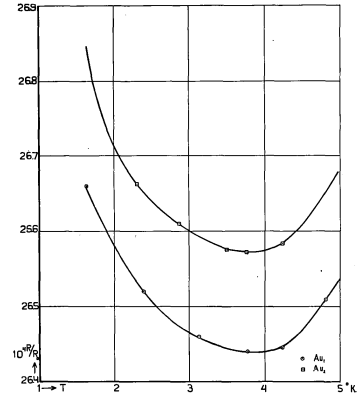


Figure 1.1: Resistivity minimum for  $Au$  (gold). Figure from [1].

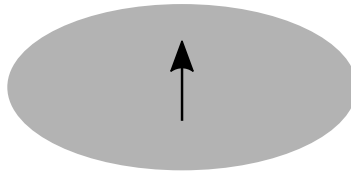


Figure 1.2: Schematic representation of the Kondo model. The gray area depicts the bulk electrons couple to the local magnetic impurity (black arrow).

At the time, these type of divergences were unprecedented in many body systems and it took another eleven years before the first solutions were found. In the meantime the quest for solving the model became known as the *Kondo problem*, and later this model would become a test ground for newly developed many-body techniques.

In 1975 Wilson proposed the first approach for solving the physics of the Kondo model.[4] Using numerical renormalization group (NRG) he obtained the low temperature behavior of spin 1/2 Kondo

model. Later in 1980 Wiegmann [5] and Andrei [6] used the Bethe ansatz to get a solution for both the high and low temperature regime, confirming Wilson results for low  $T$ .

In this thesis we will not review the work on NRG or Bethe ansatz. We will however discuss another technique for finding solutions of the Kondo model. This technique, called bosonization, offers an elegant way to find exact solutions for the Kondo model in certain fine tuned cases. We will also discuss spin chain construction showing Kondo like behavior, in an attempt to find solutions for the model.

What we have discussed above is the original one-channel Kondo model. From 1980 onwards there has also been great interest in the multi-channel Kondo model, an extension of the original one-channel Kondo model. In this case several electron baths are coupled to the same impurity. These baths are not coupled directly, and the electrons from different channels can only interact via the impurity. In Figure 1.3 we see two examples of multi-channel Kondo models. The interest in the multiple channels was raised, because the physics described is qualitatively different from the one-channel Kondo model. In the multi-channel Kondo model there is non-Fermi liquid behavior and due to an overscreening effect there is a finite coupling fixed point, while the one-channel is characterized by Fermi liquid behavior at strong coupling (we will see this in Chapter 2).[7]

Realizing the multi-channel Kondo model is experimentally very difficult. Completely separating the baths is a real challenge. Generally finding solutions for multiple channels is also more difficult. In one special case, two channels, we can find exact solutions using bosonization. Furthermore, it turns out that there are spin chain constructions that exhibit multi-channel Kondo behavior, also yielding results for the two- and four-channel case. Unfortunately, there are no other multi-channel Kondo models solved so far. In this thesis we are trying to understand what makes these two cases special and whether we can find extension to realize other multi-channel Kondo models.

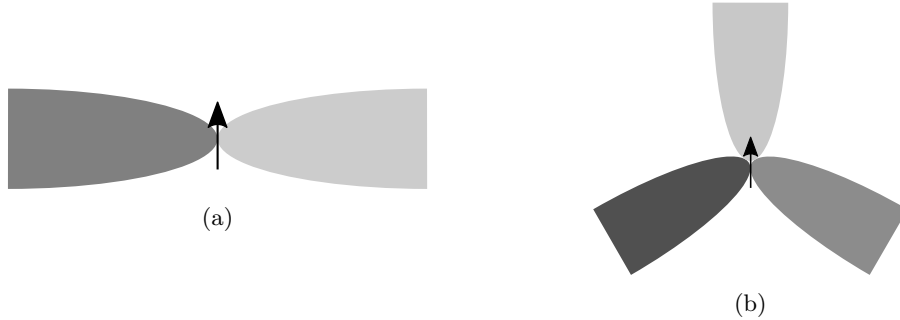


Figure 1.3: Two- (a) and three- (b) channel Kondo models schematically depicted. The different shades of gray denote different conduction electron baths. These baths all interact with the magnetic impurity, but do not directly interact with each other.

The main objective of the first part of this thesis is to give an overview of the solvable multi-channel Kondo model using two approaches, bosonization and spin chain constructions. We also discuss the limitations of these approaches and debate whether we can find solvable multi-channel Kondo model beyond these limitations.

In this chapter we will introduce the Kondo model along with the multiple channels. Also we will discuss the physical justification of the Kondo model, by showing the relation to the microscopic Anderson Impurity Model.

Then in Chapter 2 we discuss a perturbative approach to the Kondo model. We will encounter divergences, which we quantify by discussing the renormalization group flow. Here we will already see the different physical behavior between the one-channel and multi-channel Kondo model. Also we see that this perturbative analysis breaks down because of strong coupling. In Chapter 3 we will approach the Kondo Problem using bosonization. We will see how the one- and two-channel Kondo model can be solved and we discuss why it is difficult to find solutions for other channels. Finally,



Chapter 4 contains examples of spin chain constructions that have two- and four-channel Kondo like behavior. This connection makes it possible to transfer results from (well studied) spin chains to multi-channel Kondo models. In this chapter we will also discuss the search for spin chains that relate other multi-channel Kondo models.

## 1.1 Kondo Hamiltonian

First we are going to take a look at the one-channel Kondo model. The multi-channel case is a straightforward extension. As mentioned before, the Kondo model is a magnetic impurity model. A bath of conduction electrons is coupled to a spin degree of freedom at the origin. Figure 1.2 displays the bulk electrons in gray with the local magnetic impurity in the middle. Generically there can be multiple magnetic impurities, but in this thesis we only consider one. We will also only discuss spin 1/2 bath electrons and spin 1/2 impurities (unless otherwise stated). The three dimensional Hamiltonian for the one-channel Kondo model is

$$H = H_0 + H_{\text{int}} = \sum_{\vec{k}, \sigma=(\uparrow, \downarrow)} (\epsilon_{\vec{k}} - \mu) c_{\vec{k}\sigma}^\dagger c_{\vec{k}\sigma} + \sum_{\substack{i=x,y,z \\ \sigma, \sigma'=(\uparrow, \downarrow)}} J_i \psi_\sigma^\dagger(0) \tau_{\sigma\sigma'}^i \psi_{\sigma'}(0) S^i \quad (1.1)$$

with

$$c_{\vec{k}\sigma} = \int d^3x \psi_\sigma(\vec{x}) e^{-i\vec{x}\vec{k}}; \quad (1.2)$$

$$c_{\vec{k}\sigma}^\dagger = \int d^3x \psi_\sigma^\dagger(\vec{x}) e^{-i\vec{x}\vec{k}}. \quad (1.3)$$

Here  $c_{\vec{k}\sigma}$  and  $c_{\vec{k}\sigma}^\dagger$  are respectively the spin 1/2 bath electron annihilation and creation operators in momentum space and  $\psi_\sigma(\vec{x})$  and  $\psi_\sigma^\dagger(\vec{x})$  their counterparts in real space. The first term of (1.1) is the non-interacting Hamiltonian with  $\epsilon_{\vec{k}}$  the single particle energy and  $\mu$  the chemical potential. The second term describes the interaction with the impurity spin  $S^i$ , where  $\tau^i$  are the Pauli matrices corresponding to spin 1/2 and  $J_i$  the coupling constants.

For the multi-channel Kondo model we simply have to add a channel index  $a$  and we find

$$H_{\text{multi}} = \sum_{a=1}^n \left( \sum_{\vec{k}, \sigma} (\epsilon_{\vec{k}} - \mu) c_{\vec{k}\sigma a}^\dagger c_{\vec{k}\sigma a} + \sum_{\substack{i=x,y,z \\ \sigma, \sigma'=(\uparrow, \downarrow)}} J_i \psi_{\sigma a}^\dagger(0) \tau_{\sigma\sigma'}^i \psi_{\sigma' a}(0) S^i \right), \quad (1.4)$$

where  $n$  is the number of channels. We see that every channel/bath is described by the free Hamiltonian and all baths couple at  $x = 0$  to the spin impurity.

## 1.2 Kondo Model from Anderson Impurity Model

We have become familiar with the Kondo Hamiltonian in the previous section. This model is only an effective model. In this section we will derive the Kondo model from a microscopic theory, the Anderson impurity model (AIM). Here we give the main ingredients for this derivation. We will only sketch the steps, the full derivation is in Appendix A.

In 1961 Anderson proposed an extension of a model by Friedel[8] to give a microscopic description of a fermionic impurity model.[9] The AIM consists of spinful bath and impurity fermions coupled via spin exchange. The impurity fermions also interact with each other through Coulomb coupling.

$$H = \sum_{k\sigma} \left[ \epsilon_k c_{k\sigma}^\dagger c_{k\sigma} + (V_k d_\sigma^\dagger c_{k\sigma} + V_k^* c_{k\sigma}^\dagger d_\sigma) \right] + \sum_{\sigma} \epsilon_d n_{d\sigma} + U n_{d\uparrow} n_{d\downarrow}. \quad (1.5)$$

The  $c_{k\sigma}$  are the conduction electrons as usual with the single particle energy  $\epsilon_k$ . The impurity fermions are  $d_\sigma$  and they couple to the conduction fermions with  $V_k$  and  $V_k^*$ . Adding a fermion to the impurity site comes with a cost  $\epsilon_d$ , since  $n_{d\sigma}$  is the number operator for the impurity. Finally  $U$  is the Coulomb coupling.

The impurity can contain zero, one or two fermions, because there can be no spin ( $|0\rangle$ ), an up or down spin ( $|\uparrow\rangle, |\downarrow\rangle$ ) or an up and down spin ( $|\uparrow\downarrow\rangle$ ). These three sectors of the Hilbert space have energy 0,  $\epsilon_d$  and  $2\epsilon_d + U$  respectively. In Figure 1.4 we see the three energy levels and the corresponding states. On the other hand, in the Kondo model the impurity is described by a spin. This

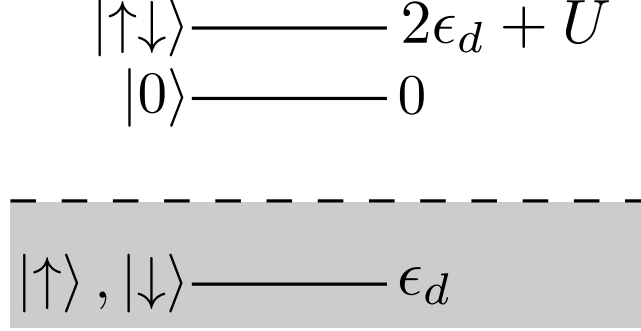


Figure 1.4: Energy levels of the impurity in the AIM with corresponding particle sectors/states.

spin is either up or down, so there is always one “particle”. If we want to derive the Kondo model from the AIM, we need the impurity to be singly occupied. Classically we would let  $\epsilon_d$  go to  $-\infty$  and let  $2\epsilon_d + U \sim 1$ , so  $U \rightarrow \infty$ . We can then shift all energies such that the impurity is singly occupied as we see in Figure 1.4. Both the zero- and two-particle sectors are at high energy and are projected out. Letting  $2\epsilon_d + U = 0$  ensures particle hole symmetry, i.e. the zero- and two-particle sectors are at the same energy. In the classical set-up the impurity would contain either an up- or a down-spin, and there would be no spin flips.

However, quantum mechanically there can still be virtual excitations to the zero and two particle sector (e.g.  $|\uparrow\rangle \rightarrow |\uparrow\downarrow\rangle \rightarrow |\downarrow\rangle$ ). These excitations give rise to the Kondo coupling.

Since we are interested in the particle sectors we write the Schrödinger equation in the following way:

$$\begin{pmatrix} H_{00} & H_{01} & H_{02} \\ H_{10} & H_{11} & H_{12} \\ H_{20} & H_{21} & H_{22} \end{pmatrix} \begin{pmatrix} |\psi_0\rangle \\ |\psi_1\rangle \\ |\psi_2\rangle \end{pmatrix} = E \begin{pmatrix} |\psi_0\rangle \\ |\psi_1\rangle \\ |\psi_2\rangle \end{pmatrix}, \quad (1.6)$$

where  $|\psi_i\rangle$  is a wave function in the  $i$ -particle sector of the Fock space. We can define projection operators  $P_i$  projecting to the respective sectors given by

$$P_0 = (1 - n_{d\uparrow})(1 - n_{d\downarrow}), \quad P_1 = n_{d\uparrow} + n_{d\downarrow} - 2n_{d\uparrow}n_{d\downarrow}, \quad P_2 = n_{d\uparrow}n_{d\downarrow} \quad (1.7)$$

The entries of the matrix in (1.6) are defined as  $H_{mn} = P_m H P_n$ . Note that  $H_{20} = H_{02} = 0$ , because in (1.5) there are no terms that create or annihilate two impurity degrees of freedom. The other entries are given by

$$H_{00} = \sum_{k\sigma} \epsilon_k c_{k\sigma}^\dagger c_{k\sigma}, \quad H_{11} = \sum_{k\sigma} \epsilon_k c_{k\sigma}^\dagger c_{k\sigma} + \epsilon_d, \quad H_{22} = \sum_{k\sigma} \epsilon_k c_{k\sigma}^\dagger c_{k\sigma} + 2\epsilon_d + U \quad (1.8)$$

$$H_{10} = \sum_{k\sigma} V_k d_\sigma^\dagger (1 - n_{d\bar{\sigma}}) c_{k\sigma}, \quad H_{21} = \sum_{k\sigma} V_k d_\sigma^\dagger n_{d\bar{\sigma}} c_{k\sigma}. \quad (1.9)$$

We can rewrite (1.6) to find an equation for the one particle state (see (A.9))

$$H_{\text{eff}}|\psi_1\rangle = (H_{10}(E - H_{00})^{-1}H_{01} + H_{11} + H_{12}(E - H_{22})^{-1}H_{21})|\psi_1\rangle = E|\psi_1\rangle. \quad (1.10)$$

Here the effective Hamiltonian  $H_{\text{eff}}$  acts on a one particle impurity state. The first term describes the impurity fermion being annihilated and a new impurity fermion being created. The second term is simply the energy of the one particle state. The third term first creates a fermion with the missing spin and then annihilates one of fermion, The first and third terms induce spin flips Using (1.8), (1.9) and after commutation we find (see (A.16)(A.21))

$$H_{10}(E - H_{00})^{-1}H_{01} \approx - \sum_{kk'\sigma\sigma'} V_k V_{k'}^* \frac{d_{\sigma}^{\dagger} c_{k\sigma} c_{k'\sigma'}^{\dagger} d_{\sigma'}}{\epsilon_{k'} - \epsilon_d}; \quad (1.11)$$

$$H_{12}(E - H_{22})^{-1}H_{21} \approx - \sum_{kk'\sigma\sigma'} V_{k'} V_k^* \frac{c_{k\sigma}^{\dagger} d_{\sigma} d_{\sigma'}^{\dagger} c_{k'\sigma'}}{U + \epsilon_d - \epsilon_{k'}}, \quad (1.12)$$

where we have assumed that  $|\epsilon_d|, U \gg |H_{00}|$  and  $E - \epsilon_d \rightarrow 0$ . To understand the latter we need to realize that  $E = E_0 + \epsilon_d$  from (1.10), where  $E_0$  is the energy of the bath.

Note that we can write the fermion degree of freedom at the impurity as a spin 1/2, when acting on the one particle Fock space.

$$\vec{S} = \sum_{\alpha\beta} d_{\alpha}^{\dagger} \frac{\vec{\sigma}_{\alpha\beta}}{2} d_{\beta}. \quad (1.13)$$

For a local impurity ( $V_k = V$ ) and  $|\epsilon_d| \gg |\epsilon_k|$  we can define  $A = -\frac{|V|^2}{\epsilon_d}$  and  $B = \frac{|V|^2}{U + \epsilon_d}$  to find (see (A.30)):

$$H_{\text{eff}} = \sum_{k\sigma} \epsilon_k c_{k\sigma}^{\dagger} c_{k\sigma} + \sum_{kk'} (A + B) c_{k\alpha}^{\dagger} \vec{\sigma}_{\alpha\beta} c_{k'\beta} \vec{S} + \frac{A - B}{2} c_{k\sigma}^{\dagger} c_{k'\sigma}, \quad (1.14)$$

The last term is a potential scattering, which vanishes if we assume particle-hole symmetry ( $2\epsilon_d + U = 0$ ). The remaining Hamiltonian is of the same form as the Kondo Hamiltonian in (1.1). Extending to multiple channels is more difficult, because we also have to suppress terms like  $c_{k\uparrow a}^{\dagger} c_{k'\downarrow b} d_{\downarrow}^{\dagger} d_{\uparrow}$  for  $a \neq b$  channel indices. These interactions couple different channels directly and should not be present in the multi-channel Kondo Hamiltonian (1.4). It is impossible to consistently derive the multi-channel Kondo model from the Anderson model.

### 1.3 Kondo Model from Three to One Dimension

In this section we are going to show that the three dimensional Kondo model put forward in the previous section can effectively be described as a one dimensional model. One of the reasons we derive this dimensional reduction is that bosonization is only applicable for one dimensional theories. Here we will derive the 3D to 1D correspondence for a general local impurity.

Suppose we have a Hamiltonian

$$H = H_0 + V, \quad (1.15)$$

where the free Hamiltonian is

$$H_0 = \int \frac{dk^3}{(2\pi)^3} \xi_k c_k^{\dagger} c_{\vec{k}} \quad (1.16)$$

and the local interaction is

$$V = \int d\vec{r} \hat{V}(\vec{r}) \psi^\dagger(\vec{r}) \psi(\vec{r}) . \quad (1.17)$$

We see that the single particle  $\xi_k = \epsilon_k - \mu$  is rotationally symmetric, because it only depends on the norm of  $\vec{k}$ . Furthermore in a local impurity model, such as the Kondo model, the interaction term is

$$\hat{V}(\vec{r}) = \hat{V} \delta(r) . \quad (1.18)$$

Hence the full Hamiltonian is rotationally symmetric. Therefore angular momentum is conserved and using the spherical wave expansion[10] we can express the fermion field in terms of momentum, total angular momentum and angular momentum in the  $z$  direction, because these are now good quantum numbers:

$$\psi(\vec{r}) = \int \frac{dk}{2\pi} \sum_{lm} \psi_{klm}(\vec{r}) c_{klm}, \quad (1.19)$$

where  $l$  is the total angular momentum and  $m = -l, -l+1, \dots, l$  the angular momentum in the  $z$  direction. The operator  $c_{klm}$  is the fermion operator in this notation and  $\psi_{klm}(\vec{r})$  is the wave function. This coefficient can be decomposed in a radial and angular part:[11]

$$\psi_{klm}(\vec{r}) = R_{kl}(r) Y_{lm}(\phi, \theta), \quad (1.20)$$

where  $R_{kl}(r)$  are the radial functions depending only on the norm of  $\vec{r}$  and  $Y_{lm}(\phi, \theta)$  the spherical harmonic functions depending only on the direction of  $\vec{r}$ . The radial functions are given by the spherical Bessel functions:[11]

$$R_{kl}(r) = 2k j_l(kr) = (-1)^l \frac{2r^l}{k^l} \left( \frac{1}{2} \frac{dr}{dr} \right)^l \frac{\sin kr}{r}. \quad (1.21)$$

For a local interaction  $\psi(\vec{r})$  only couples to the impurity at  $\vec{r} = 0$ . From the right hand side of (1.21) it is easy to see that only  $R_{k0}(r)$  is non-vanishing at  $r = 0$ . The spherical harmonic  $Y_{00}(\phi, \theta)$  is  $\frac{1}{\sqrt{4\pi}}$ . [11]

Hence we find

$$\psi(0) = \lim_{\vec{r} \rightarrow 0} \int_0^\infty \frac{dk}{2\pi} \frac{2}{\sqrt{4\pi}} \frac{\sin kr}{r} c_{k00} + \mathcal{O}(r) \quad (1.22)$$

We can drop the two zero indices from  $c_{k00}$ , so the fermion  $c_k$  only depends of the norm of the momentum. The free Hamiltonian becomes

$$H_0 = \int_0^\infty \frac{dk}{2\pi} \xi_k c_k^\dagger c_k. \quad (1.23)$$

The full impurity Hamiltonian is now effectively one dimensional:

$$H = \int_0^\infty \frac{dk}{2\pi} \xi_k c_k^\dagger c_k + \hat{V} \psi(0)^\dagger \psi(0) \quad (1.24)$$

This can easily be generalized by adding spin and channel indices, so we see that the three dimensional Kondo model can be reduced to an effective one dimensional theory.

Summarizing, we have introduced a spin impurity theory known as the Kondo model for both one- and multi-channel. This one-channel model was proposed by Kondo in 1975 as an attempt to describe the resistivity minimum observed in some metals. In the next chapters we will discuss several ways to solve the model. First in Chapter 2 we see that finding a perturbative solution is impossible due to divergences. In Chapter 3 we will see that bosonization can offer exact solution in specific cases and finally in Chapter 4 we discuss several spin chain constructions that possess Kondo like behavior.

## Chapter 2

# Kondo Renormalization Group

The physical properties of a system are encoded in the action. We can derive physical observables from expectation values of operators, e.g. the energy is given by the expectation value of the Hamiltonian. These expectation values are given by

$$\langle \hat{O} \rangle = \frac{1}{Z} \int d[\psi] \hat{O} e^{-S} , \quad (2.1)$$

for an operator  $\hat{O}$ . Here  $d[\psi]$  is path integral over the field,  $S$  is the action and  $Z = \int d[\psi] e^{-S}$  the partition function. For quadratic action these path integrals simply become Gaussian integrals, which can be work out exactly.

However, the Kondo model (1.1) is not quadratic but contains quartic interacting terms. Therefore the expectation values cannot be calculated exactly in this way. Nevertheless, we can treat the interaction perturbatively given that the coupling constant is small.

Suppose the action is given by

$$S[\psi] = S_0[\psi] + S_{\text{int}}[\psi] , \quad (2.2)$$

where  $S_0$  is the quadratic free fermion action and the interaction part  $S_{\text{int}}$  is proportional to coupling constant  $J \ll 1$ . We can perturbatively approximate (2.1) up to  $J^2$  as

$$\langle \hat{O} \rangle = \frac{1}{Z} \int d[\psi] \hat{O} e^{-S_0} e^{-S_{\text{int}}} \quad (2.3)$$

$$= \frac{1}{Z} \int d[\psi] \hat{O} e^{-S_0} \left( 1 - S_{\text{int}} + \frac{S_{\text{int}}^2}{2} \right) = \frac{Z_0}{Z} \left( \langle \hat{O} \rangle_0 - \langle \hat{O} S_{\text{int}} \rangle_0 + \frac{1}{2} \langle \hat{O} S_{\text{int}}^2 \rangle_0 \right) , \quad (2.4)$$

where  $Z_0$  is the partition function and  $\langle \hat{O} \rangle_0$  is the expectation value for with respect to  $S_0$ . We can also expand  $\frac{1}{Z}$  perturbatively to find

$$\begin{aligned} \langle \hat{O} \rangle &= \langle \hat{O} \rangle_0 - \left[ \langle \hat{O} S_{\text{int}} \rangle_0 - \langle \hat{O} \rangle_0 \langle S_{\text{int}} \rangle_0 \right] \\ &+ \frac{1}{2} \left[ \langle \hat{O} S_{\text{int}}^2 \rangle_0 - 2 \langle \hat{O} S_{\text{int}} \rangle_0 \langle S_{\text{int}} \rangle_0 - \langle \hat{O} \rangle_0 (\langle S_{\text{int}}^2 \rangle_0 - 2 \langle S_{\text{int}} \rangle_0^2) \right] . \end{aligned} \quad (2.5)$$

This is an expansion up to second order in  $S_{\text{int}}$ , third order gives terms like  $\langle \hat{O} S_{\text{int}}^3 \rangle_0$  with a factor  $-\frac{1}{3!} = -\frac{1}{6}$ .

In diagrammatic language the second (and higher) order term correspond to fermion loops.

Kondo did resistivity calculations using third order perturbation theory. Even though he could explain the resistivity minimum found in some metals, he could not extend the solutions to low temperturs

be cause the results blew up in this regime.

In 1970 Anderson invented a way to obtain renormalization group equations for the coupling constants, known as *a Poor man's scaling*. [12]

Here we are going to discuss a variation of this argument to show that the coupling constants for the Kondo model diverge and a perturbative approach is impossible.

There is a general rule to determine whether the corrections as a result of the interactions contribute to the physical properties of the system and can therefore let the perturbative analysis diverge. [13] Doing a scale dimension analysis of the action, the scaling of the coupling constant ( $J$ ) can be determined.

If  $J \propto L^{-\alpha}$  for  $\alpha > 0$  the interaction is irrelevant, if  $J \propto L^\alpha$  the interaction is relevant and finally if  $J \propto L^0$  the interaction is marginal and we have to further investigate the contribution. In a bit we will see that the Kondo model belongs to the last category.

## 2.1 One-Channel

We are going to look at the one-channel interactions first. To start we have to write down the Kondo action. Recall that the Kondo Hamiltonian (1.1) is given by

$$H_{\text{int}} = \frac{J_z}{2} \left( \psi_\uparrow^\dagger(0) \psi_\uparrow(0) - \psi_\downarrow^\dagger(0) \psi_\downarrow(0) \right) S^z + \frac{J_\perp}{2} \left( \psi_\uparrow^\dagger(0) \psi_\downarrow(0) S^- + \psi_\downarrow^\dagger(0) \psi_\uparrow(0) S^+ \right). \quad (2.6)$$

where we have worked out the Pauli matrices explicitly and used  $S^\pm = S_x \pm iS_y$ . Also we assume anisotropic coupling ( $J_z$  and  $J_\perp = J_x = J_y$ ).

In (1.13) we identified the spin impurity with a fermion degree of freedom, i.e.  $S_z = \frac{1}{2}(d_\uparrow^\dagger d_\uparrow - d_\downarrow^\dagger d_\downarrow)$ ,  $S^+ = d_\uparrow^\dagger d_\downarrow$ ,  $S_- = d_\downarrow^\dagger d_\uparrow$ . We can rewrite (2.6) in terms of these fermions:

$$H_0 = \sum_{k,\sigma} (\epsilon_k - \mu) c_{k\sigma}^\dagger c_{k\sigma} + \sum_\sigma \lambda d_\sigma^\dagger d_\sigma \quad (2.7)$$

$$H_{\text{int}} = \frac{J_z}{4} \left( \psi_\uparrow^\dagger(0) \psi_\uparrow(0) - \psi_\downarrow^\dagger(0) \psi_\downarrow(0) \right) (d_\uparrow^\dagger d_\uparrow - d_\downarrow^\dagger d_\downarrow) + \frac{J_\perp}{2} \left( \psi_\uparrow^\dagger(0) \psi_\downarrow(0) d_\downarrow^\dagger d_\uparrow + \psi_\downarrow^\dagger(0) \psi_\uparrow(0) d_\uparrow^\dagger d_\downarrow \right) \quad (2.8)$$

Since the spin-fermion transformation requires that the fermion is singly occupied (i.e.  $\sum_\sigma d_\sigma^\dagger d_\sigma = 1$ ) we have to add a term to the free Hamiltonian. Coleman showed that adding  $\sum_\sigma \lambda d_\sigma^\dagger d_\sigma$  ensures that the fermion remains in the one particle Fock space if  $\lambda \rightarrow \infty$ . [14]

From this Hamiltonian we can derive the action

$$S = T \sum_{\omega_n, \sigma} \int \frac{dk}{(2\pi)} c_{k\sigma}^\dagger (i\omega_n - (\epsilon_k - \mu)) c_{k\sigma} + T \sum_{\omega_n, \alpha} d_\alpha^\dagger (i\omega_n - \lambda) d_\alpha - \frac{J_z}{4} \left( \psi_\uparrow^\dagger(0) \psi_\uparrow(0) - \psi_\downarrow^\dagger(0) \psi_\downarrow(0) \right) (d_\uparrow^\dagger d_\uparrow - d_\downarrow^\dagger d_\downarrow) - \frac{J_\perp}{2} \left( \psi_\uparrow^\dagger(0) \psi_\downarrow(0) d_\downarrow^\dagger d_\uparrow + \psi_\downarrow^\dagger(0) \psi_\uparrow(0) d_\uparrow^\dagger d_\downarrow \right), \quad (2.9)$$

where we have replaced the time integral by the Matsubara sum with fermionic Matsubara frequencies  $\omega_n = \frac{(2n+1)\pi}{\beta}$  ( $\beta = \frac{1}{k_B T}$ ).

From dimensional analysis we see that both  $d$  and  $c_{k\sigma}$  scale as  $L^0$ , therefore  $J_{z,\perp} \propto L^0$  as well and the Kondo interactions are marginal. This means we have to further investigate whether they contribute. Along the lines of Feynman diagrams we can define propagators and vertices. The propagators for

$c_{k\sigma}$  and  $d_\alpha$  are given by

$$\begin{array}{c} \text{---} \longrightarrow \text{---} \\ \text{---} \longrightarrow \text{---} \end{array} \quad \begin{array}{c} \frac{1}{i\omega_n - (\epsilon_k - \mu)} \\ \frac{1}{i\omega_n - \lambda} \end{array} \quad \begin{array}{c} c_{k\sigma} \\ d_\alpha \end{array}. \quad (2.10)$$

The two interactions in (2.9) are

$$\begin{array}{c} \begin{array}{ccc} \sigma & & \sigma \\ & \searrow \quad \nearrow & \\ & \otimes & \\ & \swarrow \quad \searrow & \\ \alpha & & \alpha \end{array} & \sigma \alpha \frac{J_z}{4} \\ \hline \begin{array}{ccc} \sigma & & -\sigma \\ & \searrow \quad \nearrow & \\ & \blacksquare & \\ & \swarrow \quad \searrow & \\ -\sigma & & \sigma \end{array} & \frac{J_\perp}{2} \end{array} \quad (2.11)$$

The two different vertices are depicted by a crossed circle ( $J_z$ ) and a square ( $J_\perp$ ). We see that the sign of the  $J_z$ -vertex depends on the spin of the conduction fermion ( $\sigma$ ) and the impurity ( $\alpha$ ). Here spin up (down) corresponds to  $\sigma, \alpha = 1$  ( $-1$ ).

The momenta are left out, because the the vertices are momentum independent. This does not mean that momentum integrals can also be dropped.

We can now return to the perturbative expansion to calculate the corrections to the four point functions related to the vertices above. For instance

$$\langle c_{k\sigma}^\dagger c_{k'\sigma} d_\alpha^\dagger d_\alpha \rangle = \langle c_{k\sigma}^\dagger c_{k'\sigma} d_\alpha^\dagger d_\alpha \rangle_0 - \Gamma_{12,z}^{\sigma\alpha} \quad (2.12)$$

is related to the upper vertex. We have used  $\psi_\sigma(0) = \sum_k c_{k\sigma}$ . The first and second order corrections are given by  $\Gamma_{12,z}^{\sigma\alpha}$ , where the first order is simply the vertex in (2.11). The divergences in second order later give rise to the renormalization group (RG) flow.

The corrections are diagrammatically given by

$$\begin{array}{c} \Gamma_{12,z}^{\sigma\alpha} = \begin{array}{ccc} \sigma & & \sigma \\ & \searrow \quad \nearrow & \\ & \text{---} \otimes \text{---} & \\ & \swarrow \quad \searrow & \\ \alpha & & \alpha \end{array} \\ \hline \Gamma_{12,\perp}^{\sigma} = \begin{array}{ccc} \sigma & & -\sigma \\ & \searrow \quad \nearrow & \\ & \text{---} \blacksquare \text{---} & \\ & \swarrow \quad \searrow & \\ -\sigma & & \sigma \end{array} \end{array} \quad (2.13)$$

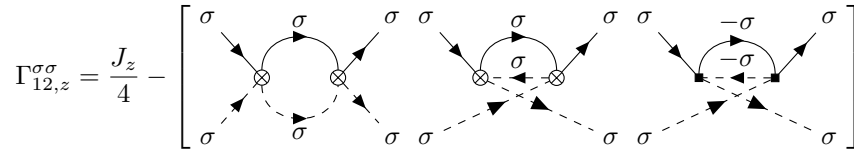
We can now also say a word on the multitude of terms in (2.5). For instance the sum of the four second order terms ensures that only certain diagrams remain. These are called one particle irreducible (1PI),

meaning the diagram is connected after cutting one propagator. Diagrams such as the following are suppressed

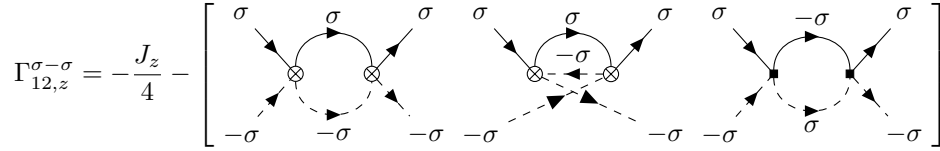


$$(2.14)$$

The diagrams that do contribute to the  $z$ -four point function are

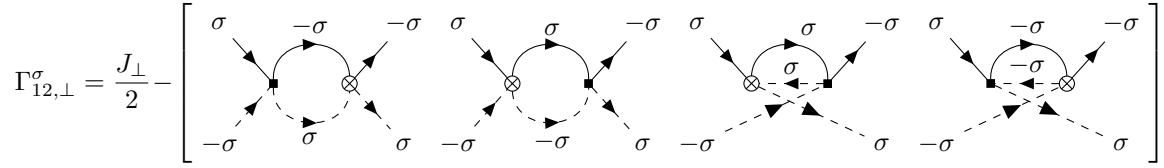


$$\Gamma_{12,z}^{\sigma\sigma} = \frac{J_z}{4} - \left[ \text{diagrams} \right] \quad (2.15)$$



$$\Gamma_{12,z}^{\sigma-\sigma} = -\frac{J_z}{4} - \left[ \text{diagrams} \right] \quad (2.16)$$

and the perpendicular corrections are

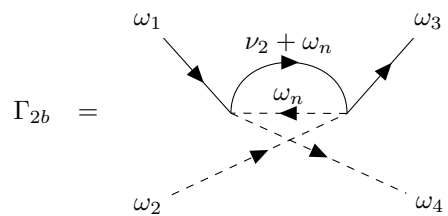


$$\Gamma_{12,\perp}^{\sigma} = \frac{J_{\perp}}{2} - \left[ \text{diagrams} \right] \quad (2.17)$$

If we take the factor from the vertices out, the spin indices can be dropped because only the vertex operators depend on the spin. We are left with two diagrams we need to calculate:



$$\Gamma_{2a} = \quad (2.18)$$



$$\Gamma_{2b} = \quad , \quad (2.19)$$



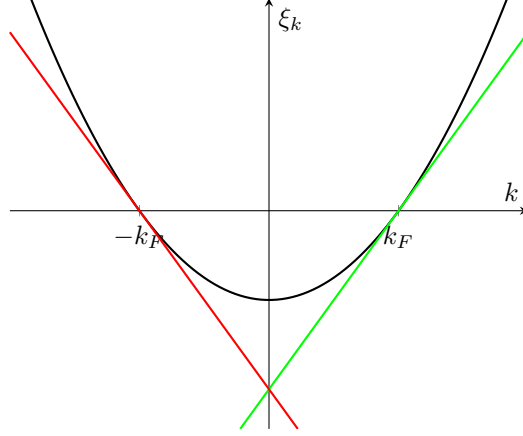


Figure 2.1: Linearization of the free energy at the Fermi surface.

where  $\nu_1 = \omega_1 + \omega_2$  and  $\nu_2 = \omega_1 - \omega_4$ . Hence the diagrams (2.15), (2.16) and (2.17) become

$$\Gamma_{12,z}^{\sigma\sigma} = \frac{J_z}{4} - \left( \frac{J_z^2}{16} \Gamma_{2a} + \frac{J_z^2}{16} \Gamma_{2b} + \frac{J_{\perp}^2}{4} \Gamma_{2b} \right) \quad (2.20)$$

$$\Gamma_{12,z}^{\sigma-\sigma} = -\frac{J_z}{4} - \left( \frac{J_z^2}{16} \Gamma_{2a} + \frac{J_z^2}{16} \Gamma_{2b} + \frac{J_{\perp}^2}{4} \Gamma_{2a} \right) \quad (2.21)$$

$$\Gamma_{12,\perp}^{\sigma} = \frac{J_{\perp}}{2} + \frac{J_z J_{\perp}}{4} (\Gamma_{2a} - \Gamma_{2b}) \quad (2.22)$$

First we take a look at  $\Gamma_{2a}$ :

$$\Gamma_{2a} = -T \sum_{\omega_n} \int \frac{dk}{2\pi} \frac{1}{i\omega_n + i\nu_1 - \xi_k} \frac{1}{-i\omega_n - \lambda} = T \sum_{\omega_n} \int \frac{dk}{2\pi} \frac{1}{i\omega_n + i\nu_1 - \xi_k} \frac{1}{i\omega_n + \lambda} \quad (2.23)$$

The minus sign in the middle term comes from the closed fermion loop.

We can work out the Matsubara sum using  $\sum_{\omega_n} f(i\omega_n) = \beta \sum_{i=1}^l \eta_F(z_i) \text{Res}_{z_i} f$  (see (B.4)), where  $\eta_F$  is the Fermi-Dirac distribution and  $z_i$  the poles of  $f$ .

$$\Gamma_{2a} = \int \frac{dk}{2\pi} \frac{1}{\xi_k - i\nu_1 + \lambda} (n_F(\xi_k) - n_F(-\lambda)) \quad (2.24)$$

We let  $T \rightarrow 0$ , then  $n_F(\epsilon) \rightarrow \theta(-\epsilon)$ . Where  $\theta$  is the heavy side function. Since  $\lambda$  is positive  $n_F(-\lambda)$  goes to 1.

$$\Gamma_{2a} = - \int \frac{dk}{2\pi} \frac{1}{\xi_k - i\nu_1 + \lambda} \theta(\xi_k) \quad (2.25)$$

We have impose a cut off  $\Lambda$  on the energy around the Fermi surface  $\mu = \frac{k_F^2}{2m}$  to remove the UV divergences. The cut off allows us to linearize the momentum around the Fermi points  $\xi_k = \frac{k_F}{m} (\pm k - k_F) = v_F (\pm k - k_F)$ . Figure 2.1 shows the linearized spectrum. We can now substitute  $u = \xi_k$ . Note that we have to add a factor 2 to account for both Fermi points ( $\pm k_F$ ).

$$\Gamma_{2a} = -2 \frac{1}{2\pi v_F} \int_{-\Lambda}^{\Lambda} du \frac{1}{u - i\nu_1 + \lambda} \theta(u) = -2 \frac{1}{2\pi v_F} \int_0^{\Lambda} du \frac{1}{u - i\nu_1 + \lambda} \quad (2.26)$$

The cut off is much larger than the  $\lambda$ , so the first diagram is

$$\Gamma_{2a} = -2 \frac{1}{2\pi v_F} \log \left( \frac{\Lambda}{\lambda - i\nu_1} \right). \quad (2.27)$$

Now  $\Gamma_{2b}$  is similar,

$$\Gamma_{2b} = -T \sum_{\omega_n} \int \frac{dk}{2\pi v_F} \frac{1}{i\omega_n + i\nu_2 - \xi_k} \frac{1}{i\omega_n - \lambda} \quad (2.28)$$

Along the same lines we obtain

$$\Gamma_{2b} = 2 \frac{1}{2\pi v_F} \log \left( \frac{\Lambda}{\lambda + i\nu_2} \right) \quad (2.29)$$

Since  $\lambda \gg i\nu_1, i\nu_2$  we can conclude

$$\Gamma_{2a} = -\Gamma_{2b} = -2 \frac{1}{2\pi v_F} \log \left( \frac{\Lambda}{\lambda} \right) \quad (2.30)$$

Now we can plug this into (2.20):

$$\Gamma_{12,z}^{\sigma\alpha} = \sigma\alpha \left[ \frac{J_z}{4} - \frac{1}{\pi v_F} \frac{J_\perp^2}{4} \log \left( \frac{\Lambda}{\lambda} \right) \right] \quad (2.31)$$

$$\Gamma_{12,\perp}^{\sigma} = \frac{J_\perp}{2} - \frac{1}{\pi v_F} \frac{J_z J_\perp}{2} \log \left( \frac{\Lambda}{\lambda} \right) \quad (2.32)$$

These corrections have to be independent of the cut off. Changing the cut off from  $\Lambda$  to  $\Lambda'$  for a general correction  $\Gamma_g = g(\Lambda) - A \log \left( \frac{\Lambda}{\lambda} \right)$  gives

$$g(\Lambda) - A \log \left( \frac{\Lambda}{\lambda} \right) = g(\Lambda') - A \log \left( \frac{\Lambda'}{\lambda} \right) \quad (2.33)$$

$$= g(\Lambda') - A \log \left( \frac{\Lambda'}{\Lambda} \right) - A \log \left( \frac{\Lambda}{\lambda} \right) \quad (2.34)$$

Hence we see that  $g(\Lambda) = g(\Lambda') - A \log \left( \frac{\Lambda'}{\Lambda} \right)$ . The cut offs are strictly positive so we can write  $\Lambda = \Lambda_0 e^l$  and  $\Lambda' = \Lambda_0 e^{l-\delta l}$ :

$$g(l) = g(l - \delta l) + A\delta l \quad (2.35)$$

For small  $\delta l$  we obtain the RG-flow

$$\frac{dg(l)}{dl} = A \quad (2.36)$$

Applying this to (2.31) and (2.32) we get the following RG-equations:

$$\frac{d\tilde{J}_z(l)}{dl} = \tilde{J}_\perp^2 \quad (2.37)$$

$$\frac{d\tilde{J}_\perp(l)}{dl} = \tilde{J}_z \tilde{J}_\perp \quad (2.38)$$

where  $\tilde{J} = \frac{J}{\pi v_F}$ .

This flow is depicted in Figure 2.2.

In the ferromagnetic case (i.e.  $\tilde{J}_z < 0$ ) the perpendicular coupling flows to zero for  $|\tilde{J}_\perp| < |\tilde{J}_z|$ . In the isotropic ferromagnetic case  $\tilde{J}_z = |\tilde{J}_\perp| < 0$  both couplings vanish and the impurity decouples from the bath. If  $|\tilde{J}_\perp| > \tilde{J}_z$ , meaning spin flipping ( $\tilde{J}_\perp$ ) is dominant over aligning spin ( $\tilde{J}_z$ ), the coupling flows towards the anti-ferromagnetic regime.

The anti-ferromagnetic coupling always blows up as we see in Figure 2.2. Locally the system behaves

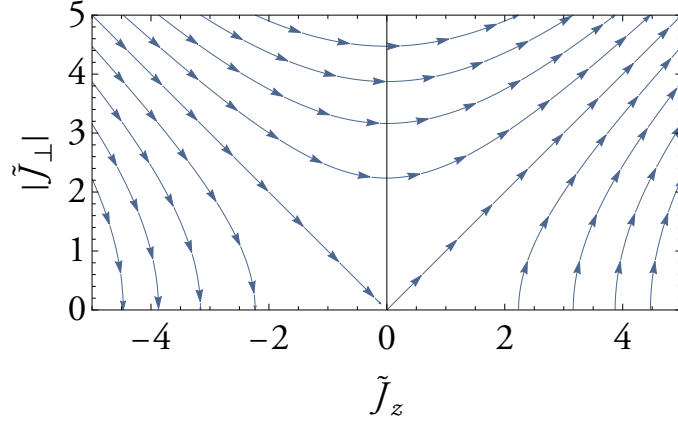


Figure 2.2: RG-flow of the anisotropic one-channel Kondo model.

a Fermi liquid. In the strong coupling limit the RG breaks down and the coupling becomes isotropic, this energy scale is known as the Kondo temperature ( $T_K$ ). In the isotropic limit we can easily solve the RG equation:

$$\tilde{J}(l) = \frac{J_0}{1 - \tilde{J}_0 l} \quad (2.39)$$

The coupling becomes of the order of 1 at  $T_k$  for  $l = \frac{1 - \tilde{J}_0}{\tilde{J}_0}$  and blows up right after. Past this point conventional RG is therefore not valid anymore.

Also higher order correction will not prevent the interaction to run to strong coupling.[15] Hence perturbative analysis is not valid for the Kondo model and there is a need for other approaches. In Chapter 3 we will see that with bosonization is one of those techniques, giving exact results and in Chapter 4 we recognize the Kondo effect in spin chain constructions.

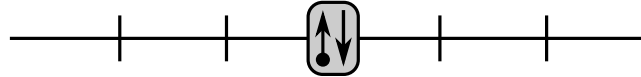


Figure 2.3: Due to the strong coupling fixed point the impurity spin traps a bath electron with opposite spin, resulting in a singlet ground state.

Nevertheless, at this strong coupling fixed point we can say something about the ground state. For strong anti-ferromagnetic coupling the impurity spin tends to trap a conduction fermion with opposite spin as we see in Figure 2.3. The arrow with the circled tail is the impurity spin. This spin-couple form as singlet  $\frac{1}{\sqrt{2}} (|\uparrow_d \downarrow_c\rangle + |\downarrow_d \uparrow_c\rangle)$ , with  $d$  the impurity spin and  $c$  the trapped conduction fermion spin. The impurity is screened and excluded from the system.[15]

## 2.2 Multi-Channel

In this section we will see that the multi-channel Kondo model exerts qualitatively different physical behavior than the one-channel Kondo model. In this case we will also take the two-loop corrections into account. This two loop RG will show that there is a finite fixed point for the coupling constants. This finite fixed point lies energetically beyond the Kondo temperature ( $T_K$ ). We therefore have to

let the system first run to  $T_K$ . In Figure 2.2 we see that the coupling flows to isotropy as it approaches the strong coupling limit ( $T_K$ ). So here we have to consider the isotropic Kondo interaction.

The action for the isotropic  $n$ -channel Kondo model is just an extension of the one-channel case (2.9):

$$\begin{aligned}
S = \sum_{a=1}^n & \left[ T \sum_{\omega_n, \sigma} \int \frac{dk}{2\pi} c_{k\sigma a}^\dagger (i\omega_n - (\epsilon_k - \mu)) c_{k\sigma a} + T \sum_{\omega_n, \alpha} d_\alpha^\dagger (i\omega_n - \lambda) d_\alpha \right. \\
& - \frac{J}{4} \left( \psi_{\uparrow a}^\dagger(0) \psi_{\uparrow a}(0) - \psi_{\downarrow a}^\dagger(0) \psi_{\downarrow a}(0) \right) \left( d_\uparrow^\dagger d_\uparrow - d_\downarrow^\dagger d_\downarrow \right) \\
& \left. - \frac{J}{2} \left( \psi_{\uparrow a}^\dagger(0) \psi_{\downarrow a}(0) d_\downarrow^\dagger d_\uparrow + \psi_{\downarrow a}^\dagger(0) \psi_{\uparrow a}(0) d_\uparrow^\dagger d_\downarrow \right) \right] \quad (2.40)
\end{aligned}$$

From this action we find the same propagators (2.10) and vertices (2.11) as in the one-channel case, although the conduction fermion propagators now carry a channel index.

Furthermore, we work in the large  $n$  limit, where  $n$  is the number of channels. Therefore we only have to consider diagrams containing a bath fermion loop. These diagrams are proportional to  $n \gg 1$  and therefore dominate the other corrections.

Before we calculate the two-loop contributions for the coupling constants we see that there is also a contribution that renormalizes the impurity fermion operators. Note that we can write the free action of the impurity as

$$d_\alpha^\dagger G_0^{-1} d_\alpha, \quad (2.41)$$

where  $G_0 = i\omega - \lambda$  is the bare Green's function. We can find a two-loop diagrams that contribute to the total Green's function, and from the Dyson equation we see that

$$G(\Lambda)^{-1} = G_0^{-1} - \Sigma(\Lambda) \quad (2.42)$$

The self energy diagrams are given by

$$\Sigma = \sum_{\sigma} \text{---} \alpha \text{---} \bigcirc \text{---} \alpha \text{---} + \text{---} \alpha \text{---} \bigcirc \text{---} \alpha \text{---} = \frac{3nJ^2}{8} \Sigma_1 \quad (2.43)$$

Here the fermion loops are displayed with a thick line, meaning there is a summation over the channels. The two loop diagram we need to calculate is

$$\Sigma_1 = \text{---} \omega \text{---} \bigcirc \text{---} \omega \text{---} \quad (2.44)$$

$$= T^2 \sum_{\omega_n, \omega_m} \int \frac{dk}{2\pi} \frac{dk'}{2\pi} \frac{1}{i(\omega_m - \omega_n) + (i\omega - \lambda)} \frac{1}{i\omega_n - \xi_k} \frac{1}{i\omega_m - \xi_{k'}}. \quad (2.45)$$

Working out the Matsubara summations using (B.4) we obtain

$$\Sigma_1 = \int \frac{dk}{2\pi} \frac{dk'}{2\pi} \frac{\eta_F(\xi_{k'})}{(i\omega - \lambda) + \xi_{k'} - \xi_k} (\eta_F(-\lambda + \xi_k + i\omega) - \eta(\xi_k)). \quad (2.46)$$

Letting  $T \rightarrow 0$  we see that  $\eta_F(x) \rightarrow \theta(-x)$ . Note that  $\lambda \gg 1$  so  $\eta_F(-\lambda + \xi_k + i\omega) - \eta(\xi_k) \rightarrow \theta(\xi_k)$ . We linearize the energy and find

$$\Sigma_1 = \frac{4}{(2\pi v_F)^2} \int_0^\Lambda du du' \frac{1}{(i\omega - \lambda) - (u + u')}. \quad (2.47)$$

In the end we have to renormalize the operators, so we are only interested in terms proportional to  $(i\omega - \lambda)$ . Expanding (2.47) in this term gives

$$\Sigma_1 = -(i\omega - \lambda) \frac{1}{(\pi v_F)^2} \int_0^\Lambda du du' \frac{1}{(u + u')^2} \quad (2.48)$$

$$= -(i\omega - \lambda) \frac{1}{(\pi v_F)^2} \log(\Lambda), \quad (2.49)$$

where all non leading order terms have been dropped. Hence the self energy is

$$\Sigma = -(i\omega - \lambda) \frac{3nJ^2}{8(\pi v_F)^2} \log(\Lambda). \quad (2.50)$$

And we find

$$d_\alpha^\dagger G^{-1} d_\alpha = d_\alpha^\dagger G_0^{-1} \left( 1 - \frac{3nJ^2}{8(\pi v_F)^2} \log(\Lambda) \right) d_\alpha = \tilde{d}_\alpha^\dagger G_0^{-1} \tilde{d}_\alpha, \quad (2.51)$$

with  $\tilde{d} = d\sqrt{Z}$  the renormalized operators. Here  $Z = 1 - \frac{3nJ^2}{8(\pi v_F)^2} \log(\Lambda)$ . The impurity operators are now still in the unrenormalized form  $d$ . To correct for this we rescale the coupling constant  $J \rightarrow \frac{J}{\Lambda}$  to find

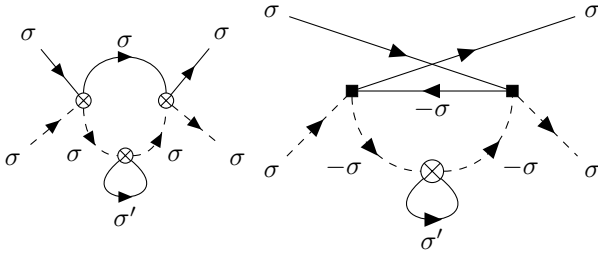
$$J d^\dagger d c^\dagger c = \frac{J}{Z} \tilde{d}^\dagger \tilde{d} c^\dagger c \quad (2.52)$$

giving an indirect contribution to the renormalization of  $J$ .

We will now determine the contributions to the direct renormalization of  $J$ . The one-loop diagrams are given by the one-channel corrections in Section 2.1. For the two-loop corrections we are only going to consider diagrams containing a closed fermion loop (e.g. loop not connected to external fermion propagators). Before we calculate the two-loop contributions we can exclude some diagrams. For instance diagrams with a tadpole fermion loop,


(2.53)

does not contribute, since it is proportional to  $\sum_{\sigma=\pm 1} \sigma = 0$ . Besides, if it were non-zero, it would have been absorbed by a renormalization of the impurity propagator. Nevertheless, it means that these fermion loop diagrams vanish:



Another diagram we can encounter is

$$(2.54)$$

However we already see that

$$(2.55)$$

is proportional to  $T \sum_{\omega_n} \frac{1}{i\omega_n + i\nu_1 - \lambda} \frac{1}{i\omega_n - \lambda} = \eta_F(\lambda) \left( \frac{1}{-\nu_1} + \frac{1}{\nu_1} \right) = 0$ . Therefore (2.54) does not contribute either. Concluding the only possible two loop contributions to the vertices containing a fermion loop are:

$$\Gamma_{3,z}^{\sigma\sigma} = \sum_{\sigma'} \left[ \text{Diagram 1} + \text{Diagram 2} \right] = -n \frac{J^3}{32} \Gamma_3 \quad (2.56)$$

$$\Gamma_{3,z}^{\sigma-\sigma} = \sum_{\sigma'} \left[ \text{Diagram 1} + \text{Diagram 2} \right] = n \frac{J^3}{32} \Gamma_3 \quad (2.57)$$

$$\Gamma_{3,\perp}^{\sigma} = \left[ \text{Diagram} \right] = -n \frac{J^3}{16} \Gamma_3 \quad (2.58)$$

The summation over the channels gives the factor  $n$ , we see on the right hand side.

We are now faced with calculating just one diagram:

where  $\nu = \omega_2 - \omega_1$  (bosonic Matsubara frequency), and  $\omega = -\omega_4$  (fermionic Matsubara frequency). This diagram is given by:

$$\Gamma_3 = (-1)^2 T^2 \sum_{\omega_n, \omega_m} \int \frac{dk}{2\pi} \frac{dk'}{2\pi} \frac{1}{i(\omega_n + \nu) - \lambda} \frac{1}{i\omega_n - \lambda} \frac{1}{i(\omega_n + \omega_m + \omega) - \xi_k} \frac{1}{i\omega_m - \xi_{k'}}, \quad (2.60)$$

with  $\xi_k = \epsilon_k - \mu$  and  $T = \frac{1}{\beta}$  the temperature. Using (B.4) we can work out the Matsubara summations and find:

$$\Gamma_3 \int \frac{dk}{2\pi} \frac{dk'}{2\pi} \frac{\eta_F(\xi_{k'}) \eta_F(\xi_k - \xi_{k'} - i\omega)}{(i(\omega - \nu) + \xi_{k'} - \xi_k + \lambda)(i\omega + \xi_{k'} - \xi_k + \lambda)} \quad (2.61)$$

All terms containing  $\eta_F(\lambda)$  have been dropped, because this Fermi-Dirac distribution vanishes even for finite temperatures. Furthermore, some terms cancel out and we remain with this double integral. Using  $\frac{1}{AB} = \frac{1}{B-A} \left[ \frac{1}{A} - \frac{1}{B} \right]$  we find

$$\Gamma_3 = \int \frac{dk}{2\pi} \frac{dk'}{2\pi} \left[ \frac{1}{i(\omega - \nu) + \xi_{k'} - \xi_k + \lambda} - \frac{1}{i\omega + \xi_{k'} - \xi_k + \lambda} \right] \frac{-\eta_B(\xi_k - \xi_{k'})}{i\nu} \eta_F(\xi_{k'}), \quad (2.62)$$

where we have used that  $\eta_F(\alpha + i\omega) = -\eta_B(\alpha)$ , with  $\omega$  a fermion Matsubara frequency and  $\eta_B$  the Bose-Einstein distribution.

Now we let the temperature go to zero, which gives  $\eta_F(\alpha) \rightarrow \theta(-\alpha)$  and  $\eta_B(\alpha) \rightarrow -\theta(-\alpha)$ , with  $\theta$  the heavy side function. We find

$$\Gamma_3 = \int \frac{dk}{2\pi} \frac{dk'}{2\pi} \left[ \frac{1}{i(\omega - \nu) + \xi_{k'} - \xi_k + \lambda} - \frac{1}{i\omega + \xi_{k'} - \xi_k + \lambda} \right] \frac{\theta(\xi_{k'} - \xi_k)}{i\nu} \theta(-\xi_{k'}) \quad (2.63)$$

As we did in the one-channel case the spectrum can be linearized and the momentum integrals become energy integrals:

$$\Gamma_3 = 4 \int_{-\Lambda}^{\Lambda} \frac{du'}{2\pi v_F} \int_{-\Lambda}^{\Lambda} \frac{du}{2\pi v_F} \left[ \frac{1}{i(\omega - \nu) + u' - u + \lambda} - \frac{1}{i\omega + u' - u + \lambda} \right] \frac{\theta(u' - u)}{i\nu} \theta(-u') \quad (2.64)$$

For small  $i\nu$  we recognize  $\frac{1}{A-u-i\nu} - \frac{1}{A-u} = i\nu \frac{d}{du} \frac{1}{A-u}$  and we can work out the first integral:

$$\Gamma_3 = -\frac{4}{(2\pi v_F)^2} \int_{-\Lambda}^0 du' \frac{1}{i\omega + u' + \Lambda + \lambda} \quad (2.65)$$

where we have dropped the term  $u = u'$  because it will be linear in  $\Lambda$  in the end, and therefore is not leading order.

Working out the remaining integral results in

$$\Gamma_3 = -\frac{4}{(2\pi v_F)^2} \log \left( \frac{\Lambda + \lambda + i\omega}{\lambda + i\omega} \right) = -\frac{4}{(2\pi v_F)^2} \log \left( \frac{\Lambda}{\lambda} \right) \quad (2.66)$$

We can now combine this with (2.31) and (2.32) to find

$$\Gamma_{123,z}^{\sigma\alpha} = \sigma\alpha \left[ \frac{J}{4} - \left( \frac{1}{\pi v_F} \frac{J^2}{4} - \frac{nJ^3}{32(\pi v_F)^2} \right) \log \left( \frac{\Lambda}{\lambda} \right) \right] \quad (2.67)$$

$$\Gamma_{123,\perp}^{\sigma} = \frac{J}{2} - \left( \frac{1}{\pi v_F} \frac{J^2}{2} - \frac{nJ^3}{16(\pi v_F)^2} \right) \log \left( \frac{\Lambda}{\lambda} \right) \quad (2.68)$$

Here  $\Gamma_{123}$  denotes the vertex contributions up to third order (two loop).

Note that both contributions are the same, as they should in the isotropic limit. Recall that the self energy also contributes to the renormalization of  $J$ :

$$\frac{J}{Z} \approx J + \frac{3nJ^3}{8(\pi v_F)^2} \log(\Lambda) \quad (2.69)$$

Expanding (2.67) up to  $J^3$  gives

$$\frac{1}{4} \left[ \tilde{J} - \left( \tilde{J}^2 - n\tilde{J}^3 \left( \frac{1}{8} + \frac{3}{8} \right) \right) \log(\Lambda) \right] \quad (2.70)$$

$$= \frac{1}{4} \left[ \tilde{J} - \left( \tilde{J}^2 - \frac{n\tilde{J}^3}{2} \right) \log(\Lambda) \right], \quad (2.71)$$

where  $\tilde{J} = \frac{J}{\pi v_F}$ .

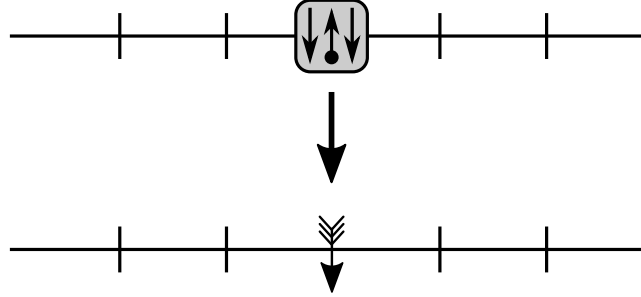


Figure 2.4: [Upper] Anti-ferromagnetic strong coupling limit, binding of two anti-aligning conduction electron spins with the impurity spin. [Lower] Effective anti-ferromagnetic chain with opposite spin and effective Kondo coupling.

And we obtain the following RG-flow

$$\frac{d\tilde{J}(l)}{dl} = \tilde{J}^2 - \frac{n}{2} \tilde{J}^3 \quad (2.72)$$

There is a finite coupling fixed point at  $\tilde{J} = \frac{2}{n}$ . At this stable fixed point the system is described by a non Fermi liquid.[10, 15]

We can make the existence of this finite stable fixed point intuitively clear in the two-channel case, following the explanation in Gianmarchi (2004).[15] First of all note that the  $J = 0$  fixed point is unstable as we see in Figure 2.2. Now suppose there is no finite fixed point. The system flows to the strong coupling limit according to Figure 2.2. In this strong coupling fixed point the system favors to anti-align the conduction spins with the impurity spin at the origin. Therefore the impurity spin (e.g. up) binds two fermions with opposite spin (e.g. down), one for each channel. This we see in the upper picture of Figure 2.4. The arrow with circled tail is the impurity spin and the other arrows the bath electrons. This behaves as an effective spin down impurity, see the lower picture of Figure 2.4. These bath electrons that are bound to the spin can still hop in and out with coupling constant  $t$



(tight binding chain). This results in a weak effective Kondo coupling, which in its turn would flow to strong coupling. Hence the strong coupling limit is not stable either. Therefore one would expect there to be a finite fixed coupling, as we saw in (2.72).

For  $n$  small (e.g. two-channel) this finite coupling fixed point is still too large and the results of a perturbative analysis are not valid.

In the next chapter we will see that bosonization and spin chains can help us understand the low- $n$ -channel Kondo models better.



## Chapter 3

# Bosonization for the Kondo Model

Bosonization has been developed in the late 1970s after Coleman and Mandelstam[16, 17], and Mattis and Luther[18, 19] independently derived that the correlation functions for Dirac fermions can be expressed by the correlation functions of free bosons.[10]

It has proven to be useful for solving one dimensional metals and was essential in understanding an interacting itinerant electron system, known as the Tomanaga-Luttinger Liquid.

In this chapter we will use bosonization to find exact solutions for both one- and multi-channel Kondo models. First, we will briefly introduce the important ingredients of bosonization. In Appendix C there is a more comprehensive discussion. There are different conventions for defining the bosonization framework. In this thesis we will stick with the set-up Von Delft uses, because it is elegant and short in notation.[20] Then we will use bosonization to get exact results for the one- and two-channel Kondo models in Sections 3.3 and 3.4. Finally, in Section 3.5 we give an outlook for bosonization and the Kondo model.

Before we proceed to technical details of bosonization, it is important to underline that there are special circumstances for bosonization to be applicable.

First of all, we need a finite density of states at the Fermi surface. For the one-dimensional Kondo model we are going to discuss, this means we have to be able linearize the Hamiltonian close to the Fermi point, i.e. describe the fermion by a Dirac theory. Furthermore bosonization is only applicable in one dimension. Fortunately, in Section 1.3 we saw that because of rotational symmetry the three dimensional Kondo Hamiltonian can be reduced to an effective one dimensional theory.

We underline the difference between one dimension and higher dimensions using Figure 3.1. Figure 3.1a depicts a quadratic spectrum in one dimension with a Fermi surface. Suppose we excite a fermion from below the Fermi surface with a finite amount of energy to above the Fermi surface. We see that the dispersion allows this fermion to hop only to one point. On the other hand, Figure 3.1b shows a projection of a two dimensional Fermi surface. Now suppose there is fermion at  $k$  with  $|\vec{k}| < k_F$  excited above the Fermi surface, it can go to any unoccupied state on the dashed circle. Hence the state is smeared out over this circle, therefore a excitation in energy does not relate one-to-one to a momentum change. This energy-momentum relation is essential for bosonization, hence one dimension is special.

Note that in Figure 3.1a we only show  $k > 0$ , this is allowed because we integrated out the rotational degrees of freedom leaving only a radial (positive) component. This has two major advantages. First, it makes the definitions of the bosons simpler. Secondly, after linearization we do not have to care about the filled Fermi sea for the right movers (i.e. linearization around  $+k_F$ ) for negative  $k$ .

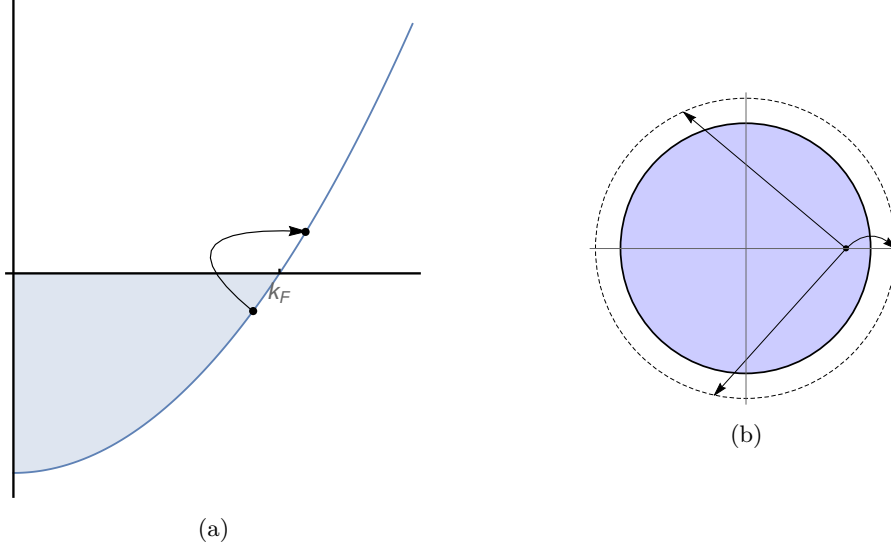


Figure 3.1: Excitations from below the Fermi surface ( $E_k$ ) to above ( $E_{k+q}$ ) for one dimension (a) and two dimensions (b). The spectrum for two dimensions is projected in the  $k_x, k_y$ -plane. For one dimension there is only one point the excited particle can go to, for two dimensions there is a whole circle (dashed).

### 3.1 Bosonization Ingredients

There is a very natural way to relate a boson with fermions, because the density fermion operator behaves as a boson. Bosonization uses this fact to construct boson operators:  $b \propto \psi^\dagger \psi$ . We already see that a great advantage of this boson representation is the fact that fermion density-density interaction is quadratic in bosonic language,  $\psi^\dagger \psi \psi^\dagger \psi \propto b^\dagger b$ .

More explicitly the bosonization identity, relating fermions to the new boson operators is

$$\psi_\sigma(x) = F_\sigma a^{-1/2} e^{-i \frac{2\pi}{L} (\hat{N}_\sigma - \frac{1}{2} \delta_b) x} e^{-i \phi_\sigma(x)}, \quad (3.1)$$

where  $a$  is the lattice spacing,  $\hat{N}_\sigma$  the fermion number operator and  $L$  the length of the system. The factor  $F_\sigma$  is a Klein factor. Without the latter  $\psi$  (and  $\psi^\dagger$ ) would conserve particle number ( $\phi \propto \psi^\dagger \psi$ ), while it should annihilate (create) a particle. Furthermore, it ensures the anti-commutation relations are satisfied since:

$$\{F_\sigma^\dagger, F_{\sigma'}\} = 2\delta_{\sigma\sigma'} \text{ and } F_\sigma F_\sigma^\dagger = F_\sigma^\dagger F_\sigma = 1 \quad (3.2)$$

The boson field  $\phi_\sigma(x)$  is given by

$$\phi_\sigma(x) = \varphi_\sigma(x) + \varphi_\sigma^\dagger(x) = - \sum_{q>0} \frac{1}{\sqrt{n_q}} (e^{-iqx} b_{q\sigma} + e^{iqx} b_{q\sigma}^\dagger) e^{-aq/2} \quad (3.3)$$

where  $q = \frac{2\pi n_q}{L}$  with  $n_q \in \mathbb{Z}$  and boson operators

$$b_{q\sigma} = \frac{-i}{\sqrt{n_q}} \sum_k c_{k-q\sigma}^\dagger c_{k\sigma} \quad (3.4)$$

$$b_{q\sigma}^\dagger = \frac{i}{\sqrt{n_q}} \sum_k c_{k+q\sigma}^\dagger c_{k\sigma} \quad (3.5)$$

The  $b_{q\sigma}$  satisfies canonical commutation relations:

$$[b_{q\sigma}, b_{q'\sigma'}] = \delta_{qq'} \delta_{\sigma\sigma'} \quad (3.6)$$

and  $\phi$  satisfies

$$[\phi_\sigma(x), \phi_{\sigma'}(x')] \stackrel{L \gg (x-x') \rightarrow 0}{=} -\delta_{\sigma\sigma'} 2\pi i \operatorname{sgn}(x-x') \quad (3.7)$$

$$[\phi_\sigma(x), \partial_x \phi_{\sigma'}(x')] \stackrel{L \gg (x-x') \rightarrow 0}{=} \delta_{\sigma\sigma'} 2\pi i \left[ \delta(x-x') - \frac{1}{L} \right] \quad (3.8)$$

Where  $\operatorname{sgn}(x)$  is the sign function, analytically continued in 0 (i.e.  $\operatorname{sgn}(0) = 0$ ). The free linearized fermion Hamiltonian

$$H_0 = \sum_{\sigma, k} v_F k :c_{k\sigma}^\dagger c_{k\sigma}: = \sum_{\sigma} \int_{-L/2}^{L/2} \frac{dx}{2\pi} : \psi_\sigma^\dagger(x) i v_F \partial_x \psi_\sigma(x) :, \quad (3.9)$$

in the bosonization language is (see (C.26))

$$H_0 = \sum_{\sigma} \int_{-L/2}^{L/2} \frac{dx}{2\pi} \frac{v_F}{2} :(\partial_x \phi_\sigma(x))^2:, \quad (3.10)$$

where we have introduced the notion of normal ordering  $:O:$ , to take care of the divergences resulting from the linearization.

Note that we have normalized the fermion operators  $\psi$  to  $2\pi$ , for notational purposes.

### 3.1.1 Bosonized Kondo Hamiltonian

The bulk Hamiltonian for the Kondo model is given by the single particle energy, so (3.10) describes the fermion bath. The Kondo interaction (2.6) we can write as

$$H_{\text{int}} = H_z + H_\perp = \frac{J_z}{2L} \sum_{\substack{k, k' \\ \sigma=(\uparrow, \downarrow)}} \sigma :c_{k\sigma}^\dagger c_{k'\sigma}: S^z + \frac{J_\perp}{4\pi} \left( : \psi_\uparrow^\dagger(0) \psi_\downarrow(0) : S^- + : \psi_\downarrow^\dagger(0) \psi_\uparrow(0) : S^+ \right) \quad (3.11)$$

where we have written the  $z$ -interaction in terms of the momentum operators and the  $\perp$ -interaction in terms of the spatial operators. The  $\sigma$  in front of the fermion operators is  $+1$  for  $\sigma = \uparrow$  and  $-1$  for  $\sigma = \downarrow$ . Here we will translate the one-channel Kondo Hamiltonian to boson language. For the multi-channel, we just have to add a summation over the channel numbers. Using (3.3) and (3.4) the  $z$ -interaction becomes

$$\begin{aligned} H_z &= \frac{J_z}{2L} \sum_{k, k', \sigma} \sigma :c_{k\sigma}^\dagger c_{k'\sigma}: S_z \\ &= \frac{J_z}{2L} \sum_{\sigma} \sigma \left[ \sum_{q>0} \sum_k \left( c_{k-q\sigma}^\dagger c_{k\sigma} + c_{k+q\sigma}^\dagger c_{k\sigma} \right) \right] S_z \\ &= \frac{J_z}{4\pi} \sum_{\sigma} \sigma \partial_x \phi_\sigma(0) S_z \end{aligned} \quad (3.12)$$

In the last line we recognized the derivative of the boson operator  $\phi$ .

We can define two new boson operators, satisfying the same commutations relations as  $\phi_\sigma$ :

$$\begin{aligned} \phi_\rho(x) &= \frac{1}{\sqrt{2}} (\phi_\uparrow(x) + \phi_\downarrow(x)) \\ \phi_s(x) &= \frac{1}{\sqrt{2}} (\phi_\uparrow(x) - \phi_\downarrow(x)) \end{aligned} \quad (3.13)$$

These are the charge  $\phi_\rho$  and the spin  $\phi_s$ . Using this transformation the  $z$ -interactions becomes

$$H_z = \frac{J_z}{2\sqrt{2}\pi} \partial_x \phi_s(0) S_z \quad (3.14)$$

Hence the charge field decouples from the  $z$ -interactions, only the spin operators couple to the magnetic impurity. Intuitively this makes sense, because the Kondo interactions are spin interactions. Also the  $\perp$ -interaction couples only to the spin part:

$$H_\perp = \frac{J_\perp}{4\pi} (: \psi_\uparrow^\dagger(0) \psi_\downarrow(0) : S^- + \text{h.c.}) \quad (3.15)$$

$$= \frac{J_\perp}{4\pi a} (e^{i\sqrt{2}\phi_s(0)} S^- + \text{h.c.}) \quad (3.16)$$

Hence the Kondo model is a boundary sine-Gordon model:

$$H = \int_{-L/2}^{L/2} \frac{dx}{2\pi} \frac{1}{2} \left( :(\partial_x \phi_\rho(x))^2: + :(\partial_x \phi_s(x))^2: \right) + \frac{J_z}{2\sqrt{2}\pi} \partial_x \phi_s(0) S_z + \frac{J_\perp}{4\pi a} (e^{i\sqrt{2}\phi_s(0)} S^- + \text{h.c.}) \quad (3.17)$$

The charge carrying operators  $\phi_\rho$  do not couple to the impurity, so we can integrate these operator out leaving only the  $\phi_s$ . From now on we drop the index  $s$  and write  $\phi \equiv \phi_s$ .

We now use a technical trick, to further simplify the Hamiltonian. Define a unitary canonical transformation as

$$W = e^{i\gamma S_z \phi(0)} \quad (3.18)$$

Letting this canonical transformation act in the following way  $\tilde{H} = WHW^\dagger$  we obtain after working out the commutations

$$\tilde{H} = WHW^\dagger = \int_{-L/2}^{L/2} \frac{dx}{2\pi} \frac{1}{2} :(\partial_x \phi(x))^2: + \left( \frac{J_z}{2\sqrt{2}\pi} - 2\pi v_F \gamma \right) \partial_x \phi(0) S_z + \frac{J_\perp}{4\pi a} (e^{i(\sqrt{2}-\gamma)\phi(0)} S^- + \text{h.c.}). \quad (3.19)$$

We can still freely choose constant  $\gamma$  in the canonical transformation.

In the next sections this canonical transformation proves essential in finding exact solutions for the one- and multi-channel Kondo model.

## 3.2 Renormalization Group One-Channel

Before we discuss how we can derive exact solutions for the Kondo model using bosonization we rederive the RG equation in the one-channel case. However, as we will see bosonization will make it possible to derive an exact RG-flow for the  $J_z$  coupling

Note that if we set  $\gamma = \frac{J_z}{4\pi^2 \sqrt{2} v_F \pi}$  the  $S_z$ -coupling in (3.19) disappears and the  $J_z$  dependence remains only in sine-Gordon term. The only interaction term is the perpendicular interaction.

We can write down a full action from (3.19)

$$S = S_0 + S_\perp \quad (3.20)$$

with

$$S_\perp = -\frac{J_\perp}{4\pi a} \int d\tau (e^{i(\sqrt{2}-\gamma)\phi(\tau,0)} S^-(\tau) + e^{-i(\sqrt{2}-\gamma)\phi(\tau,0)} S^+(\tau)) \quad (3.21)$$

Notice that there is a imaginary time  $\tau$  in the argument as well.  $\phi(\tau, x)$  and  $S^\pm(\tau)$  are the time evolved operators.

To calculate the RG-flow we only have to treat  $J_\perp$  perturbatively.

In Appendix C.6 the boson one-loop correction are worked out yielding the following RG-equations:

$$\frac{d\gamma(l)}{dl} = (\sqrt{2} - \gamma)^3 \frac{J_\perp^2 v_F^2}{16\pi^2 a^2 \Lambda^2} \quad (3.22)$$

$$\frac{dJ_\perp(l)}{dl} = \left(1 - \frac{(\sqrt{2} - \gamma)^2}{2}\right) J_\perp \quad (3.23)$$

Remarkably these equations are now exact for  $\gamma$  (related to  $J_z$ ) and only second order in  $J_\perp$ . This is the first nice result we obtain from bosonization. Expand both equations up to second order to rediscover the conventional-RG equations (2.37),(2.38). Still the anti-ferromagnetic Kondo coupling blows up, so this perturbative approach does not give a satisfactory solution.

We have to add one remark, the RG-equation for  $\gamma$  does not concur with the equation found by Giamarchi.[15] He obtained  $(\sqrt{2} - \gamma)$  in stead of  $(\sqrt{2} - \gamma)^3$ .

### 3.3 One-Channel Kondo - Toulouse Limit

We return to the canonically transformed Hamiltonian (3.19)

$$H_{\text{int}} = \left( \frac{J_z}{2\sqrt{2}\pi} - 2\pi v_F \gamma \right) \partial_x \phi(0) S_z + \frac{J_\perp}{4\pi a} (e^{i(\sqrt{2}-\gamma)\phi(0)} S^- + \text{h.c.}). \quad (3.24)$$

If we now choose  $\gamma = \sqrt{2} - 1$  the perpendicular interaction is proportional to  $e^{i\phi(0)}$ . If we compare this with (3.1) we notice that the scaling dimension of this perpendicular term is now the same as a fermion, i.e. the pre-factor in the exponent for the  $\phi$  is the same ( $\pm 1$ ).

Note that we need a Klein factor ( $F$ ) to be able to refermionize the Hamiltonian, i.e.  $F e^{i\phi(0)} \propto \hat{\psi}(0)$  with  $\hat{\psi}$  the new fermion operator.

We also note that the spin impurity system is a two level system. A single impurity fermion is a two level system as well, so we can write this spin in terms of a fermion. The spin up corresponds with occupation number one, while spin down with occupation number zero through

$$S_z = d^\dagger d - \frac{1}{2}, \quad (3.25)$$

where  $d^\dagger$  and  $d$  are respectively the fermion creation and annihilation operators. This means that  $S^+$  and  $S^-$  need to create and annihilate a fermion, so we need them to change particle number. This can be artificially added a Klein factor, so  $S^+ F = d^\dagger$  and  $S^- F = d$ .

Combining both transformations results we find the  $\perp$  term

$$\frac{J_\perp}{4\pi a} e^{i\phi(0)} S^- = \frac{J_\perp}{4\pi a} e^{i\phi(0)} F^2 S^- = \frac{J_\perp}{4\pi\sqrt{a}} \hat{\psi}^\dagger(0) d. \quad (3.26)$$

For the  $z$ -interaction we can reverse steps from (3.12) to find  $\partial_x \phi(0) = \hat{\psi}^\dagger(0) \hat{\psi}(0)$ . The Kondo Hamiltonian is therefore equivalent to an interacting resonant level model:

$$\tilde{H} = H_0 + \left( \frac{J_z}{2\sqrt{2}\pi} - 2\pi v_F (\sqrt{2} - 1) \right) \hat{\psi}^\dagger(0) \hat{\psi}(0) \left( d^\dagger d - \frac{1}{2} \right) + \frac{J_\perp}{4\pi\sqrt{a}} \left( \hat{\psi}^\dagger(0) d + \text{h.c.} \right) \quad (3.27)$$

Here the bath electrons interact with a spinless singly occupied impurity at the Fermi level, see Figure 3.2. The electron can hop in and out ( $J_\perp$ -term) and interact via density-density interaction ( $J_z$ -term).

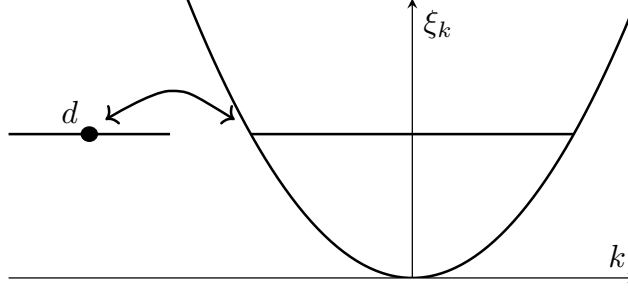


Figure 3.2: Resonant level model. Interaction of the bath electrons at the Fermi surface with the quantum dot ( $d$ ).

Taking a closer look at the  $z$ -coupling we see that if  $J_z = 4\pi^2\sqrt{2}v_F(\sqrt{2} - 1)$ , the density-density interaction vanishes and only hopping remains. This critical value for  $J_z$  is known as the Toulouse limit and in the resulting resonant level model is exactly solvable.[21] Physical properties of the impurity is now very easy to derive. This is the most important result of the bosonization approach for the one-channel Kondo model.

From this quadratic model it is easy to calculate physical observables.[15]

Furthermore in the interacting resonant level model one can do a perturbative analysis and find exact results away from this fine-tuned point, as was shown by Majumbar et al.[22]

### 3.4 Two-Channel - Emery-Kivelson Solution

We have seen that the one-channel Kondo model can be solved with bosonization, however this is not unique to the one-channel case. For two-channel there is an equivalent approach using bosonization, known as the Emery-Kivelson solution.[23]

We start with an two-channel extension of the bosonized Hamiltonian (3.19):

$$H = \int_{-L/2}^{L/2} \frac{dx}{2\pi} \frac{v_F}{2} \left( :(\partial_x \phi_1(x))^2: + :(\partial_x \phi_2(x))^2: \right) + \frac{J_z}{2\sqrt{2}\pi} [\partial_x \phi_1(0) + \partial_x \phi_2(0)] S_z + \frac{J_\perp}{4\pi a} \left[ \left( e^{i\sqrt{2}\phi_1(0)} + e^{i\sqrt{2}\phi_2(0)} \right) S^- + \text{h.c.} \right] \quad (3.28)$$

Again, we can do a transformation of the operators, but now we transform the operators from the different channels.

$$\phi_S = \frac{1}{\sqrt{2}} (\phi_1 + \phi_2), \quad \phi_A = \frac{1}{\sqrt{2}} (\phi_1 - \phi_2) \quad (3.29)$$

where  $S$  denotes the symmetric and  $A$  denotes the anti-symmetric operator. Again these operators satisfy boson commutation relations. The Hamiltonian (3.28) then becomes

$$H = \int_{-L/2}^{L/2} \frac{dx}{2\pi} \frac{v_F}{2} \left[ :(\partial_x \phi_S(x))^2: + :(\partial_x \phi_A(x))^2: \right] + \frac{J_z}{2\pi} \partial_x \phi_S(0) S_z + \frac{J_\perp}{2\pi a} \left[ e^{i\phi_S(0)} \cos(\phi_A(0)) S^- + \text{h.c.} \right] \quad (3.30)$$

Just as in the one-channel case we can do a canonical transformations

$$W = e^{i\phi_S(0)S_z} \quad (3.31)$$



such that the factor  $e^{i\phi_S(0)}$  disappears in (3.30):

$$\tilde{H} = WHW^\dagger = H_{0,S} + H_{0,A} + \left[ \frac{J_z}{2\pi} - 2\pi v_F \right] \partial_x \phi_S(0) S_z + \frac{J_\perp}{2\pi a} [\cos(\phi_A(0)) S^- + \text{h.c.}] \quad (3.32)$$

If we now impose

$$J_z^* = 4\pi^2 v_F, \quad (3.33)$$

which is known as the Emery-Kivelson line, the  $z$ -term vanishes. Hence only the anti-symmetric part of the boson operators couples to the impurity.

The field  $\phi_A$  appears in  $e^{\pm i\phi_A(0)}$ , again this term has the same scaling dimension of a fermion operator (3.1). Hence we can refermionize

$$\hat{\psi}(x) = F a^{-1/2} e^{-i\phi_A(x)} \quad (3.34)$$

where  $F$  is the Klein factor. The impurity can be written in terms of fermion operators as  $d^\dagger = S^+ F$  and  $d = S^- F$ . Again we find an effective resonant level model:

$$\tilde{H} = H_{0,S} + H_{0,A} + \frac{J_\perp}{4\pi\sqrt{a}} \left[ (\hat{\psi}^\dagger(0) + \hat{\psi}(0))d + d^\dagger(\hat{\psi}^\dagger(0) + \hat{\psi}(0)) \right] \quad (3.35)$$

$$= H_{0,S} + H_{0,A} + \frac{J_\perp}{4\pi\sqrt{a}} (d^\dagger - d)(\hat{\psi}^\dagger(0) + \hat{\psi}(0)) \quad (3.36)$$

In this case both the conduction electrons and the impurity couple as Majoranas, so only half the degrees of freedom couples. This resonant level model is exactly solvable and well studied.[23]

Again using a perturbative approach for the interacting resonant level model one can calculate physical observables away from the Emery-Kivelson solution.[22]

In the next section we will discuss if there are other multi-channel Kondo models that can be solved exactly using bosonization.

### 3.5 Beyond

We would like to extend this nice construction for two channels using bosonization to find exact solutions for other  $n$ -channel Kondo models. It turns out to be rather difficult. Here we are going to show why the two-channel case is so special, and why we cannot extend this approach to general  $n$ . Again we start with the multi-channel Kondo model (1.4), in the bosonic language

$$H = \int_{-L/2}^{L/2} \sum_{\lambda=1}^n \frac{dx}{2\pi} \frac{v_F}{2} :(\partial_x \phi_\lambda(x))^2: + \sum_{\lambda=1}^n \left[ \frac{J_z}{2\sqrt{2}\pi} \partial_x \phi_\lambda(0) S_z + \frac{J_\perp}{4\pi a} \left( e^{i\sqrt{2}\phi_\lambda(0)} S^- + \text{h.c.} \right) \right] \quad (3.37)$$

We require some transformation analogous to the symmetric vs. anti-symmetric (SA) transformation for the two-channel Kondo model (3.29) such that the  $z$  interaction is proportional to one transformed operator. In the two-channel Kondo model we saw that the  $z$  term was proportional to  $\partial_x \phi_S(0) S_z$ , which we could then eliminate from the Hamiltonian using a canonical transformation (3.31) and the proper choice of  $J_z$  (3.33). For the multi-channel Kondo this would relate to

$$\partial_x \chi_1(0) S_z \quad (3.38)$$

for some choice of  $\chi_1$  in

$$\begin{pmatrix} \chi_1 \\ \chi_2 \\ \vdots \\ \chi_n \end{pmatrix} = O \begin{pmatrix} \phi_1 \\ \phi_2 \\ \vdots \\ \phi_n \end{pmatrix} \quad (3.39)$$

with  $O \in O(n)$  an orthogonal matrix (i.e. orthonormal rows and columns,  $O^\top = O^{-1}$ ). Note that the first row of  $O$  needs to be  $(\frac{1}{\sqrt{n}}, \frac{1}{\sqrt{n}}, \dots, \frac{1}{\sqrt{n}})$ , to ensure that (3.38) is satisfied.

We also need to be able to do the refermionization in the perpendicular term of the interaction, as we did for the two-channel Kondo model (3.34). After recognizing that

$$\begin{pmatrix} \phi_1 \\ \phi_2 \\ \vdots \\ \phi_n \end{pmatrix} = O^\top \begin{pmatrix} \chi_1 \\ \chi_2 \\ \vdots \\ \chi_n \end{pmatrix} \quad (3.40)$$

we see consequently  $\phi_i = \frac{1}{\sqrt{n}}\chi_1 \pm \frac{1}{\sqrt{2}}\chi_j$ , to make sure that we obtain the right scaling dimension through  $e^{\pm i\sqrt{2}\frac{1}{\sqrt{2}}\chi_j}$ . From this equation we see that  $\phi_i$  and  $\chi_j$  can not both be normalized correctly unless  $n = 2$ .

So the two-channel Kondo model is special in this approach.

However, there is one more case where bosonization can help out. For the four-channel Kondo model as similar approach yields an interactive solution, as was shown by Fabrizio and Gogolin in 1994.[24]

They derived that the low energy physics of four channels with spin 1/2 bath electrons is equivalent to one-channel spin 1. Meaning we need to solve a four-channel Kondo model.

Again we can do a spin-charge-decomposition (similar to (3.13)) and canonically transform the Hamiltonian to find:

$$H = H_0 + \frac{2J_\perp}{\pi a} \cos\left(\sqrt{\frac{3}{2}}\phi(0)\right) S_x \quad (3.41)$$

It turns out that this corresponds to [10, 24]

$$H_{\text{TLL},0} + 2J_\perp(\Psi_R^\dagger(0)\Psi_L(0) + \text{h.c.}) \quad (3.42)$$

where  $H_{\text{TLL},0}$  is the interacting bulk Hamiltonian of the Tomonaga-Luttinger liquid (TLL) and the second term a local scattering of the TLL-fermions.

This identification is based on the fact that the TLL fermions are proportional to  $e^{i\sqrt{2K}\phi}$ , where  $\sqrt{2K}$  is not necessarily 1. Furthermore, in this case the Tomonaga-Luttinger parameter  $K$  is equal to  $\frac{3}{4}$ , which means the interaction between the bath-electrons is repulsive. The impurity-TLL is well studied, hence we can find some low energy physical properties for four-channel Kondo model in this way.[10]

As with the Emery-Kivelson solution this approach is not extendible to other multi-channel Kondo models. For higher channel Kondo model there are simply no transformations that bring the Hamiltonian in a nice refermionizable form.

Bosonization offered exact solutions for both the one- and two-channel case and gave a interactive solution for the four-channel case in the form of a impurity Tomonaga-Luttinger liquid. However, it appears there is no other solvable  $n$ -channel Kondo models using bosonization.

In the next chapter we will discuss that a mapping from spin chains to Kondo models, presenting another approach to find physical properties of the Kondo model.

## Chapter 4

# Spin Chains to Kondo Models

As we have seen in previous sections, the  $n$ -channel Kondo model is only solvable in some special cases. Again it is quite remarkable that adding only a single impurity can cause such great challenges in finding solutions. Here we present another technique to solve the Kondo model for some special cases. We recognize the Kondo effect in a specific spin chain construction. This allows to translate results from these well studied spin models to derive the physics of certain Kondo models. In this chapter we will first take a look at the XX-chain and derive that it shows four-channel Kondo behavior in the right topology (Section 4.1) as discovered by Crampé and Trombettoni in 2013.[25] Then we will discuss the Ising chain in Section 4.2. Inspired by the four-channel mapping, Tsvetlik came up with a mapping from Ising chains to the two-channel Kondo model.[26] Subsequently, Giuliano et al. merged these two mappings, by connecting the XX and Ising model using a XY-model.[27] They concluded that the XY-chain can only produce two- and four-channel Kondo effects. In Section 4.3 we will see what this mapping entails. Finally, in Section 4.4 we will discuss whether we can find other  $n$ -channel Kondo behavior.

### 4.1 XX to Four-Channel Kondo

The XX-chain is the isotropic XY-model given by

$$H_{XX} = \frac{J}{2} \sum_{j=1}^{L-1} \sigma^x(j) \sigma^x(j+1) + \sigma^y(j) \sigma^y(j+1), \quad (4.1)$$

where  $J$  is the coupling constant,  $L$  the length of the chain, and  $\sigma^i$  the spin operators given by the Pauli matrices. If we define the spin raising and lowering operators as  $\sigma^\pm = \frac{1}{2}(\sigma^x \pm i\sigma^y)$ , the XX chain (4.1) can be rewritten as

$$H_{XX} = J \sum_{j=1}^{L-1} \sigma^+(j) \sigma^-(j+1) + \sigma^-(j) \sigma^+(j+1), \quad (4.2)$$

#### 4.1.1 Star Junction

For the mapping to the Kondo model we combine three XX-chains. This is done by coupling the first lattice site of the chain pairwise with XX coupling. Figure 4.1 schematically shows this star junction. The different chains are denoted by  $\alpha = 1, 2, 3$  and the corresponding spin operators are  $\sigma_\alpha(j)$ . For

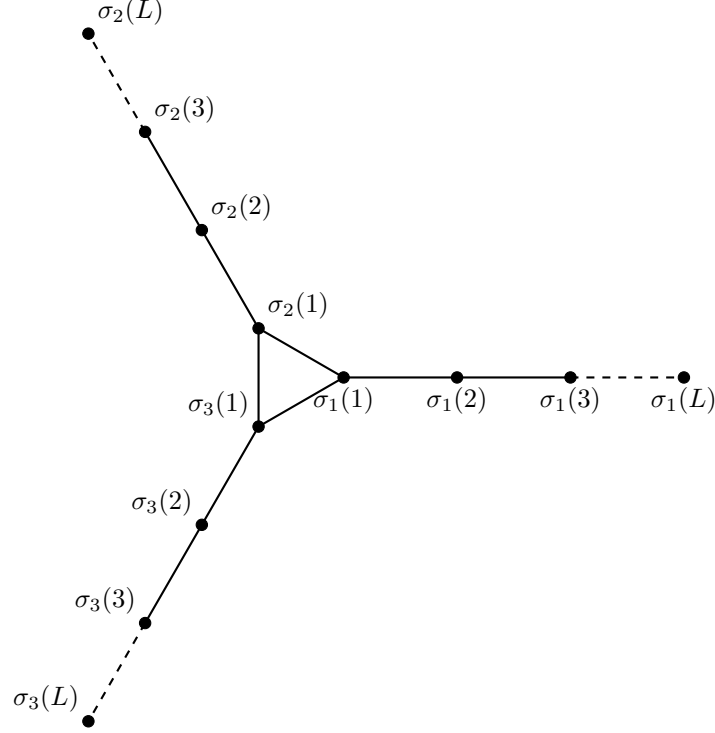


Figure 4.1: Star junction for three spin chains. The chain are pairwise coupled at the first lattice site

all three chain we have a copy of (4.2) and the coupling Hamiltonian is

$$H_{c,XX} = J_c \sum_{\alpha=1,2,3} \sigma_{\alpha}^{+}(1) \sigma_{\alpha+1}^{-}(1) + \sigma_{\alpha}^{-}(1) \sigma_{\alpha+1}^{+}(1) , \quad (4.3)$$

where we use  $\sigma_4 = \sigma_1$  so the chains are cyclic connected with  $J_c$  as coupling constant. The full Hamiltonian now becomes:

$$H_{XX} = J \sum_{j=1}^{L-1} \sum_{\alpha=1,2,3} \sigma_{\alpha}^{+}(j) \sigma_{\alpha}^{-}(j+1) + \sigma_{\alpha}^{-}(j) \sigma_{\alpha}^{+}(j+1) + J_c \sum_{\alpha=1,2,3} \sigma_{\alpha}^{+}(1) \sigma_{\alpha+1}^{-}(1) + \sigma_{\alpha}^{-}(1) \sigma_{\alpha+1}^{+}(1) \quad (4.4)$$

### 4.1.2 Jordan-Wigner Transformation

The Kondo model is a fermion model, so we have to rewrite the spin chain in fermions. Here we are going to use an extension of the normal Jordan-Wigner transformation (JW) to obtain effective fermion chains.

The JW was first proposed by Pascual Jordan and Eugene Wigner in 1928 to consistently transform spin operators on a one dimensional lattice into fermion operators. For a single chain the JW is given by

$$\tilde{c}(j) = \left( \prod_{k=1}^{j-1} \sigma^z(k) \right) \sigma^{-}(j) \quad (4.5)$$

This construction ensures that these new fermion operators satisfy canonical anti-commutation relations:

$$\{\tilde{c}^{\dagger}(j), \tilde{c}(k)\} = \delta_{jk}. \quad (4.6)$$

In this case we have a generalization to three coupled chains. If we naively use the above JW, the fermions in different chains would commute rather than anti-commute:

$$[\tilde{c}_\alpha^\dagger(j), \tilde{c}_\beta(k)] = 0 \quad \text{for } \alpha \neq \beta \quad (4.7)$$

Here we need to alter the JW with an additional factor, the Klein factor. This factor ensures anti-commutation relations.

For three chains we can even define the Klein factor explicitly.

For these Klein factors we need an auxiliary space  $\simeq \mathbb{C}^2$ . Essentially this adds additional degrees of freedom to the Hilbert space, which are not explored by the original Hamiltonian (4.4). We define additional Pauli matrices  $\sigma^x(0)$ ,  $\sigma^y(0)$  and  $\sigma^z(0)$  with site number 0 that act on this space. Now we can introduce the Klein factors

$$\eta^x = \sigma^x(0) \prod_{k=1}^L \sigma_2^z(k) \sigma_3^z(k), \quad \eta^y = \sigma^y(0) \prod_{k=1}^L \sigma_1^z(k) \sigma_3^z(k), \quad \eta^z = \sigma^z(0) \prod_{k=1}^L \sigma_1^z(k) \sigma_2^z(k) \quad (4.8)$$

These operators satisfy the anti commutation relations:

$$\{\eta^\alpha, \eta^\beta\} = 2\delta_{\alpha\beta}. \quad (4.9)$$

We can check that they are self-adjoint and they also satisfy the Clifford algebra:

$$\eta^{\alpha\dagger} = \eta, \quad \eta^x \eta^y = i\eta^z \quad (4.10)$$

So the  $\eta$ 's possess the same properties as the Pauli matrices, hence they represent spin 1/2.

If we define the naive JW for the three chains as:

$$\tilde{c}_\alpha(j) = \left( \prod_{k=1}^{j-1} \sigma_\alpha^z(k) \right) \sigma_\alpha^-(j), \quad \tilde{c}_\alpha^\dagger(j) = \left( \prod_{k=1}^{j-1} \sigma_\alpha^z(k) \right) \sigma_\alpha^+(j) \quad (4.11)$$

Then we can write the modified JW as

$$c_\alpha = \eta^\alpha \tilde{c}_\alpha(j) \text{ and } c_\alpha^\dagger = \eta^\alpha \tilde{c}_\alpha^\dagger(j), \quad (4.12)$$

with  $\alpha = 1, 2, 3$  and  $\eta^1 = \eta^x, \eta^2 = \eta^y, \eta^3 = \eta^z$ . Fully written out this becomes:

$$c_\alpha(j) = \eta^\alpha \left( \prod_{k=1}^{j-1} \sigma_\alpha^z(k) \right) \sigma_\alpha^-(j) \quad (4.13)$$

$$c_\alpha^\dagger(j) = \eta^\alpha \left( \prod_{k=1}^{j-1} \sigma_\alpha^z(k) \right) \sigma_\alpha^+(j) \quad (4.14)$$

We also see that

$$\sigma_\alpha^z(j) = 1 - 2c_\alpha^\dagger(j)c_\alpha(j) \quad (4.15)$$

as usual. The inverted expressions of (4.13) and (4.14) are

$$\begin{aligned} \sigma_\alpha^-(j) &= \eta^\alpha \left( \prod_{k=1}^{j-1} (1 - 2c_\alpha^\dagger(k)c_\alpha(k)) \right) c_\alpha(j) \\ \sigma_\alpha^+(j) &= \eta^\alpha \left( \prod_{k=1}^{j-1} (1 - 2c_\alpha^\dagger(k)c_\alpha(k)) \right) c_\alpha^\dagger(j) \end{aligned} \quad (4.16)$$

Note that  $\eta^x$  anti-commutes with  $\tilde{c}_2(j)$  and  $\tilde{c}_3(j)$  and commutes with  $\tilde{c}_1(j)$ ,  $\eta^y$  and  $\eta^z$  satisfy similar (anti-) commutation relations. Putting this all together gives the correct anti-commutation relation:

$$\{c_\alpha^\dagger(j)c_\beta(k)\} = \delta_{\alpha\beta}\delta_{jk} \quad (4.17)$$

We can use the JW to write the spin Hamiltonian in terms of spinless fermions.

### 4.1.3 Mapping

Now we return to the XX Hamiltonian (4.4) and plug in the JW (4.16). We obtain

$$\begin{aligned} H_{XX} = & -J \sum_{j=1}^{J-1} \sum_{\alpha} c_\alpha^\dagger(j)c_\alpha(j+1) + c_\alpha^\dagger(j+1)c_\alpha(j) \\ & + iJ_c \left[ \eta^z (c_1^\dagger(1)c_2(1) - c_2^\dagger(1)c_1(1)) + \eta^x (c_2^\dagger(1)c_3(1) - c_3^\dagger(1)c_2(1)) + \eta^y (c_3^\dagger(1)c_1(1) - c_1^\dagger(1)c_3(1)) \right] \end{aligned} \quad (4.18)$$

Still the  $\alpha$  indices denote the different chains, in a moment we will see that these indices can also be interpreted as a spin degree of freedom.

We can rewrite the interaction between the chains as

$$\sum_{\alpha,\beta} J_c \left[ \eta^z c_\alpha^\dagger S_{\alpha\beta}^z c_\beta + \eta^x c_\alpha^\dagger S_{\alpha\beta}^x c_\beta + \eta^y c_\alpha^\dagger S_{\alpha\beta}^y c_\beta \right] = \sum_{\alpha,\beta,i} J_c \eta^i c_\alpha^\dagger S_{\alpha\beta}^i c_\beta, \quad (4.19)$$

where we have introduced  $S^i$

$$S^x = \begin{pmatrix} 0 & 0 & 0 \\ 0 & 0 & -i \\ 0 & i & 0 \end{pmatrix}, \quad S^y = \begin{pmatrix} 0 & 0 & i \\ 0 & 0 & 0 \\ -i & 0 & 0 \end{pmatrix}, \quad S^z = \begin{pmatrix} 0 & -i & 0 \\ i & 0 & 0 \\ 0 & 0 & 0 \end{pmatrix}. \quad (4.20)$$

Note that these matrices are an  $\mathfrak{su}(2)$  representation in three dimensions, which corresponds to spin 1. The XX Hamiltonian in fermion language is

$$H_{XX} = -J \sum_{j=1}^{J-1} \sum_{\alpha} c_\alpha^\dagger(j)c_\alpha(j+1) + c_\alpha^\dagger(j+1)c_\alpha(j) + \sum_{\alpha,\beta,i} J_c \eta^i c_\alpha(1)^\dagger S_{\alpha\beta}^i c_\beta(1) \quad (4.21)$$

Fourier transforming the tight binding part ( $J$ ), taking the continuum limit and renaming the parameters gives a Kondo-like Hamiltonian:

$$H_{XX} = \sum_{k,\sigma} (\epsilon_k - \mu) c_{k\sigma}^\dagger c_{k\sigma} + \sum_{\alpha,\beta,i} J_i \eta^i \psi_\alpha(0)^\dagger S_{\alpha\beta}^i \psi_\beta(0) \quad (4.22)$$

where  $\eta^i$  is the impurity spin 1/2 degree of freedom. If we compare this to (1.1) we see one difference. In this case the conduction electrons are spin 1, since the  $\alpha$  index in  $c_\alpha(j)$  can take three values and they are coupled through a spin 1 matrix representation. Spin 1 conduction electrons are rather strange and not physical, however we can now use an elegant result from Fabrizio and Zaránd.[28] They showed that for multi-channel exchange models, such as Kondo, there is a mapping between models with different spin and channel number. The low energy behavior of a model with conduction electron spin  $s$  and channel number  $N_f$  is equivalent to a model with  $s^*$  and  $N_f^*$  if

$$N_f s(s+1)(2s+1) = N_f^* s^*(s^*+1)(2s^*+1). \quad (4.23)$$

The impurity spin in both models is identical. Using this fact the 1-channel spin 1 Kondo model from (4.21) has the same low energy behavior as a four-channel spin 1/2 Kondo model. Notice that

this is the same identification we made in Section 3.5 for the bosonized four-channel Kondo model. Hence the low energy behavior of the 3-star junction XX model and the four-channel Kondo model are equivalent.

Therefore we can translate the low energy physical properties from the the 3-star junction XX model to the four-channel Kondo model.

## 4.2 Ising Chain to Two-Channel Kondo

It turns out that the four-channel Kondo model is not unique for showing up in spin chain systems. Here we will show that the two-channel Kondo effect is found in the Ising chain, as was shown by Tsvelik (2013). [26]

Again we consider a 3-star junction as shown in Figure 4.1, in this case transverse field Ising chains:

$$H_{\text{Ising}} = \sum_{j=1}^{L-1} \sum_{\alpha=1}^3 [-J\sigma_{\alpha}^x(j)\sigma_{\alpha}^x(j+1) + h\sigma_{\alpha}^z(j)] \quad (4.24)$$

$$+ J_{12}\sigma_1^x(1)\sigma_2^x(1) + J_{23}\sigma_2^x(1)\sigma_3^x(1) + J_{31}\sigma_3^x(1)\sigma_1^x(1) \quad (4.25)$$

The first line is the bulk Hamiltonian with a nearest neighbor coupling  $J$  and spin flip term with coupling  $h$ . In the second line we see the coupling of the first sites of the chain with Ising interaction. Again we can rewrite the Hamiltonian using Jordan-Wigner transformations.

From (4.16) and  $\sigma^{\pm} = \frac{1}{2}(\sigma^x \pm i\sigma^y)$  we obtain

$$\sigma_{\alpha}^x(j) = \eta^{\alpha} \left( \prod_{k=1}^{j-1} (1 - 2c_{\alpha}^{\dagger}(k)c_{\alpha}(k)) \right) (c_{\alpha}(j) + c_{\alpha}^{\dagger}(j)) \quad (4.26)$$

Plugging this in into (4.25) gives

$$H_{\text{Ising}} = \sum_{j=1}^{L-1} \sum_{\alpha=1}^3 [-J[c_{\alpha}^{\dagger}(j) - c_{\alpha}(j)][c_{\alpha}^{\dagger}(j+1) + c_{\alpha}(j+1)] + hc_{\alpha}^{\dagger}(j)c_{\alpha}(j)] \quad (4.27)$$

$$+ i\epsilon_{\alpha\beta\gamma}\eta^{\alpha}J_{\beta\gamma}[c_{\beta}^{\dagger}(1) + c_{\beta}(1)][c_{\gamma}^{\dagger}(1) + c_{\gamma}(1)] \quad (4.28)$$

where we recognized that the  $\eta$ 's satisfy the Clifford algebra (4.10)  $\eta^{\beta}\eta^{\gamma} = i\epsilon_{\alpha\beta\gamma}\eta^{\alpha}$  ( $\epsilon_{\alpha\beta\gamma}$  is the Levi-Civita tensor).

It is now helpful to rewrite the fermions in terms of Majoranas:

$$\chi_{R,\alpha}(x = ja) = \frac{1}{\sqrt{2a}}(\omega^*c_{\alpha}(j) + \omega c_{\alpha}^{\dagger}(j)), \quad \chi_{L,\alpha}(x = ja) = \frac{1}{\sqrt{2a}}(\omega c_{\alpha}(j) + \omega^*c_{\alpha}^{\dagger}(j)) \quad (4.29)$$

where  $\omega = e^{i\pi/4}$  satisfying and  $a$  the lattice spacing. If we then take the continuum limit we the bath becomes

$$\sum_{\alpha=1}^3 \int_0^{\infty} dx \, i\hat{J} [\chi_{R,\alpha}(x)\partial_x\chi_{R,\alpha}(x) - \chi_{L,\alpha}(x)\partial_x\chi_{L,\alpha}(x)] - (J - h)\chi_{L,\alpha}(x)\chi_{R,\alpha}(x) \quad (4.30)$$

where we used  $\chi(x = (j+1)a) = \chi(x = ja) + a\partial_x\chi(x = ja)$  and  $\hat{J} = Ja$ . If we impose that  $h = J$  (critical Ising coupling) only the kinetic term remains.

The interaction term becomes

$$i\epsilon_{\alpha\beta\gamma}\eta^{\alpha}\hat{J}_{\beta\gamma}[\chi_{R,\beta} + \chi_{L,\beta}][\chi_{R,\gamma} + \chi_{L,\gamma}] \quad (4.31)$$

Since the  $\chi_{R/L}$  only lives in the positive half of the real line we can define a chiral fermion over the full real line

$$\chi_\alpha(x) = \theta(x)\chi_{R,\alpha}(x) + \theta(-x)\chi_{L,\alpha}(x), \quad (4.32)$$

where  $\theta(x)$  is the heavy side function regularized at  $\theta(0) = \frac{1}{2}$ . So the effective Hamiltonian of the Ising chain in terms of Majorana fermions is

$$H_{\text{eff}} = \int_{-\infty}^{\infty} dx \, i\hat{J}\chi_\alpha(x)\partial_x\chi_\alpha(x) + i\epsilon_{\alpha\beta\gamma}\eta^\alpha \frac{\hat{J}_{\beta\gamma}}{2}\chi_\beta(0)\chi_\gamma(0) \quad (4.33)$$

This might seem a lot of work to get another complicated expression. Actually this Hamiltonian has the same low energy behavior as the two-channel Kondo model. This has been proven by Coleman and Ioffe.[29] We will not go into detail, because it is very tedious to derive. It relies on the fact that a spinful fermion can be represented by three Majorana fermions. In this case three Majoranas from different chains. This paper shows that the two-channel Kondo model has the same low energy behavior as

$$H_{2\text{ck}} = \int_{-\infty}^{\infty} dx \, itv\vec{\psi}(x) \cdot \partial_x\psi(x) + iJ_c b\vec{S}\vec{\psi}(0) \times \vec{\psi}(0) \quad (4.34)$$

where  $\vec{\psi}$  is a three-vector with Majorana entries. If we define  $\vec{\chi} = (\chi_1, \chi_2, \chi_3)^\top$ , we recognize that  $\epsilon_{\alpha\beta\gamma}\chi_\beta(0)\chi_\gamma(0) = \vec{\chi}(0) \times \vec{\chi}(0)$ . So the effective 3-star junction Ising chain corresponds to the two-channel Kondo model with  $tv = J$  and  $J_c = \frac{J_{\beta\gamma}}{2}$ .

### 4.3 In Between XX and Ising

We have seen that both the XX and Ising chain correspond to a multi-channel Kondo model. We can now investigate the models in between these two fine tuned cases, following the work from Guiliano et al. (2016).[27] Therefore we look at XY chain with a transverse field on 3-star junction:

$$\begin{aligned} H_{\text{XY}} = & \sum_{j=1}^{L-1} \sum_{\alpha=1}^3 \left[ \frac{J}{2} \left( \sigma_\alpha^x(j)\sigma_\alpha^x(j+1) + \gamma_1\sigma_\alpha^y(j)\sigma_\alpha^y(j+1) \right) + \frac{h}{2}\sigma_\alpha^z(j) \right] \\ & + \sum_{\alpha=1}^3 \frac{J_{\alpha,\alpha+1}}{2} (\sigma_\alpha^x(1)\sigma_{\alpha+1}^x(1) + \gamma_2\sigma_\alpha^y(1)\sigma_{\alpha+1}^y(1)) \end{aligned} \quad (4.35)$$

This model is in between the XX and the Ising chain. If  $\gamma_1 = \gamma_2 = 1$  and  $h = 0$  we rediscover the XX chain and if  $\gamma_1 = 0$  and  $\gamma_2 = 0$  it becomes the Ising chain. Again we can do a Jordan-Wigner transformation:

$$\begin{aligned} H_{\text{XY}} = & - \sum_{j=1}^{L-1} \sum_{\alpha=1}^3 \frac{J}{2} (1 + \gamma_1)(c_\alpha^\dagger(j)c_\alpha(j+1) + c_\alpha^\dagger(j+1)c_\alpha(j)) \\ & + \sum_{j=1}^{L-1} \sum_{\alpha=1}^3 \frac{J}{2} (1 - \gamma_1)(c_\alpha^\dagger(j+1)c_\alpha^\dagger(j) + c_\alpha(j)c_\alpha(j+1)) + \sum_{j=1}^L \sum_{\alpha=1}^3 hc_\alpha^\dagger(j)c_\alpha(j) \\ & + \sum_{\alpha=1}^3 i \frac{J_{\alpha,\alpha+1}}{2} \eta^{\alpha+2} \left( (1 + \gamma_2)c_\alpha^\dagger(1)c_{\alpha+1}(1) + (1 - \gamma_2)c_\alpha^\dagger(1)c_{\alpha+1}^\dagger(1) - \text{h.c.} \right) \end{aligned} \quad (4.36)$$

We only have to consider  $\gamma_1, \gamma_2 \in [0, 1]$ , for values outside this interval we can do a rescaling of  $J, J_{\alpha,\alpha+1}$  or do a particle hole inversion to get  $\gamma_1, \gamma_2$  in the interval.

If we go to momentum space we find that the bulk spectrum is given by

$$E_{\text{XY}}^\pm = \pm \sqrt{(h + J(1 + \gamma_1)\cos(k))^2 + (J(1 - \gamma_1)\sin(k))^2} \quad \text{with } k \in ]-\pi, \pi] \quad (4.37)$$



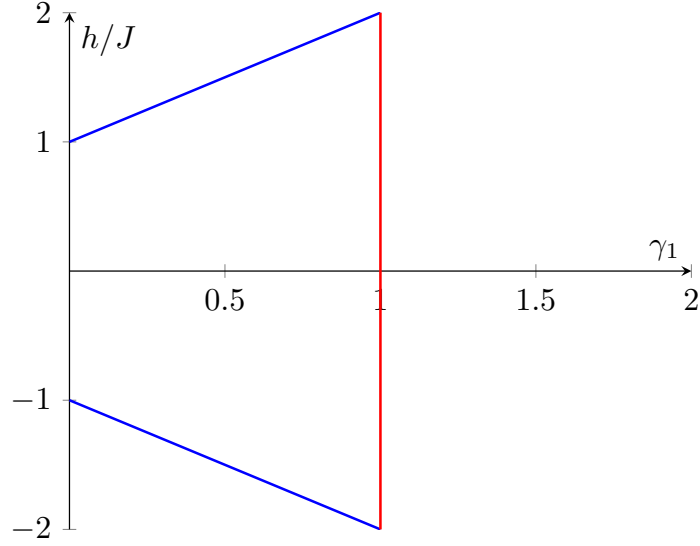


Figure 4.2: Phase diagram for the XY model. The lines denote the parameter conditions for a gapless XY theory. At  $\gamma_1 = 0$  and  $h/J = \pm 1$  sits the Ising chain and these points correspond to the two-channel Kondo model (Section 4.1). At  $\gamma_1 = 1$ ,  $H/J = 0$  we find the XX chain, hence the four-channel Kondo model (Section 4.2).

The Kondo model is gapless in the bulk, hence for a “spin chain-Kondo”- connection the bulk of this JW fermion chain needs to be gapless as well. For the two bulk parameters  $\gamma_1$  and  $h$  we can derive a phase diagram show in Figure 4.2, displaying the gapless regions.

If  $\gamma_1 = 1$  the bulk is a tight binding chain, which is gapless for all  $h$ . This corresponds the red line in Figure 4.2 and is a XX-model with transverse field ( $h$ ). If  $\gamma_1 < 1$  we recognize the Kitaev chain[30] with chemical potential  $\mu = -h$ , fermion hopping  $t = J(1 + \gamma_1)$  and superconductivity  $\Delta = J(1 - \gamma_1)$ . The spectrum is gapless if there exists a  $k$  for which both squares are zero. Since  $\gamma_1 < 1$  we need  $\sin(k) = 0$  so  $k = 0, \pi$ . This gives  $h = \pm J(1 + \gamma_1)$  as a gapless lines for the XY model, these are known as the Kitaev lines and are denoted by the blue lines in the phase diagram.

The four-channel Kondo model from Section 4.1 is the critical XX-model at  $h = 0$ . The two-channel Kondo models from Section 4.2 are at the Kitaev lines at  $\gamma_1 = 0$ , as we saw before these are critical Ising models.

The remaining question is, what happens on the lines between the special point. It was shown by Guiliano et al.[27] that these lines correspond either to the two- or four-channel Kondo model.

Using Poor Man’s Renormalization Group [12] they showed that there are two separate cases. In both cases the Kitaev lines correspond to the two-channel Kondo model. The argument goes as follows, if  $\gamma_1 \neq 1$  there is no spin rotational symmetry around the  $z$ -axis in the bulk and hence the four-channel Kondo model is less relevant here and only the two-channel remains.

Along the XX line the two cases are separated. If we tune  $\gamma_2$  to 1 the rotational symmetry in the boundary term is maintained and the line corresponds to four-channel Kondo model. Again if  $\gamma_2 \neq 1$  the symmetry is broken and the line corresponds to two-channel Kondo.

## 4.4 Beyond

As we have seen in the previous section there is no easy way to find a mapping to from a 3-star junction spin chain to an non-(4,2)-channel Kondo model since the transverse field XY model can only correspond two- or four-channel.

One approach would be to increase number of chains and follow the derivation for the four-channel Kondo model. For instance we take four chains, which would then correspond to the four possible spins for a spin  $3/2$  bath electron  $(-3/2, -1/2, 1/2, 3/2)$ . To get the Kondo interaction one has to find Klein factors  $(F_1, F_2, F_3, F_4)$  for the chains, such that the product of any two is a linear combination of three operators  $(\eta_1, \eta_2, \eta_3)$  satisfying the Clifford algebra. They should also be of such a form that we would find a representation of spin  $3/2$   $(S^x, S^y, S^z)$  as we did in (4.20) for spin 1. The combination of these properties makes it very difficult if not impossible to find these Klein factors. Possibly, using Lie algebra theory it can be proven that such a construction does not exist.

There is however another field of spinlike chains to be explored, namely the parafermions.[31] These spinlike particles are an extension of spin  $1/2$  particles. The latter can only take spin values at  $\pm 1$  in the complex plane (in fact  $\pm 1/2$ ), while  $Z_m$ -invariant parafermions can have spin  $e^{i\frac{2\pi k}{m}}$  for  $k = 0, 1, \dots, m$ . These systems have not been studied a lot yet, but seem to give rise to interesting physical behavior, such as topological insulators with zero energy Marjorana modes.[32, 33]

## Chapter 5

# Conclusion and Discussion - Kondo Model

In this part of the thesis we have given a view on two approaches for finding solutions for the Kondo model. The main focus of this part of the thesis was understanding the limitations of these solutions and trying to extend these approaches beyond these limitations.

In Chapter 1 we have introduced the one- and multi-channel Kondo model, a local magnetic impurity model. We have shown that the one-channel Kondo model can be derived from the microscopic Anderson impurity model, offering a physical framework for the model. We have also derived that we can reduce the three-dimensional Kondo model to an effective one-dimensional theory because of rotational symmetry around the local impurity.

Then in Chapter 2 we started with the naive perturbative analysis of the Kondo interactions. For the one-channel Kondo model, we calculated the one-loop corrections for the coupling constant. We obtained diverging contributions and the interactions flow to strong coupling. Therefore this perturbative approach is not valid for the one channel Kondo model. For the  $n$ -channel Kondo model in the large  $n$  limit we found a stable finite fixed coupling point in the isotropic limit at  $J = \frac{2}{n}$ . Hence the multi-channel and one-channel Kondo model exhibit different physical behavior. However, this perturbative analysis is still not valid for low  $n$ -channel Kondo model, since the fixed point is of the order of the Kondo temperature  $T_K$ , the point where the perturbative approach breaks down. We therefore discussed two different approaches for finding solution in the remainder of this part.

In Chapter 3 we used bosonization to solve the one- and two-channel models. By rewriting the Dirac fermion theory in terms of bosons we observed that only the spin degrees of freedom couple to the impurity and the charge field decouples. By doing a canonical transformation we were able to rewrite the Kondo Hamiltonian in the form of an interacting resonant level model. Finally, we imposed  $J_z = 4\pi^2\sqrt{2}v_F(\sqrt{2} - 1)$ , the Toulouse limit, to get rid of the interaction and we saw that the one-channel Kondo model is equivalent to the exactly solvable resonant level model. In the two-channel case we separated the two boson fields for the two channels in a symmetric and an anti-symmetric part. The symmetric operators decouple from the impurity after doing a canonical transformation and imposing  $J_z = 4\pi^2v_F$ . This is known as the Emery-Kivelson solution.[23] Again we recover a resonant level model. In this case coupling Majorana impurity fermions with Majorana conduction electrons. It was shown in the literature that perturbation theory is suitable for finding physical properties away from these fine tuned points.[22]

Then we discussed the difficulty in finding extensions to other multi-channel Kondo models. It

turned out that it is not possible to find other solutions along the lines of the Emery-Kivelson solution. Nevertheless, we reviewed that the four-channel Kondo model can be solved through a mapping to an interacting conduction electron theory known as the Tomonaga-Luttinger liquid.[24] Finally in Chapter 4 we discussed several spin chain constructions that show rich behavior in the form of the Kondo effect. Using an extension of regular Jordan-Wigner transformations we reviewed the mapping proposed by Crampé and Trombettoni.[25] They showed the equivalence between the four-channel Kondo model and the XX 3-star junction. We also discussed the two-channel Kondo effect in the Ising 3-star junction first derived by Tsvetik.[26] Ultimately, we followed a recent paper from Gogolin et al. which describes the Kondo model in transverse field XY 3-star junction. In the limiting cases this model is either the XX-chain or the Ising chain, containing respectively a four-channel or a two-channel Kondo effect. Gogolin et al. showed that all gapless XY-chain are either equivalent to the two- or four-channel Kondo model.

Therefore, we concluded that in this 3-star spin chain junction there are no possibilities for finding other multi-channel Kondo behavior. Deriving other spin chain-Kondo mappings asks for other spin chain constructions. However, for instance the 4-channel junction already comes with major challenges when it comes to constructing suitable Klein factors for the Jordan-Wigner transformation.

We also suggested that parafermion chains might be hiding Kondo like behavior, although there is no clear evidence pointing in this direction. These spinlike object do however seem to possess rich physics.

All in all we have seen that many bright physicist have put a lot of effort into finding solutions to the multi-channel Kondo model. This has led to a great deal of papers discussing a variety of techniques and mappings, of which we have only discussed two in this thesis. However, the other techniques such as Bethe ansatz and numerical renormalization group neither offer solutions to other multi-channel Kondo models.

Concluding, the one-, two- and four-channel Kondo models are solvable and well understood. However, extending the approaches discussed in this thesis to other multi-channel Kondo models seems very challenging.

## Part II

# Quantum Quenching the Kitaev Chain



## Chapter 6

# Introduction to Kitaev Chain and Quantum Quench

The second part of this thesis discusses quantum quenches for the Kitaev chain. The Kitaev chain is a topological insulator, showing topological effect in the form of a Majorana edge mode. In this thesis we discuss the effect of a quantum quench on these Majorana edge modes. A quantum quench is a shift in system parameters. In Figure 6.1 we see schematic display of a quench. At time  $\tau < 0$  the system is in set-up 1 and at time  $\tau = 0$  the system parameters are changed to set-up 2. Experimentally, we can for instance view a quench in chemical potential as a change in gate voltage. The gate regulates the chemical potential in the chain. In this thesis we prepare the system in the Majorana edge modes for time  $\tau < 0$  and discuss how this state evolves after the quench.

The dynamical properties of the quantum quench of the Kitaev chain have already been studied using a dynamical topological order parameter[34], information recovery[35] and entanglement spectra[36]. In this thesis we will use a different approach by explicitly studying the wave function before and after the quench. Furthermore, we will mostly discuss the long time averaged properties of the system, i.e. we let the system relax after the quench.

In the remainder of this chapter we will introduce the Kitaev chain. Then in Chapter 7 we will discuss the technical details of the quench for the Kitaev chain. Finally, in Chapter 8 we present the results of quantum quenching the Kitaev chain.

### 6.1 Kitaev Chain

The Kitaev chain is a hot topic and widely studied over the last 15 years. The model was proposed by Kitaev in 2001 [30] and has been taken up enthusiastically by the physics and computer science community, because it is a likely candidate for a stable quantum bit (qbit). The experimental realization of a qbit would greatly advance computer power and would reshape the digital world as we know it. A quantum bit is a conventional computer bit on steroids. Nowadays computers use conventional bits to store information. These discrete bits are binary and can be either 0 or 1. A

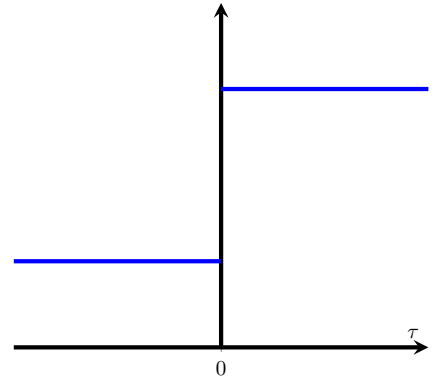


Figure 6.1: Example of a quantum quench. For  $\tau < 0$  the parameters of the system are set 1 and the parameters change to set 2 at  $\tau = 0$ .

quantum computer on the other hand stores informations using qbits. Theoretically these continuous qbits can take any value in  $\mathbb{C}$ , yielding endlessly more capacity to store information. Experimentally, this is easier said than done.

A qbit system is a system with a two-fold degenerate ground state, i.e.  $|\psi_0\rangle$  and  $|\psi_1\rangle$  at the same energy. From these two states the ground state can be any linear combination of the two

$$|\alpha\rangle = \frac{1}{\sqrt{1+|\alpha|^2}} [|\psi_0\rangle + \alpha |\psi_1\rangle] , \quad (6.1)$$

where  $\alpha \in \mathbb{C}$  is the degree of freedom storing the information. In a clean system a degenerate ground state is easy to realize, but physical systems are never perfectly clean. In general the qbits are very sensitive to decoherence, and as a result the two states hybridize and split in energy.

We can for example, following Kondo (2001) [30], consider the simplest possible qbit, a non interacting spin with no Zeeman term. The two states  $|\uparrow\rangle$  and  $|\downarrow\rangle$  are at the same energy. The first form of decoherence comes in the form of a quantum error, a spin flip  $\delta\sigma^x$ . This error causes the two states to interact and hybridize ( $E \rightarrow \pm\delta$ ), hence the information is lost.

The second error, is a phase error. Suppose we have a chain of multiple qbits. At every site there is a slight error  $\delta_i\sigma_z$ , this changes the sign in front of  $|\downarrow\rangle$  with respect to  $|\uparrow\rangle$  at every site in a different way. Consistently retrieving information from the qbits becomes impossible.

Kitaev proposed a scheme to get rid of these two errors.[30]

He argued that using spinless fermion qbits instead of spinlike qbits removes the quantum error. For this spinless qbit an empty site is  $|\psi_0\rangle = |0\rangle$  and an occupied site is  $|\psi_1\rangle = a^\dagger |0\rangle$ , where  $a^\dagger$  is the fermion creation operator. For spinless fermions this error would correspond the creation or annihilation of a fermion, which is not charge conserving. In other word a quantum error would correspond to the operator  $\delta(a^\dagger + a)$ , which does not exist in any feasible theory. However, there can be two-site errors, when a fermion hops from one qbit site to another. This can be avoided by keeping the qbit sites far enough apart.

For the second problem we have do a mathematical trick. At every site the fermion creation and annihilation operators are given by  $a_j^\dagger$  and  $a_j$ , we can define two Majoranas

$$\xi_{2j-1} = i(a_j^\dagger - a_j), \quad \xi_{2j} = (a_j^\dagger + a_j) . \quad (6.2)$$

In the Majorana language a phase error is now given by  $a_j^\dagger a_j = \frac{1}{2}(1 + i\xi_{2j-1}\xi_{2j})$ . If we move the two Majorana sites  $2j-1$  and  $2j$  far away from each other, this error will not occur either. So there is no Majorana interaction.

However, Majoranas are difficult to realize both experimentally and physically. In his paper Kondo suggested a theoretical superconducting model that can produce these two fold degenerate Majoranas.[30]

## 6.2 Kitaev Hamiltonian

The Kitaev chain is a spinless fermion chain, containing hopping and p-wave superconductivity. Note that truly spinless fermions cannot exist, but we can realize this system by imposing strong Zeeman interaction for spinful fermions. This projects out one of the spins (e.g.  $|\downarrow\rangle$ ), remaining with an effective spinless theory (only  $|\uparrow\rangle$ ). Experimentally realizing a one dimensional p-wave superconductor is very difficult.[37, 38]

The Hamiltonian of the Kitaev chain is

$$H = -\mu \sum_{i=1}^L \left( c_i^\dagger c_i - \frac{1}{2} \right) - \frac{1}{2} \sum_{i=1}^{L-1} \left( t c_i^\dagger c_{i+1} + \Delta c_i c_{i+1} + \text{h.c.} \right), \quad (6.3)$$



where  $\mu$  is the chemical potential,  $t$  the hopping potential and  $\Delta$  the superconductivity parameter. In this thesis we will assume  $\Delta$  to be real. One can also choose  $\Delta$  complex, but the phase can be removed in a canonical transformation of the operators. The second quantized operators  $c_i^\dagger$  and  $c_i$  respectively create and annihilate a fermion at lattice site  $i$ . The chain is  $L$  sites long with open boundary conditions and note that the summation in the second term only runs up to  $L - 1$ , since it contains  $c_{i+1}$  in summand. As we have seen in Part I, Chapter 4, the Jordan-Wigner transformed XY-chain is equivalent to the Kitaev chain.

Because of the superconducting terms the Hamiltonian is not particle number conserving. These terms ( $c_{i+1}^\dagger c_i^\dagger$ ,  $c_i c_{i+1}$ ) create or annihilate two fermions. Nevertheless, particle number modulo 2 is conserved. This means there are two particle sectors for a Kitaev state, either 0 or 1 (mod 2). This is called parity.

Because of the superconductivity terms we have to introduce Nambu vectors

$$\vec{C} = (c_1, \dots, c_n, c_1^\dagger, \dots, c_n^\dagger)^\top. \quad (6.4)$$

in order to write the Hamiltonian (6.3) in matrix form:

$$H = \vec{C}^\dagger \mathcal{H} \vec{C} \quad (6.5)$$

where

$$\mathcal{H} = \begin{pmatrix} D & T \\ -T & -D \end{pmatrix}, \quad D = \begin{pmatrix} -\frac{\mu}{2} & -\frac{t}{4} & 0 & \dots \\ -\frac{t}{4} & -\frac{\mu}{2} & -\frac{t}{4} & \\ 0 & -\frac{t}{4} & -\frac{\mu}{2} & \ddots \\ \vdots & & \ddots & \ddots \end{pmatrix}, \quad T = \begin{pmatrix} 0 & -\frac{\Delta}{4} & 0 & \dots \\ \frac{\Delta}{4} & 0 & -\frac{\Delta}{4} & \\ 0 & \frac{\Delta}{4} & 0 & \ddots \\ \vdots & & \ddots & \ddots \end{pmatrix} \quad (6.6)$$

One of the consequences of going to the Nambu-vector language is doubling of the spectrum. In Figure 6.2a we see the spectrum for 30 sites with  $\mu = 2$  and  $\Delta = t$ . Due to the particle-hole doubling every particle eigenvalue (blue) has a hole eigenvalue (red) partner, with  $E_{\text{hole}} = -E_{\text{particle}}$ . Hence the spectrum of the doubled Hamiltonian is particle-hole symmetric. Note that the Hamiltonian itself is particle-hole anti-symmetric ( $H \rightarrow -H$ ). Because of this redundancy in degrees of freedom we can ignore the states with  $E < 0$ , the nonnegative energy states describe the full system.

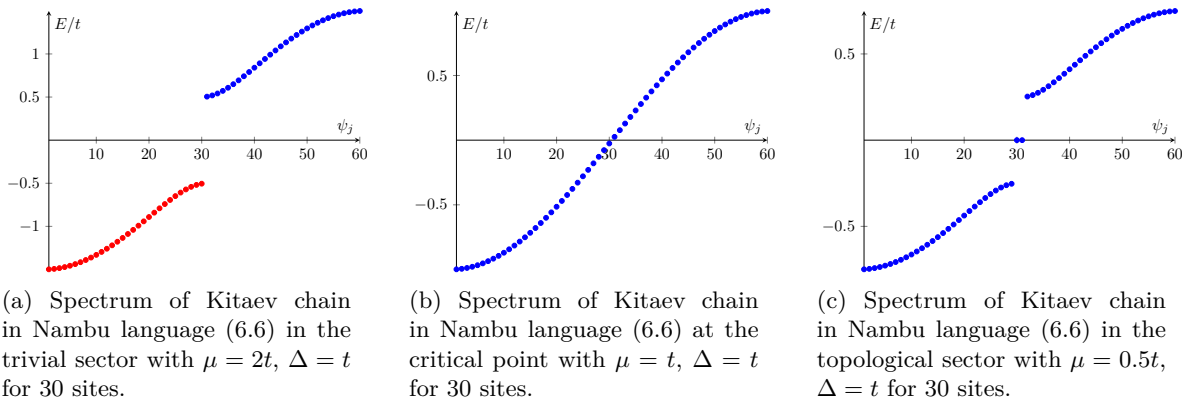


Figure 6.2

Furthermore, we see that each of these eigenvalues  $E_i$  (Figure 6.2a) corresponds to an eigenstate  $\psi_i$  of the Hamiltonian matrix (6.6). In fermion language the eigenstates of the Hamiltonian (6.3) are

$$\Psi_k = \vec{C}^\dagger \psi_k. \quad (6.7)$$

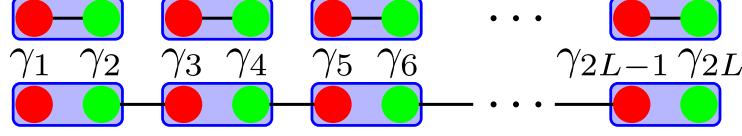


Figure 6.3: [Upper chain] Split of fermions in Majoranas in the Kitaev chain. [Lower chain] Coupling (black lines) of Majoranas in new fermions. The first ( $\gamma_1$ ) and the last Majorana ( $\gamma_{2L}$ ) remain uncoupled.

These eigenstates are a superposition of creation and annihilation operators  $\Psi_k = \psi_{1k}c_1^\dagger + \dots + \psi_{Lk}c_L^\dagger + \psi_{L+1k}c_1 + \dots + \psi_{2Lk}c_L$  and therefore is neither a (delocalized) particle nor a hole. In the next section we will see that in some cases it represents a Majorana (particle + hole). Using the Bogoliubov-de-Gennes (BdG) we can diagonalize the Hamiltonian

$$H = \vec{C}^\dagger \mathcal{H} \vec{C} = \vec{C}^\dagger \psi \hat{E} \psi^\dagger \vec{C}, \quad (6.8)$$

where  $\psi = (\psi_1, \dots, \psi_n)$  is the matrix of the eigenvectors and  $\hat{E}$  the diagonal matrix with entries  $E_1 \leq E_2 \dots \leq E_n$ . The eigenstates form an orthonormal basis of the Hilbert space.

### 6.2.1 Majorana Edge Modes

In one special nontrivial case, we can easily obtain the ground state of the Kitaev chain by hand. Consider  $\mu = 0$  and  $t = \Delta$ :

$$H = -\frac{t}{2} \sum_{i=1}^{L-1} \left( c_i^\dagger c_{i+1} + c_i c_{i+1} + c_{i+1}^\dagger c_i + c_{i+1}^\dagger c_i^\dagger \right) \quad (6.9)$$

This Hamiltonian is very suitable for introducing the notion of Majorana fermions. We define

$$\gamma_{2i-1} = i(c_i^\dagger - c_i), \quad \gamma_{2i} = c_i^\dagger + c_i, \quad (6.10)$$

and the other way around

$$c_i = \frac{1}{2}(\gamma_{2i} + i\gamma_{2i-1}), \quad c_i^\dagger = \frac{1}{2}(\gamma_{2i} - i\gamma_{2i-1}). \quad (6.11)$$

Notice the distinction with the Majoranas defined in (6.2), here we are dealing with interacting Majoranas on a single chain. The Majorana operators split the complex fermion  $c_i$  in two real fermions  $\gamma_{2i-1}$  and  $\gamma_{2i}$ . The upper chain of Figure 6.3 depicts the fermions (blue boxes) being split into two Majoranas. These Majorana satisfy

$$\gamma_i^\dagger = \gamma_i, \quad \{\gamma_i, \gamma_j\} = 2\delta_{ij}, \quad \gamma_i^2 = 1 \quad (6.12)$$

And we can rewrite the Hamiltonian (6.9):

$$H = \frac{it}{2} \sum_{i=1}^{L-1} \gamma_{2i} \gamma_{2i+1}. \quad (6.13)$$

This Hamiltonian suggests that we have to pair the Majoranas from neighboring sites ( $\gamma_{2i}$  and  $\gamma_{2i+1}$ ), so we define new fermion operators  $\tilde{c}_i^\dagger = \frac{1}{2}(\gamma_{2i} - i\gamma_{2i+1})$ . These new fermions correspond to the lower

chain in Figure 6.3, the black lines depict the new coupling. In terms of these new fermions the Hamiltonian becomes

$$H = t \sum_{i=1}^{L-1} (\tilde{c}_i^\dagger \tilde{c}_i - 1) \quad (6.14)$$

For  $t \neq 0$  the system is gapped because adding a fermion  $\tilde{c}_i^\dagger$  costs energy  $t$ . Furthermore, there are two Majoranas ( $\gamma_1$  and  $\gamma_{2L}$ ) that completely drop out of the Hamiltonian. Hence they do not contribute to the energy. If we combine these remaining degrees of freedom into a new fermion  $f^\dagger = \frac{1}{2}(\gamma_{2L} - i\gamma_1)$ , we see that this state is at zero energy ( $Hf^\dagger = 0$ ). It is a delocalized fermion built up out of two Majoranas. These Majoranas live at of a gapped bulk, therefore we call this a Majorana Edge Mode (MEM). Concluding, the MEM does not contribute to the energy, so the ground state is two fold degenerate. The MEM is either occupied or empty:

$$|\text{GS}_1\rangle = |0\rangle, \quad |\text{GS}_2\rangle = f^\dagger |0\rangle = \frac{1}{2}(\gamma_{2L} - i\gamma_1) |0\rangle, \quad (6.15)$$

where  $|0\rangle$  is the filled Fermi sea, so all states with  $E < 0$  filled. The second state ( $|\text{GS}_2\rangle$ ) is the MEM. These two states live in a different particle sector, because for the MEM there is an additional delocalized fermion present. The first ground state has zero parity, while the second (MEM) ground state has parity one. As we mentioned before, this parity distinction protects a ground state against hybridization (i.e. there is no physically reasonable Hamiltonian that maps  $|\text{GS}_1\rangle$  to  $|\text{GS}_2\rangle$  or vice versa). Furthermore, note that we have constructed a delocalized fermion, satisfying the second requirement. As put forth by Kitaev, to avoid phase errors the Majorana fermions need to be far apart and not interacting.

This is not the only parameter set for which there is a gapped bulk system with zero energy edge modes, but it is only case we can do by hand. In Figure 6.2c we see the spectrum for a 30-site Kitaev chain with  $\mu = 0.5t$  and  $\Delta = t$ . The system is an insulator since the bulk is gapped. The two zero modes in the middle denote the particle-hole pair MEM. Recall that this spectrum is for the Nambu language, so we can ignore  $E < 0$  (filled Fermi sea for vacuum) and take only one state at  $E = 0$ .

In Figure 6.2b we see the system at the critical point ( $\mu = \Delta = t$ ). This point is critical, because the system becomes gapless at this point. We also see that for  $\mu = 2$  in Figure 6.2a there is no zero modes.

It turns out that there is a MEM for  $|\mu| < |t|$ . We can therefore call the Kitaev chain a topological insulator. In the bulk it behaves like an insulator, but at the edge there is non-trivial behavior that is robust against smooth changes in parameters. In fact the non-trivial or topological edge effect disappear only after the system has passed a gapless point ( $\mu = \pm t$ ). Therefore we call the region with MEM the topological sector and without MEM the trivial sector. In Figure 6.4 we see the phase diagram for the Kitaev chain.

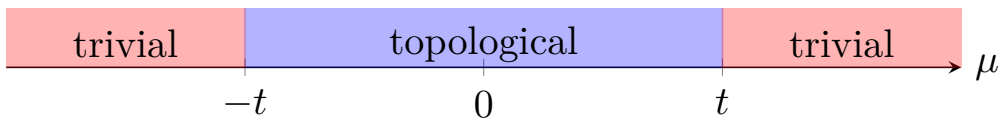


Figure 6.4: Phase diagram for the Kitaev chain for the chemical potential  $\mu$ . The topological and trivial sectors are separated by gapless points,  $\mu = \pm t$ .

Before we discuss the effect of disorder on the MEM we have to make a side note. As we saw in the example the MEMs are perfectly localized in the special case  $\mu = 0$ ,  $\Delta = t$  (only the sites at the very edge are occupied). For other parameter sets we can only find numerical results. In Figure 6.5 we see the absolute value of the MEM wave function for several topological systems. Recall that the MEM is actually the fermion comprised of two Majoranas. In this picture we only see the

first half of the Nambu-vector, because the second half is identical. Notice that for increasing  $\mu$  the delocalization of edge modes increases as well. For an infinite system this would not be a problem, but since numerically we are dealing with finite system sizes the delocalization affects the energy. For  $\mu = 0.7$  (green) and  $\mu = 0.9$  (red) the two MEMs overlap in the middle of the chain and feel each other. So as the system approaches the gapless point the two Majoranas hybridize and the energy of the edge modes does not vanish completely. In this figure we looked at a small system (30 sites), so this effect is very strong. Nevertheless, for all finite system sizes the edge modes have finite energy. So we have to implement a numerical cut off  $10^{-15}$ , to be able to view these edge modes as zero energy MEMs.

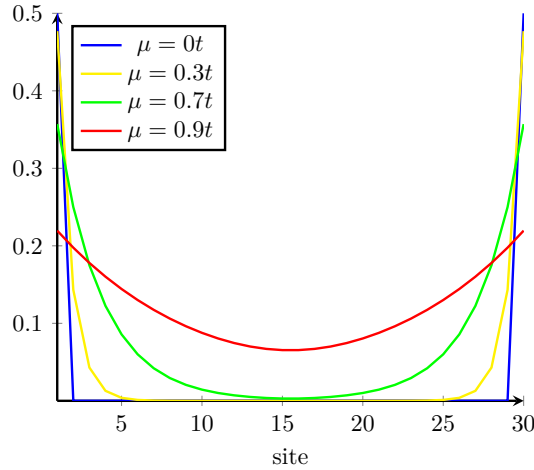


Figure 6.5: MEM for the Kitaev chain of 30 sites with  $\Delta = t = 1$  for several chemical potentials ( $\mu$ ). For low  $\mu$  the states are localized at the edge, however as  $\mu$  approaches  $t$  the edge modes pierce into the bulk and overlap.

### 6.3 Disorder

A physical system is rarely perfectly clean. Here we take a quick look at the effect of disorder on the Majorana edge modes. The disorder will be introduced in the chemical potential. The chemical potential becomes site dependent  $\mu_i = \mu + \delta\mu_i$ , with  $\delta\mu_i$  the fluctuation of the chemical potential at site  $i$ . These fluctuations are randomly picked from  $[-\delta\mu, \delta\mu]$ . Figure 6.6a displays the spectrum of the same system as in Figure 6.2c, but now there is a random disorder in the chemical potential  $\delta\mu = 0.5t$ . The overall shape of the spectrum is not much affected, the system is still gapped and the zero modes still exist. The bulk states on the other hand have become more localized. We see in Figure 6.6b the absolute value of a wave function bulk state for the non-disordered (blue) and the disordered case (red) for approximately the same energy. Disorder forces the bulk states to localize, this is known as Anderson Localization.

On the other hand, in Figure 6.6c depicts a Majorana edge mode, again for both the non-disordered (blue) and the disordered case (red). Here we see that the edge mode is almost unchanged by the disorder.

This indicates that the Majorana edge modes are very robust against the effects of disorder as we would expect in a topological system.

We have seen that the MEMs are present in a static system, even with disorder. We now wonder what happens to the MEMs once the system is altered. How does a sudden change in parameters, a

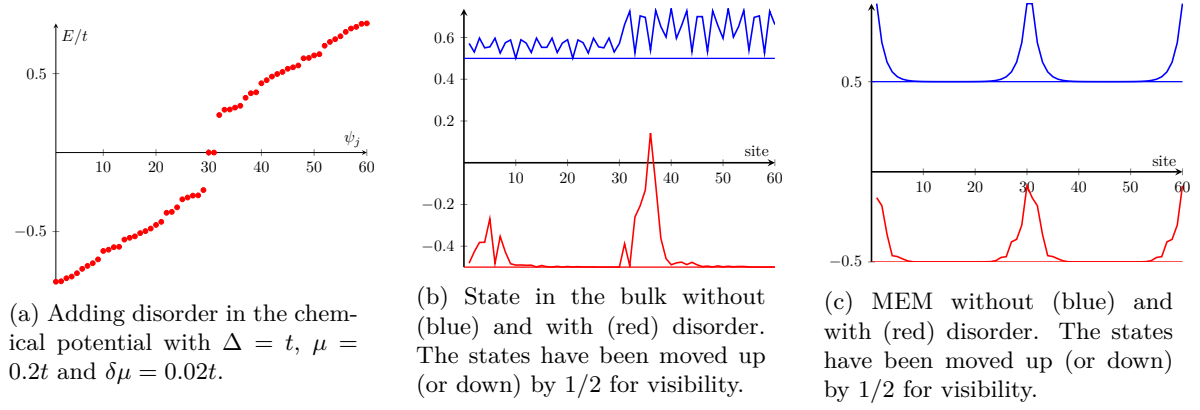


Figure 6.6

quantum quench, affect the MEM? In the next chapter we will work out the details of the quantum quench for the Kitaev chain. We will also derive measures to determine the survival of the wave function after the quench. Using these measures we will investigate the evolution of the MEM in Chapter 8.



## Chapter 7

# Technical Details Quench

We have seen that the Kitaev chain is a topological insulator with a Majorana edge mode as a ground state for specific parameters. Also we have seen that these MEMs are very robust against static disorder in chemical potential. We can now wonder whether these MEMs can also withstand quantum quenches. Do the Majorana edge modes survive a change in chemical potential or superconductivity? A quantum quench generally pumps a lot of energy in or out of the system, so this might have a significant effect on the MEM. Notice that the Majorana ground state is a single particle state. This makes the quench dynamics very simple. We do not have to care about Slater determinants or Pfaffians as one would in a many body system, but we can straightforwardly calculate the time evolution after the quench.

In this chapter we will introduce the technical details necessary for the quench. We will also discuss how to determine the survival of a MEM after a quench.

First, the Hamiltonian of the quench is given by

$$H(\tau) = \begin{cases} H_1 & \text{if } \tau < 0 \\ H_2 & \text{if } \tau > 0 \end{cases} \quad (7.1)$$

where  $H_1$  is in the topological sector. The initial state ( $|\text{ini}\rangle$ ) is a MEM for  $H_1$ . The time evolution of this state after the quench is simply given by

$$|\text{fin}(\tau)\rangle = e^{-i\tau H_2} |\text{ini}\rangle \quad (7.2)$$

This fully governs the evolution of the MEM after the quench. We will use  $\tau$  for the real time in order to avoid confusion with the hopping constant  $t$ .

### 7.1 Projected Overlap

We would like to define a measure for the survival of the MEM after the quench. Since a quantum quench is a very rigorous way to pump energy in or out of the system, starting with the energy of the MEM is the first guess.

However, we have to be careful with the term energy, because the time evolved MEM is not an eigenstate of  $H_2$ . We can on the other hand use the projected overlap (PO), which is closely related to the concept of energy:

$$\text{PO} = \langle \text{fin}(\tau) | H_2 | \text{fin}(\tau) \rangle \quad (7.3)$$

The PO seems an obvious measure for the survival of the MEM. Nevertheless, as we will prove here the PO defined above will always remain zero for a MEM, regardless of the quenched Hamiltonian. First of all note that

$$\text{PO} = \langle \text{ini} | H_2 | \text{ini} \rangle, \quad (7.4)$$

because  $H_2$  commutes with the time evolution operator.

Recall that we can diagonalize  $H_1$  and  $H_2$  using an eigenvalue decomposition (6.5):

$$H_1 = \hat{\Gamma} E_1 \hat{\Gamma}^\dagger = \vec{C}^\dagger \hat{\gamma} \hat{E}_1 \hat{\gamma} \vec{C}, \quad H_2 = \Psi E_2 \Psi^\dagger = \vec{C}^\dagger \psi \hat{E}_1 \psi \vec{C} \quad (7.5)$$

where  $\gamma$  and  $\psi$  are the eigenvector matrices of  $\mathcal{H}_1$  and  $\mathcal{H}_2$ . For notational convenience we would like to drop these  $\vec{C}$  in quadratic terms, and we can because

$$\Gamma_k^\dagger \Psi_j = (\hat{\gamma}_k^\dagger \vec{C})(\vec{C}^\dagger \psi_j) = \sum_i (\hat{\gamma}_k^\dagger \psi_i^\dagger \psi_i \vec{C})(\vec{C}^\dagger \psi_j) = \sum_i \hat{\gamma}_k^\dagger \psi_i^\dagger \Psi_i \Psi_j = \hat{\gamma}_k^\dagger \psi_j \quad (7.6)$$

Suppose  $\gamma$  is the MEM for  $H_1$ .

Here we are going to introduce notation only used in this section. We need these definitions to coherently prove that the PO of the MEM vanishes.

First of all, we can split the states, both initial state and the eigenstates of the new Hamiltonian

$$\gamma = \begin{pmatrix} \hat{\phi} \\ \hat{\theta} \end{pmatrix}, \quad \psi_j = \begin{pmatrix} \phi_j \\ \theta_j \end{pmatrix} \quad (7.7)$$

such that  $\hat{\phi}$  and  $\phi_j$  act on the  $c_i^\dagger$ 's and  $\hat{\theta}$  and  $\theta_j$  act on  $c_i$ 's in the Nambu-vector (6.7).

We will redefine the indices for notational purposes.

The  $j$ -index denotes the eigenvalue and eigenvector of the Hamiltonian (e.g.  $\psi_j$  is the eigenvector with energy  $E_j$ ). Figure 7.1 shows three eigenvalues with the particle-hole partners. We see that  $j$  runs from  $-L$  to  $L$  ( $j = 0$  does not exist). This notation makes it easier to do particle-hole

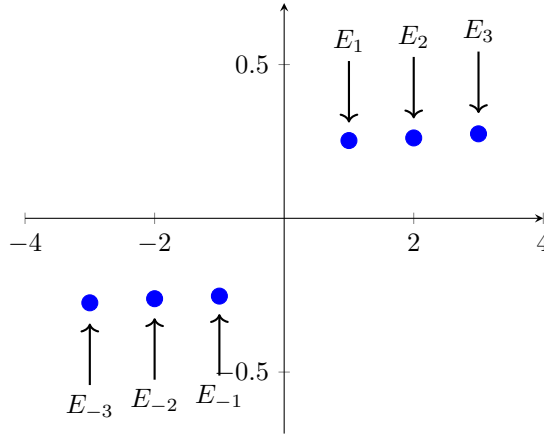


Figure 7.1: Particle-hole indices

transformations, because this transformation would correspond to  $j \rightarrow -j$ .

Furthermore the two parts of every eigenstate  $(\phi_j, \theta_j)$  are both  $L$  dimensional vectors. The entries of these vectors  $(\phi_{ij}, \theta_{ij})$  we will denote by  $i$  running from  $-L/2, \dots, L/2$ . This negative versus positive index makes chain inversion simple. Note that for  $L$  even  $i = 0$  has to be removed, and for  $L$  odd the  $i$ 's are half-integers. In Figure 7.2 we see this lattice schematically displayed.



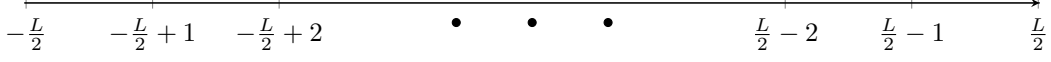


Figure 7.2: Lattice indices running from  $-\frac{L}{2}$  to  $\frac{L}{2}$  to accommodate lattice inversion.

Now we return to (7.4) and we see that

$$\text{PO} = \gamma^\dagger \psi \hat{E}_1 \psi^\dagger \gamma, \quad (7.8)$$

where  $\psi$  is the matrix of eigenvectors.

In the following step we use some results based on symmetries of the system derived in Appendix D. We continue by calculating

$$(\psi^\dagger \gamma)_j = \phi_j^\dagger \hat{\phi} + \theta_j^\dagger \hat{\theta} = \sum_{i=-L/2}^{L/2} \left( \phi_{ji}^\dagger \hat{\phi}_i + \theta_{ji}^\dagger \hat{\theta}_i \right) = \sum_{i=1}^{L/2} \left( \phi_{ji}^\dagger [\hat{\phi}_i - \beta_j \hat{\phi}_{-i}] + \theta_{ji}^\dagger [\hat{\theta}_i + \beta_j \hat{\theta}_{-i}] \right) \quad (7.9)$$

In the last step we used that the Kitaev chain is symmetric under inversion and time reversal (D.18):

$$\phi_{ji} = -\beta_j \phi_{j-i} \quad (7.10)$$

$$\theta_{ji} = \beta_j \theta_{j-i} \quad (7.11)$$

Here  $\beta_j = \pm 1$  is the symmetry factor for the  $j$ th eigenvector. Using the fact that the initial state ( $\gamma$ ) is an MEM we see (from D.38)

$$\hat{\phi}_i = +\hat{\theta}_i \quad \text{near site } -L/2 \quad (7.12)$$

$$\hat{\phi}_i = -\hat{\theta}_i \quad \text{near site } L/2 \quad (7.13)$$

We proceed by splitting the summation over the vector index ( $i$ ) to find

$$(\psi^\dagger \gamma)_j = \sum_{i=1}^{L/2} \phi_{ji}^\dagger [\hat{\phi}_i + \beta_j \hat{\theta}_{-i}] + \theta_{ji}^\dagger [\hat{\phi}_i + \beta_j \hat{\theta}_{-i}] \quad (7.14)$$

$$= \sum_{i=1}^{L/2} [\phi_{ji}^\dagger + \theta_{ji}^\dagger] [\hat{\phi}_i + \beta_j \hat{\theta}_{-i}] \quad (7.15)$$

Now using particle-hole anti-symmetry of the Hamiltonian  $E_{-j} = -E_j$  to see that

$$\text{PO} = \sum_{j=-L}^L E_j |(\psi^\dagger \gamma)_j|^2 = \sum_{j=0}^L E_j (|(\psi^\dagger \gamma)_j|^2 - |(\psi^\dagger \gamma)_{-j}|^2) \quad (7.16)$$

and also to recognize that  $\phi_{-j} = \theta_j$  and vice versa (D.8). Then we find  $|(\psi^\dagger \gamma)_j|^2 = |(\psi^\dagger \gamma)_{-j}|^2$ , so the PO vanishes for all quenches.

So we can not use the projected overlap as a measure for survival of the MEM

## 7.2 Measures: Inverse Participation Ratio and Overlap

There are two measures we are now going to present, that combined can determine the survival of the MEM rather well. The wave functions of the MEMs are by characterized two properties. First

of all the wave functions are localized, and second this localization is at the edge of the system. The second property is measured by the overlap of the evolved state with the initial state. We define

$$\text{OVR} = |\langle \text{ini} | \text{fin}(\tau) \rangle|^4. \quad (7.17)$$

If the overlap is high the weight of the wave function is at the edge. At the end of this section we will see why we have picked the fourth order. Note that there is a maximum for the overlap at 1 if  $|\text{fin}\rangle = |\text{ini}\rangle$ , so great similarity reflects in high overlap. Nevertheless, the OVR does not give to full overview in some cases. Consider for instance the two wave functions in Figure 7.3. Suppose we prepare the system in the state in Figure 7.3a and it evolves to the state in Figure 7.3b for some quench. The overlap would be zero because the states are clearly orthogonal, even though there is still a localized state.

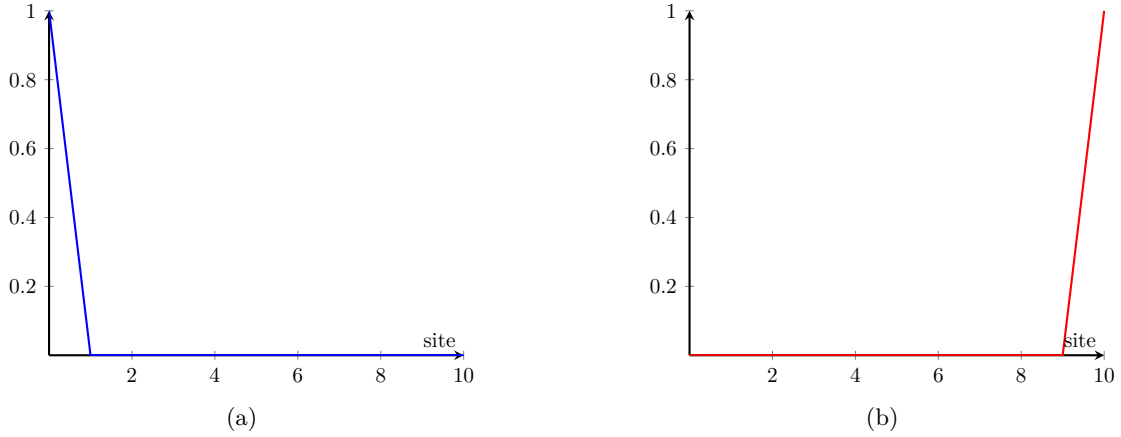


Figure 7.3: Example of two perfectly localized orthogonal states.

The second measure determines the localization. Here we are going to use the inverse participation ration (IPR) defined by Wegner in 1980.[39] For a state  $\psi$  with value  $\psi_i$  on lattice site  $i$  we define

$$\widehat{\text{IPR}} = \sum_i |\psi_i|^4 \quad (7.18)$$

The  $\widehat{\text{IPR}}$  of a perfectly localized state (e.g. Figure 7.3) is obviously 1. A fully delocalized constant state  $(\frac{1}{\sqrt{L}}, \dots, \frac{1}{\sqrt{L}})$  has  $\widehat{\text{IPR}} = \sum_i \frac{1}{L^2} = \frac{1}{L}$ , which in the thermodynamic limit ( $L \rightarrow \infty$ ) goes to zero. Hence the  $\widehat{\text{IPR}}$  becomes 1 for localized states and goes to zero for delocalized states.

For the Kitaev chain we cannot have a fully localized state in the sense of Figure 7.3a or 7.3b. The MEM for the special point ( $\mu = 0, \Delta = t$ ) is the perfectly localized edge state and the normalized wave function in Nambu language is given by  $|\gamma\rangle = (\frac{1}{2}, 0, \dots, 0, \frac{1}{2}, \frac{1}{2}, 0, \dots, 0, \frac{1}{2})^\top$ , describing Majoranas at both edges. The  $\widehat{\text{IPR}}$  of  $\gamma$  is  $\frac{4}{2^4} = \frac{1}{4}$ . We would like this state to have IPR equal to 1 so we define

$$\text{IPR} = 4\widehat{\text{IPR}} = 4 \sum_i |\psi_i|^4 \quad (7.19)$$

Finally, we give an argument for choosing the fourth order for the OVR (7.17). Using the diagonalization of  $H_2$  (7.5) we see that (when acting on the one-particle Fock space)

$$e^{-i\tau H_2} = \Psi e^{-i\tau \hat{E}_2} \Psi^\dagger = \Gamma(\Gamma^\dagger \Psi e^{-i\tau \hat{E}_2} \Psi^\dagger \Gamma) \Gamma^\dagger \quad (7.20)$$

where we have inserted  $\Gamma\Gamma^\dagger = \mathbf{I}$  and we can write  $\Lambda(\tau) = \Gamma^\dagger \Psi e^{-i\tau \hat{E}_2} \Psi^\dagger \Gamma$ . We let this act on the initial state  $\frac{1}{\sqrt{2}}(\Gamma_1 + i\Gamma_{-1})|0\rangle$  to find

$$|\text{fin}(\tau)\rangle = \Gamma_\alpha \frac{1}{\sqrt{2}}(\Lambda(\tau)_{\alpha 1} + i\Lambda(\tau)_{\alpha -1})|0\rangle \quad (7.21)$$

In this notation  $\text{IPR} \propto \Lambda^4$  and  $|\langle \text{ini} | \text{fin}(\tau) \rangle| \propto \Lambda$ , hence we choose the fourth order for the overlap. In the following chapter we will use these measures to investigate the MEM for a variety of quenches.



## Chapter 8

# Results - Kitaev Chain Quantum Quench

In this chapter we will discuss the behavior of the wave functions after the quench. Using the measures described in Section 7.2 we explore the parameter space ( $\mu$  and  $\Delta$ ) to determine whether the MEM survives or dissipates into the bulk. First we consider the Kitaev chain without disorder and we quench the chemical potential and superconductivity separately. Finally, we also implement disorder in the chemical potential to see how this affects the MEM.

### 8.1 Examples Quench

Before we discuss the quenches using the measures, let us first take a look at the explicit time evolution of the MEM. Figures 8.1 show the evolution of the MEM after two distinct quenches. In both cases the system (100 sites) was prepared in the topological sector at the special point,  $\mu = 0$  and  $\Delta = t$ . In Figure 8.1a we quenched the chemical potential to  $\mu = 2$ , the trivial sector. We see how the wave function reacts and evolves over time to become very delocalized. In this figure we see the absolute value of the wave function for several times. At time  $\tau = 0$  (blue) we see the MEM at site 1 and 100. Then very quickly the localized state dissipates into the bulk, at  $\tau = 100$  (green) it is already spread out over the whole lattice. At  $\tau = 1000$  (red) there are still some oscillations, but no localization. This suggests that the MEM disappears, because in the trivial sector there are no localized edge eigenstates it can explore. In Figure 8.1b we quench the system within the topological sector ( $\mu = 0.5$ ). We then observe that the system remains much more localized at the edges, even though the change in Hamiltonian induces some dissipation into the bulk. The inset of Figure 8.1b gives a better picture of the edge and shows that the MEM does not decay into the bulk for large time. For  $\tau = 1000$  (red) the weight of the wave function is still at the edge.

### 8.2 Chemical Potential Quench

So now we have discussed two particular examples, one extreme topological to trivial quench where the MEM disappears, and one topological to topological quench where we see that the MEM survives. We can make these statements more concrete by considering the two measures defined in Section 7.2, the inverse participation ratio (IPR) and the overlap (OVR). The IPR estimates the localization of the state is, while OVR determines the resemblance to the initial state. The combination of these two quantities gives a good indication for the survival of the original MEM.

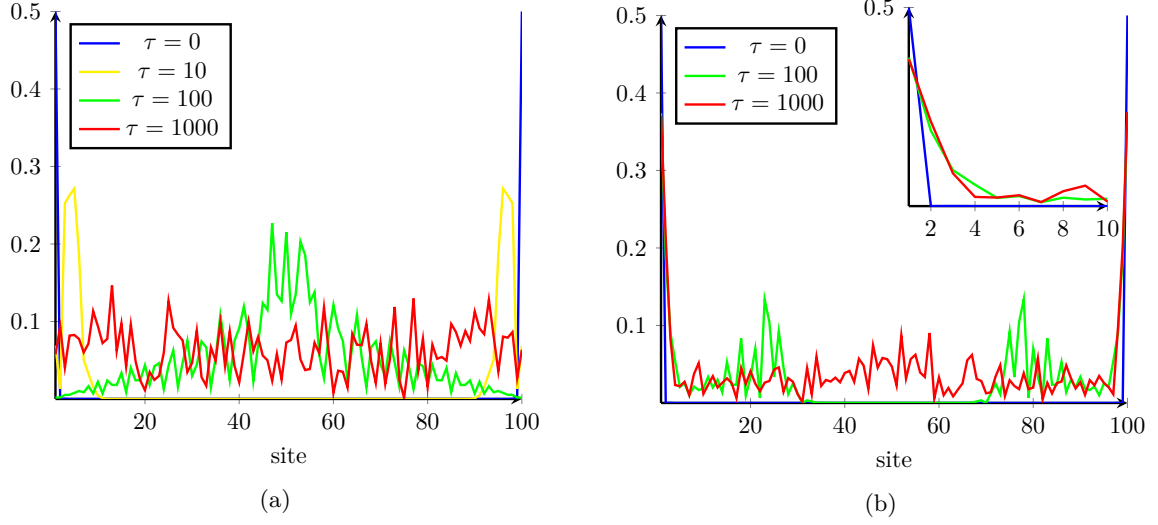


Figure 8.1: Examples of the evolution of a Majorana state after a quantum quench for the Kitaev chain from the topological sector ( $\mu = 0$ ) (a) to the trivial sector ( $\mu = 2$ ) and (b) to topological sector ( $\mu = 0.5$ ), with a lattice of 100 sites and  $\Delta = t = 1$ . Here we have plotted for different times the absolute value of the wave function for the fermions only for the particles (not the holes). The inset in (b) is a zoom at the edge of the topological-topological quench.

Here we take a look at quenches in the chemical potential. In the following sections we will use a Kitaev chain of 100 sites. It turns out that the measures (IPR and OVR) are relatively well converge thermodynamic limit for a system of 100 sites. There will still be some effects from the finite size, but these are only slight fluctuations that do not change the outcomes significantly.

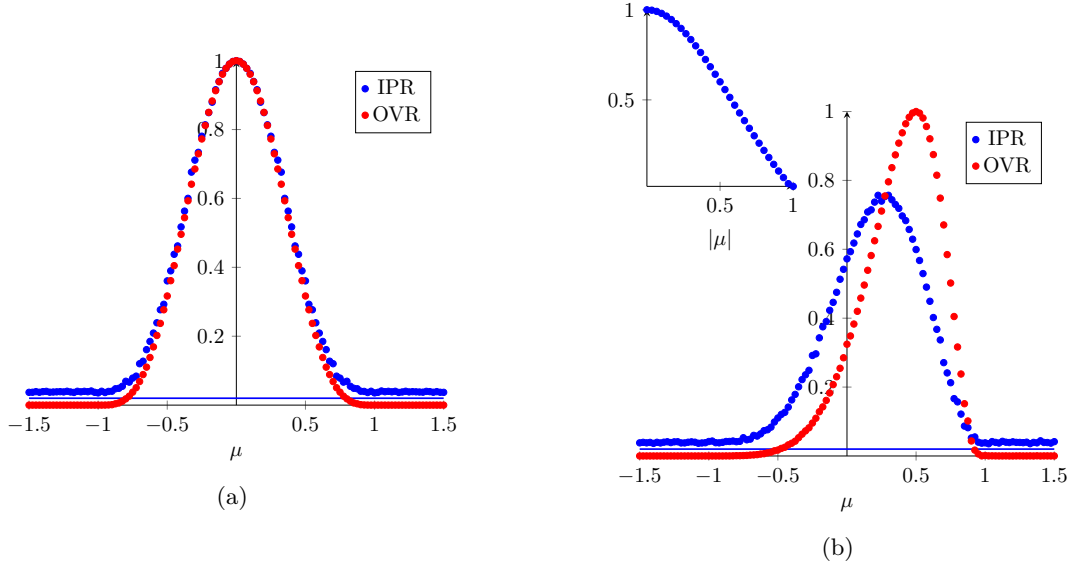


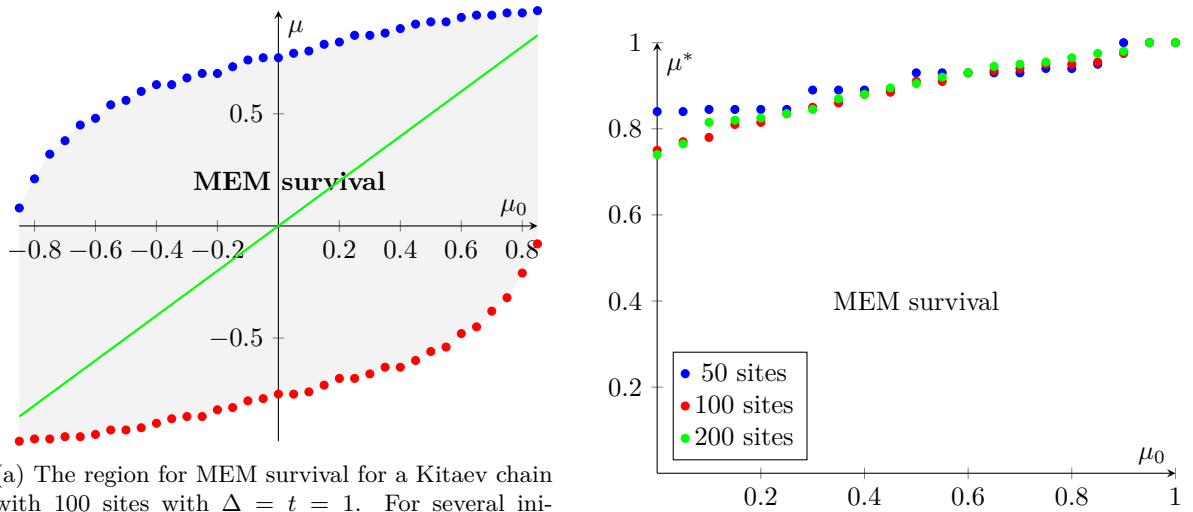
Figure 8.2: The IPR and OVR (long time average) for the wave function of the MEM quenched from  $\mu = 0$  (a) and  $\mu_0 = 0.5$  (b) to  $\mu$ . (100 sites and  $\Delta = t = 1$ ). The inset in (b) depicts the IPR for the initial MEM as a function of  $\mu$ .

In Figure 8.2 we see the results for the chemical potential quenches. The system is prepared in the topological sector. Then we prepare the state in the Majorana ground state, the MEM as we did before. We quench to various different chemical potential (horizontal axis). By taking a long time average ( $T$  between 10000 and 11000) for IPR and OVR we make sure the MEM has time to fully adjust to the new system parameters. Taking the average over a time period ensures oscillations are filtered out.

Figure 8.2a depicts IPR and OVR for a quench from  $\mu_0 = 0$  ( $\Delta = t = 1$ ). The initial has a maximally localized MEM ground state. Unsurprisingly, OVR is maximal for  $\mu = 0$ , because a state overlaps perfectly with itself. Also IPR is maximal for  $\mu = 0$ , since this is the most localized state. We also see that both quantities decay and flatten out as  $\mu$  increases. The OVR goes to zero, while the IPR approaches the blue solid line. This line (0.02) corresponds to the IPR of the constant wave function ( $\psi = (\frac{1}{\sqrt{L}}, \dots, \frac{1}{\sqrt{L}})$ ), and therefore indicates complete delocalization (CD).

For  $\mu$  outside the topological sector (see Figure 6.4) the evolved MEM becomes completely delocalized and has zero overlap with the initial state. The system in the trivial sector does not have any localized edge state the MEM can go to, therefore it is smeared out over the whole eigenstate basis.

Interestingly, we see that the MEM also disappears for certain regions in the topological sector. We can define thresholds for the measures: for the IPR  $\text{IPR}_{\text{th}} = 0.08$  (four times the CD), and for the OVR  $\text{OVR}_{\text{th}} = 0.04$ . If either of the measures is below these threshold, we conclude that the Majorana did not survive the quench. In this case (Figure 8.2a) the region of stability, or the region of survival is  $\mu \in [\mu_{\text{down}}, \mu_{\text{up}}]$ , with  $\mu_{\text{down}} = -0.75$  and  $\mu_{\text{up}} = 0.75$ . Hence even for  $|\mu| > 0.75$  in the topological sector the MEM disappears. The localized states for these chemical potential are too “orthogonal” to the original MEM and the initial state is smeared out over many new eigenstates. Note that for both IPR and OVR the maximum is at  $\mu = 0$ .



(a) The region for MEM survival for a Kitaev chain with 100 sites with  $\Delta = t = 1$ . For several initial chemical potentials  $\mu_0$  the upper  $\mu^{\text{up}}$  and lower crossover  $\mu^{\text{down}}$  are depicted in respectively blue and red. At these cross overs either the IPR of the OVR reaches the threshold value ( $\text{IPR}_{\text{th}} = 0.08$ ,  $\text{OVR}_{\text{th}} = 0.04$ ).

(b) Part of Figure 8.3a for several lattice sizes. Clearly 50 sites results in some finite size effects, while the 100 sites results have converged to the thermodynamic limit.

Figure 8.3

Figure 8.2b shows chemical potential quenches for which OVR and IPR do not agree as good as in the previous case. Here we prepare the system with  $\mu_0 = 0.5$  and both OVR and IPR qualitatively agree on the cross overs  $\mu_{\text{up}} \approx 0.9$  and  $\mu_{\text{down}} \approx -0.7$ . However, the maximums for the IPR and OVR do coincide in this case. The OVR maximizes at  $\mu_0$ , which is 0.5 in this case, since there the system

remain unchanged through the quench. However for the IPR the maximum is not at  $\mu_0$ . We see that there is a balance between the memory of the initial state and IPR maximization. The inset in Figure 8.2b shows the IPR for Majorana eigenstates as a function of chemical potential (and  $\Delta = t = 1$ ). As said before the localization is maximized for  $\mu = 0$ , and the IPR decays in the topological sector to zero at the phase transition  $\mu = t = 1$ .

Hence for  $0 < \mu < \mu_0$  the MEM is better localized. Apparently our initial MEM tries to align with these better localized states. On the other hand the further  $\mu$  and  $\mu_0$  are apart the more the MEM dissipates into the bulk, because more eigenstates get involved. The combination of both effects results in a maximum for IPR at  $\mu^{\text{IPR}} \approx 0.25$ .

In two specific cases (Figure 8.2a and Figure 8.2b) we have looked at the two measures after the quench, concluding that there is a stability region for the MEMs. In Figure 8.3a we see this stability region plotted as a function of  $\mu_0$ , the initial chemical potential. Using the thresholds we have calculated the lower bound  $\mu_{\text{down}}$  (red) and upper bound  $\mu_{\text{up}}$  (blue) for survival of the MEM.

First, we observe that the MEM survival region is the largest for  $\mu_0 = 0$ . Furthermore, the green line denotes  $\mu = \mu_0$  and using this line we see that a system with  $\mu = 0$  is much more stable than a system with  $\mu = \pm 0.85$  at the edge of this figure. For  $\mu = 0.8$  a shift of  $\delta\mu = +0.2$  would already put the system outside the MEM survival region.

Note that the diagram runs only up to  $\mu_0 = 0.85$ , because for this lattice size (100 sites) the localization of the initial MEM is below the threshold beyond this point.

The values of  $\mu_{\text{down,up}}$  turn out to be independent of lattice, provided that the system is large enough. In Figure 8.3b we see part of Figure 8.3a for various lattice sizes. For 50 lattice sites there is clearly some finite size effects in the form of plateaus, but the 100 sites is almost indistinguishable from the 200 sites. We can therefore safely assume 100 sites is large enough for these analyses.

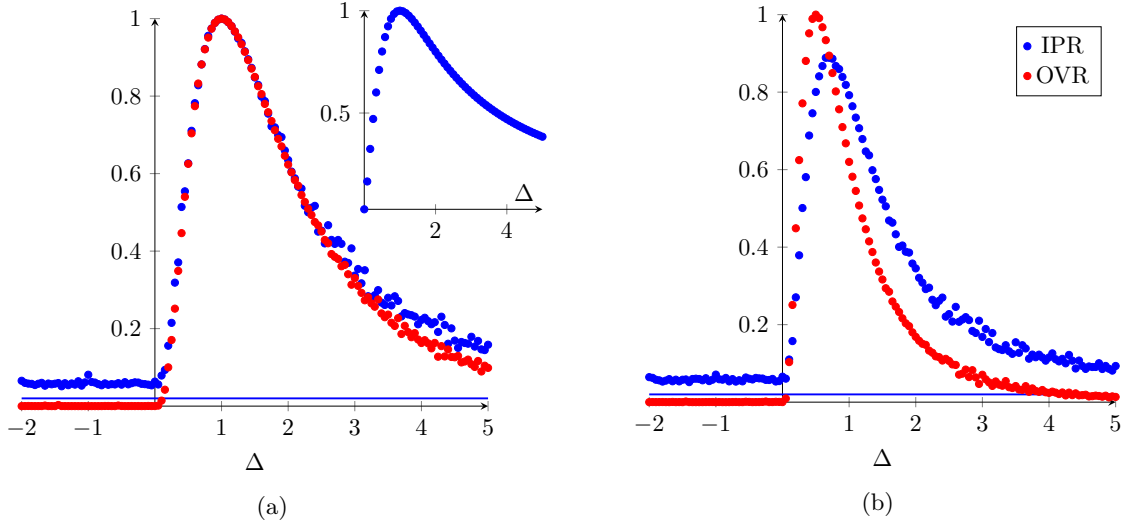


Figure 8.4: The IPR and OVR (long time average) for the wave function of the MEM quenched from  $\Delta_0 = 1$  (a) and  $\Delta_0 = 0.4$  (b) to  $\Delta$ . (100 sites and  $\mu = 0$ ,  $t = 1$ ). The inset in (a) depicts the IPR for the initial MEM as a function of  $\Delta$ .



### 8.3 Superconductivity Quench

We now also take a look at the superconductivity quench. Analogous to the chemical potential quench in Figure 8.4 we see quenches for different initial condition. The first observation is that, contrary to the chemical potential quench, the stability region does not cover negative values for  $\Delta$ . Up to now we have only considered  $\Delta > 0$ , because this term distinguishes the Kitaev chain from a simple gapless tight binding model. Therefore at  $\Delta = 0$  there is phase transition. However, this transition does not separate a topological phase from a trivial phase, but on either side there is a topological phase. In both figures we clearly see that the topological phases at both sides of the transition are different. For the quenches in Figure 8.4a the initial state is a MEM for  $\mu = 0$  and  $\Delta = t = 1$ . If we quench this to negative  $\Delta$  the MEM completely vanishes. We see this as well for different initial condition  $\Delta = 0.5$  in Figure 8.4b.

A simple explanation follows from the Hamiltonian in Majorana language (see Section 6.2.1). We showed that for  $\mu = 0$  and  $t = \Delta$  two Majoranas,  $\gamma_1$  and  $\gamma_{2L}$  do not contribute to the energy. If we do the same derivation for  $\Delta = -t$  the Majoranas operators that drop out of the Hamiltonian are  $\gamma_2$  and  $\gamma_{2L-1}$ . The even and odd Majoranas are the two different types (see (6.10)) and changing the sign of  $\Delta$  changes the Majorana type at both edges. The two types are orthogonal, so the MEM vanishes when quenching from  $\Delta_0 > 0$  to  $\Delta < 0$ . The localized states in both systems are orthogonal.

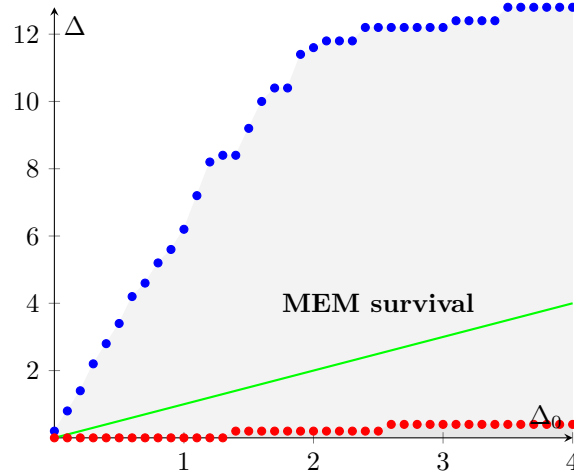


Figure 8.5: The region for MEM survival for a Kitaev chain with 100 sites with  $\mu = 0$  and  $t = 1$ . For several initial superconductivities  $\Delta_0$  the upper  $\Delta^{\text{up}}$  and lower crossover  $\Delta^{\text{down}}$  are depicted in respectively blue and red. At these cross overs either the IPR of the OVR reaches the threshold value ( $\text{IPR}_{\text{th}} = 0.08$ ,  $\text{OVR}_{\text{th}} = 0.04$ ).

Similar to the chemical potential quench the MEM does not survive all quenches within the topological sector. The lower bound for survival of the MEM are around  $\Delta_{\text{down}} = 0.1$  in both cases.

Note that we see a similar distinction between Figure 8.4a and Figure 8.4b as we saw for the chemical potential quench. Figure 8.4a is prepared in the special point ( $\Delta_0 = 1$ ), so both the IPR and OVR are maximal for  $\Delta = \Delta_0 = 1$ . On the other hand in Figure 8.4b we start at  $\Delta_0 = 0.5$ . Obviously, the overlap is again maximal at  $\Delta = \Delta_0 = 0.5$ . The IPR maximum is pulled away from  $\Delta_0$ , because for  $\Delta \in [0.5, 1]$  the available MEMs are more localized as we see in the inset of Figure 8.4a. This figure shows the IPR for the bare MEM as a function of the superconductivity.

This inset also shows the MEM slowly disappearing for  $\Delta \gg 1$ . In fact for the system used in this case (100 sites) there are no MEM in the initial system ( $H_1$ ) if  $\Delta > 25$ , because the IPR is below the threshold we defined in Section 8.2. Because of this delocalization of the Majoranas for high  $\Delta$ , the

MEM does not survive quenches to high enough  $\Delta$ .

We can make this more explicit by determining the upper and lower cross over superconductivity for several initial conditions. We see the results of this analysis in Figure 8.5. As a function of initial superconductivity ( $\Delta_0$ ) we see the the upper boundary (blue) and the lower boundary (red) for MEM survival after the quench. We only consider  $\Delta_0$  up to 4, because very high superconductivity is not physical. Furthermore, only  $\Delta_0 > 0$  is plotted here, for negative superconductivity one has to mirror the plot in both axis.

Again some caution is required when discussing the cross overs in the topological sector (recall that there is a MEM for  $|\Delta| > 0$ ). As with the chemical potential quenches it turns out that we can treat the system size of 100 sites to be close to the thermodynamic limit. Increasing the size of the system only smoothens out the plot, i.e. takes away the jumps but does not change the shape.

## 8.4 Adding Disorder

In Section 6.3 we have seen that the MEM are very robust against disorder. Here we are going to see what happens to a MEM in a disordered state, when the chemical potential is quenched. We add the disorder in the chemical potential in the form of block disorder with width  $\delta\mu$ . Note that there is particle-hole symmetry in the system, so adding a disorder  $\delta\mu_i$  to  $c_i$  means a disorder  $-\delta\mu_i$  for  $c_i^\dagger$ . This disorder shifts all energies in the spectrum up or down. Therefore we have to be careful

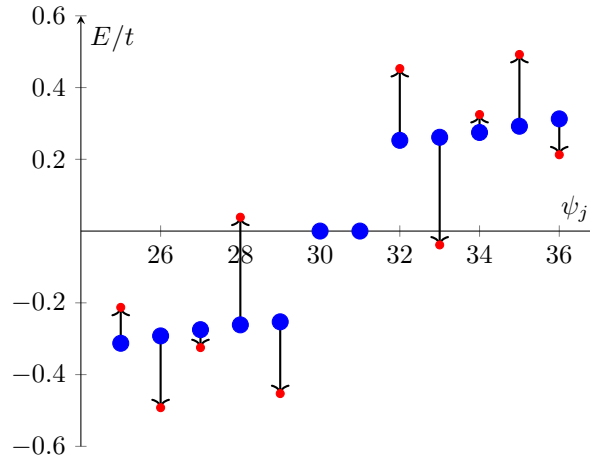


Figure 8.6: Effect of disorder spectrum, shifting of the eigenvalues.

with adding too much disorder. In Figure 8.6 we see an example of a non-disordered spectrum in blue. Adding  $\delta\mu_i$  to every site shifts all the eigenvalues in spectrum, only the zero energy states are pretty resilient against this shift, as we saw before. The black arrows depict the shift for a certain disorder. The red dots denote the new energies. In Figure 8.7 we see two spectrums for the same global parameter set ( $\mu = 0.5$ ,  $\Delta = t = 1$ ). Figure 8.7a displays the gapped spectrum without disorder, while in Figure 8.7b we see that disorder ( $\delta\mu = 1$ ) forced the gap to close. Hence we see that adding high disorder can result in the closing of the gap and this has two consequences. As we saw before in a finite lattice the “zero” eigenstates are never exactly zero, because of finite size effects, we treat them as zero below a certain threshold. For a highly disordered system energies of the bulk states can also become of the order of the “zero” energies, hence it is impossible to distinguish the MEM from the other small energy states.

Secondly, finite size effects start to play a role since the system is not an insulator anymore, i.e. the zero modes can talk to one another through the bulk.

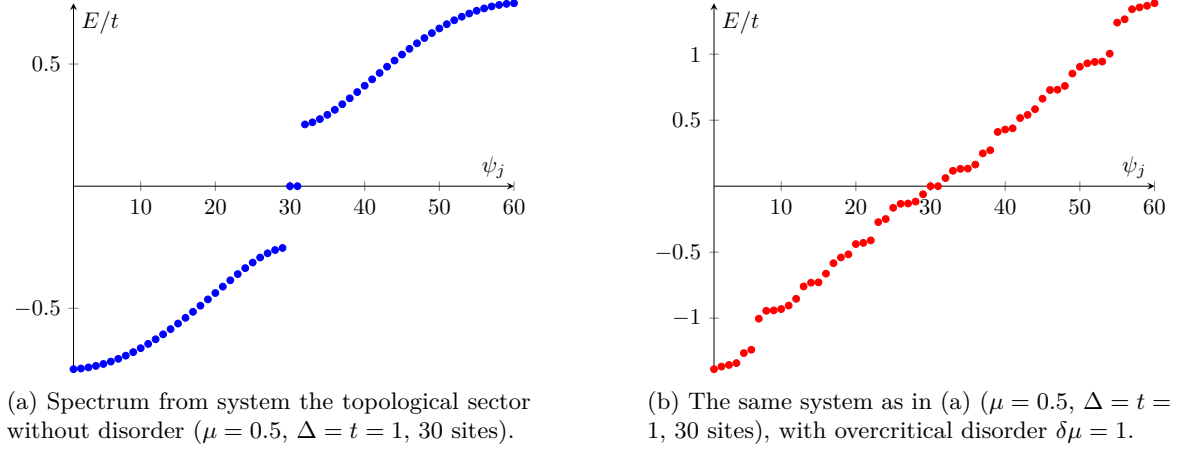


Figure 8.7

Therefore we cannot use arbitrarily large disorder, because we have to make sure the initial system is gapped. For  $\Delta = t = 1$  the size of the gap to  $E = 0$  is given by  $\Delta_{\text{gap}} = \frac{1}{2}|1 - \mu|$ . In (6.6) we see that the chemical potential enters as  $\frac{\mu}{2}$ , therefore half the disorder ( $\frac{\delta\mu}{2}$ ) should be smaller than  $\frac{1}{2}|1 - \mu|$  to avoid the gap to close. We choose the initial system to have chemical potential  $\mu_0 = 0$ , so the maximal allowed disorder is  $\delta\mu = 1$ . In all case we prepare the system with a certain chemical potential  $\mu_0$  and disorder distribution  $\delta\mu_i$ . Then we quench by only changing the global chemical potential, leaving the disorder distribution unaltered.

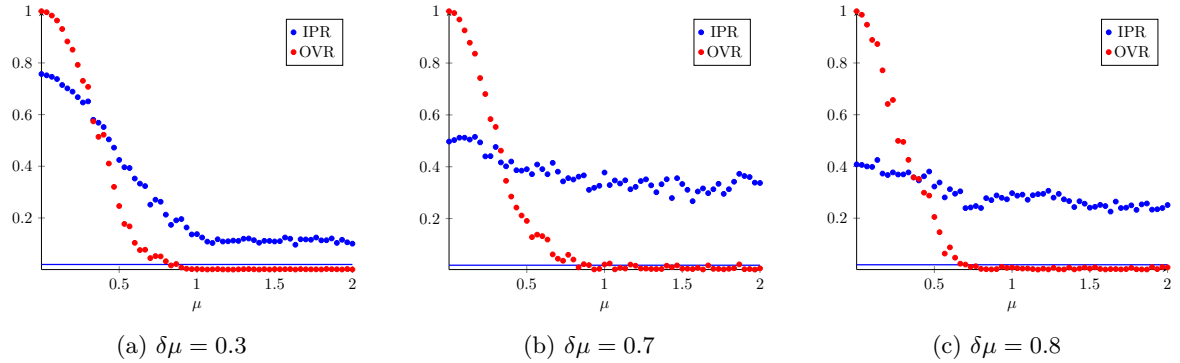


Figure 8.8: OVR and IPR for chemical potential quench ( $\mu$ ), for initial system (100 site) with  $\mu_0 = 0$ ,  $\Delta = t = 1$  for several disorder levels ( $\delta\mu$ ).

In Figure 8.8a the IPR and OVR of chemical potential quench for  $\delta\mu = 0.3$  displayed. We see that the overlap has changed very little in comparison with the non disordered case (Figure 8.2a). On the other hand, the IPR seems to level out. This is due to another localization effect, known as Anderson localization (AL).[40] This effect appears for instance in disordered chains with tight binding. Deviations in chemical potential along the chain force the system to localize. The stronger the disorder, the stronger the AL. In Figure 8.8b and 8.8c we see that for strong disorder the IPR almost completely levels out. This suggest that the state is localized equivalently when quenched to a topological and trivial system. Hence the localization is not due to the appearance of Majoranas at the edge, but rather because of the disorder, Anderson localization. In all cases the energy of the initial MEM is of the order of  $10^{-16}$ , which is below *Mathematica* working precision. As we would expect the OVR falls of as we go away from the initial condition  $\mu = 0$ .

More research needs to be done in order understand MEM survival in the presence of disorder.



## Chapter 9

# Conclusion and Discussion - Kitaev Chain Quantum Quench

In the second part of this thesis we have looked at the the quantum quench for the Kitaev chain. In particular, analyzing the wave function of a Majorana edge mode after a quench in chemical potential and superconductivity.

In Chapter 6 we have introduced the Kitaev chain, with it distinctive features. We reviewed the appearance of localized zero energy Majorana edge modes in the system. And we have seen that these topological effects manifest for certain conditions, the topological sector. Outside this sector the system is a simple insulator, the trivial sector. These different phases are separated by a gapless critical point. Also we have seen that these MEMs are very robust against disorder. These properties combined make this a good candidate for a quantum computer. This made us wonder about other experimental distortion the MEMs should overcome, for instance a sudden change in overall chemical potential. The main question of this part is: How does the Majorana edge mode behave when the Kitaev chain is subjected to a quantum quench? We attempted to answer this question by looking at the wave function of the MEM after we performed a quench.

In Chapter 7 we discussed the details of the quench. The wave functions after the quench were numerically calculated by applying the time evolution operator to the initial state for a finite size system (100 sites). We presented measures to assess the behavior of the wave function. The overlap determined the resemblance to the state before the quench and the inverse participation ratio estimated the localization of the state.

Finally in Chapter 8 we discussed the results. First we considered two specific chemical potential quenched. In both cases the initial system was in the topological phase and we prepared the state to be the MEM ( $\mu = 0$ ,  $\Delta = t = 1$ ). In one case we quenched the system to the trivial phase ( $\mu = 2$ ), and by looking at the wave function we observed that the MEM dissipated into the bulk. It delocalized and did not survive this quench. In the second case we quenched the system within topological sector ( $\mu = 0.5$ ). In this case there was still some dissipation into the bulk, but the weight of the wave function was still at the edge. In this case the MEM clearly remained in the system.

We then discussed the survival of the MEM using the IPR and OVR. First we calculated these measures explicitly for two examples of chemical potential quenches. Starting from the initial system ( $\mu_0 = 0$  and  $\mu_0 = 0.5$ ) we derived these measures as a function of  $\mu$  (chemical potential after the quench). We observed that the MEM already seems to disappear for quenches within the topological sector. Therefore we defined thresholds to determine the stable quench region as a function of the initial chemical potential. We noticed that this stability region was maximal for  $\mu_0 = 0$  and the width of this region was approximately 1.5.

Then we performed a similar analysis for the superconductivity. We determined the stability regions for small initial superconductivity. Here the region seems to grow as the initial superconductivity increases. Interestingly the MEM does not survive a quench from one topological sector to the other topological sector. At  $\Delta_0 = 0$  there is a phase transition between two different topological sectors, containing different MEM types. These two types are orthogonal and the MEM cannot survive in the other sector.

We have to mention that for both parameter quenches the finite size effects cannot be completely ignored. These are inherent to doing a numerical analysis. Even though the evidence suggests otherwise, the boundaries of the stability regions may be significantly different in the thermodynamic limit.

Finally, we have implemented disorder in the system. This adds a completely new dimension to the story. Disorder can even cause localization effects in non-topological systems such as the tight binding model. This effect is known as Anderson localization. When we add disorder to the chemical potential we see that AL starts to battle with the edge mode localization and it is difficult to determine whether there is still MEMs.

Quenching the Kitaev chain in the presence of disorder certainly demands for more extensive research.

# Appendices





## Appendix A

# Kondo Model from Anderson Impurity Model

In this appendix we will show how the Kondo model (1.1) can be derived as an effective theory from the Anderson Impurity model (AIM). The AIM is a microscopic theory, so by making this connection we obtain the physical justification for (1.1).

The idea is as follows the Anderson model couples a spinful impurity to spinful conduction electrons. The Anderson impurity can possess no particles ( $|0\rangle$ ), one particle ( $|\uparrow\rangle, |\downarrow\rangle$ ) or two particles ( $|\uparrow\downarrow\rangle$ ). In the Kondo model the impurity is a spin, hence is either up or down, so it is in the one particle sector. By projecting out the zero and two particle sectors in the AIM we can derive the Kondo impurity. In the end we let  $U$  and  $\epsilon_d$  become large and  $E - \epsilon_d$  go to zero. These quantities are defined in the following part.

The Hamiltonian of the Anderson impurity model is given by

$$H = \sum_{k\sigma} \left[ \epsilon_k c_{k\sigma}^\dagger c_{k\sigma} + (V_k d_\sigma^\dagger c_{k\sigma} + V_k^* c_{k\sigma}^\dagger d_\sigma) \right] + \sum_\sigma \epsilon_d n_{d\sigma} + U n_{d\uparrow} n_{d\downarrow}. \quad (\text{A.1})$$

The  $c_{k\sigma}$  are the conduction electrons as usual with the single particle energy  $\epsilon_k$ . The impurity fermions are  $d_\sigma$  and they couple to the conduction fermions with  $V_k$  and  $V_k^*$ . Adding a impurity fermion comes with a cost  $\epsilon_d$ , since  $n_{d\sigma}$  is the number operator for the impurity. Finally  $U$  couples both spin species of the impurity.

Since we are interested in different particles sectors we can define three sectors of the Hilbert space:

$$|\psi\rangle = \begin{pmatrix} |\psi_0\rangle \\ |\psi_1\rangle \\ |\psi_2\rangle \end{pmatrix} \quad (\text{A.2})$$

The Schrödinger equation becomes then

$$\begin{pmatrix} H_{00} & H_{01} & H_{02} \\ H_{10} & H_{11} & H_{12} \\ H_{20} & H_{21} & H_{22} \end{pmatrix} \begin{pmatrix} |\psi_0\rangle \\ |\psi_1\rangle \\ |\psi_2\rangle \end{pmatrix} = E \begin{pmatrix} |\psi_0\rangle \\ |\psi_1\rangle \\ |\psi_2\rangle \end{pmatrix}. \quad (\text{A.3})$$

The  $H_{mn}$  are the Hamiltonians coupling the different sectors. If we define projection operators  $P_i$  ( $i = 0, 1, 2$ ) projecting to each respective sector we get

$$H_{mn} = P_n H P_m \quad (\text{A.4})$$

The projection operator are explicitly given by

$$P_0 = (1 - n_{d\uparrow})(1 - n_{d\downarrow}), \quad P_1 = n_{d\uparrow} + n_{d\downarrow} - 2n_{d\uparrow}n_{d\downarrow}, \quad P_2 = n_{d\uparrow}n_{d\downarrow} \quad (\text{A.5})$$

Note that  $H_{20} = H_{02} = 0$ , because in the Hamiltonian (A.2) there is no term adding or removing two impurity fermions.

The diagonal entries are

$$H_{00} = \sum_{k\sigma} \epsilon_k c_{k\sigma}^\dagger c_{k\sigma}, \quad H_{11} = \sum_{k\sigma} \epsilon_k c_{k\sigma}^\dagger c_{k\sigma} + \epsilon_d, \quad H_{22} = \sum_{k\sigma} \epsilon_k c_{k\sigma}^\dagger c_{k\sigma} + 2\epsilon_d + U \quad (\text{A.6})$$

The two entries creating an impurity fermion are

$$H_{10} = \sum_{k\sigma} V_k d_\sigma^\dagger (1 - n_{d\bar{\sigma}}) c_{k\sigma}, \quad H_{21} = \sum_{k\sigma} V_k d_\sigma^\dagger n_{d\bar{\sigma}} c_{k\sigma}. \quad (\text{A.7})$$

Here  $\bar{\sigma}$  denotes is  $\uparrow$  if  $\sigma = \downarrow$  and vice versa. We see that  $H_{10}$  only adds a fermion with spin  $\sigma$  if the other fermion is absent and  $H_{21}$  only add a fermion if the other is present. Finally  $H_{01} = H_{10}^\dagger$  and  $H_{12} = H_{21}^\dagger$ .

From the three equation in (A.3) we can derive

$$H_{\text{eff}} |\psi_1\rangle = H_{10} |\psi_0\rangle + H_{11} |\psi_1\rangle + H_{12} |\psi_2\rangle = E |\psi_1\rangle \quad (\text{A.8})$$

$$(H_{10}(E - H_{00})^{-1}H_{01} + H_{11} + H_{12}(E - H_{22})^{-1}H_{21}) |\psi_1\rangle = E |\psi_1\rangle. \quad (\text{A.9})$$

Where we have rewritten the equations in (A.3) to find an equation for  $|\psi_1\rangle$ .

Now we can work out the first term in (A.9):

$$H_{10}(E - H_{00})^{-1}H_{01} = \sum_{kk'\sigma\sigma'} V_k V_{k'}^* d_\sigma^\dagger (1 - n_{d\bar{\sigma}}) c_{k\sigma} (E - H_{00}) c_{k'\sigma'}^\dagger (1 - n_{d\bar{\sigma}'}) d_{\sigma'} \quad (\text{A.10})$$

The strategy with both the first and the third term will be to get all sector dependence to the front and remain with only terms that depend on the bulk. We go to projector language immediately because the orthogonality of the sectors makes the derivation a lot easier.

Note that  $P_0 + P_1 + P_2 = 1$ , so we can write

$$E - H_{00}P_0 = (E - H_{00})P_0 + EP_1 + EP_2. \quad (\text{A.11})$$

Since the sectors are orthogonal it is easy to see that

$$(E - H_{00}P_0)^{-1} = (E - H_{00})^{-1}P_0 + \frac{1}{E}P_1 + \frac{1}{E}P_2. \quad (\text{A.12})$$

If we insert (A.12) in (A.10), we see that only the  $P_0$  survives:

$$(E - H_{00})^{-1} c_{k'\sigma'}^\dagger (1 - n_{d\bar{\sigma}'}) d_{\sigma'} = -(1 - n_{d\bar{\sigma}'}) d_{\sigma'} (E - H_{00})^{-1} c_{k'\sigma'}^\dagger \quad (\text{A.13})$$

$$= c_{k'\sigma'}^\dagger (1 - n_{d\bar{\sigma}'}) d_{\sigma'} (E - H_{00} - \epsilon_{k'})^{-1}, \quad (\text{A.14})$$

where we have used  $H_{00}c_{k'\sigma'}^\dagger = \sum_{k\sigma} c_{k\sigma}^\dagger c_{k\sigma} c_{k'\sigma'}^\dagger = c_{k'\sigma'}^\dagger (H_{00} + \epsilon_{k'})$  in the second line. Note that the energy  $E$  is for a one particle state. In the end we set  $|\epsilon_d|, U \gg |H_{00}|$ , so  $E \approx \epsilon_d$ . Therefore we rewrite (A.14)

$$(E - H_{00})^{-1} c_{k'\sigma'}^\dagger (1 - n_{d\bar{\sigma}'}) d_{\sigma'} = -\frac{c_{k'\sigma'}^\dagger (1 - n_{d\bar{\sigma}'}) d_{\sigma'}}{\epsilon_{k'} - \epsilon_d} \left(1 - \frac{E - \epsilon_d - H_{00}}{\epsilon_{k'} - \epsilon_d}\right)^{-1} \quad (\text{A.15})$$

If we now let  $|\epsilon_d|$  be large then using (A.12) we find:

$$H_{10}(E - H_{00})^{-1}H_{01} = - \sum_{kk'\sigma\sigma'} V_k V_{k'}^* \frac{d_{\sigma}^{\dagger}(1 - n_{d\bar{\sigma}})c_{k\sigma}c_{k'\sigma'}^{\dagger}(1 - n_{d\bar{\sigma}'})d_{\sigma'}}{\epsilon_{k'} - \epsilon_d} \quad (\text{A.16})$$

Because we only consider the one particle state the  $n_{d\bar{\sigma}}$  can be dropped in (A.16).

Next we work out the two particle virtual states in a similar fashion.

$$H_{12}(E - H_{22})^{-1}H_{21} = \sum_{kk'\sigma\sigma'} V_{k'} V_k^* c_{k\sigma}^{\dagger} n_{d\bar{\sigma}} d_{\sigma} (E - H_{22}) d_{\sigma'}^{\dagger} n_{d\bar{\sigma}'} c_{k'\sigma'} \quad (\text{A.17})$$

Now again we can write

$$(E - H_{22}P_2)^{-1} = \frac{1}{E}P_0 + \frac{1}{E}P_0 + (E - H_{22})^{-1}P_2, \quad (\text{A.18})$$

and only the  $P_2$  term remains in the product. Recall from (A.6) that  $H_{22} = H_{00} + 2\epsilon_d + U$ . And using  $H_{00}c_{k'\sigma'} = c_{k'\sigma'}(H_{00} - \epsilon_{k'})$  we find

$$(E - H_{22})^{-1}d_{\sigma'}^{\dagger} n_{d\bar{\sigma}'} c_{k'\sigma'} = d_{\sigma'}^{\dagger} n_{d\bar{\sigma}'} c_{k'\sigma'} (E - H_{00} - 2\epsilon_d - U + \epsilon_{k'})^{-1} \quad (\text{A.19})$$

$$= -\frac{d_{\sigma'}^{\dagger} n_{d\bar{\sigma}'} c_{k'\sigma'}}{U + \epsilon_d - \epsilon_{k'}} \left(1 - \frac{E - \epsilon_d - H_{00}}{U + \epsilon_d - \epsilon_{k'}}\right)^{-1}. \quad (\text{A.20})$$

We have again put the second line in a form, such that we can drop the last factor to obtain the leading order terms in  $1/U$  and  $1/\epsilon_d$ .

Plugging in (A.20) into (A.17) we find

$$H_{12}(E - H_{22})^{-1}H_{21} = - \sum_{kk'\sigma\sigma'} V_{k'} V_k^* \frac{c_{k\sigma}^{\dagger} n_{d\bar{\sigma}} d_{\sigma} d_{\sigma'}^{\dagger} n_{d\bar{\sigma}'} c_{k'\sigma'}}{U + \epsilon_d - \epsilon_{k'}}. \quad (\text{A.21})$$

This operator acts on the one particle sector we can work out the  $n_{d\bar{\sigma}} = 1$ .

Plugging (A.16) and (A.21) into (A.9) gives

$$H_{\text{eff}} = H_{00} + \epsilon_d - \sum_{kk'\sigma\sigma'} V_k^* V_{k'} \left[ \frac{d_{\sigma'}^{\dagger} c_{k'\sigma'} c_{k\sigma}^{\dagger} d_{\sigma}}{\epsilon_k - \epsilon_d} + \frac{c_{k\sigma}^{\dagger} d_{\sigma} d_{\sigma'}^{\dagger} c_{k'\sigma'}}{U + \epsilon_d - \epsilon_{k'}} \right] \quad (\text{A.22})$$

$$= H_{00} + \epsilon_d - \sum_{kk'\sigma\sigma'} A_{kk'} d_{\sigma'}^{\dagger} c_{k'\sigma'} c_{k\sigma}^{\dagger} d_{\sigma} + B_{kk'} c_{k\sigma}^{\dagger} d_{\sigma} d_{\sigma'}^{\dagger} c_{k'\sigma'} \quad (\text{A.23})$$

$$= H_{00} + \epsilon_d + \sum_{kk'\sigma\sigma'} (A_{kk'} + B_{kk'}) c_{k\sigma}^{\dagger} c_{k'\sigma'} d_{\sigma'}^{\dagger} d_{\sigma} - A_{kk'} \delta_{\sigma\sigma'} \delta_{kk'} d_{\sigma'}^{\dagger} d_{\sigma} - B_{kk'} \delta_{\sigma\sigma'} c_{k\sigma}^{\dagger} c_{k'\sigma'} \quad (\text{A.24})$$

$$= H_{00} + \epsilon_d + \sum_{kk'\sigma\sigma'} (A_{kk'} + B_{kk'}) c_{k\sigma}^{\dagger} c_{k'\sigma'} d_{\sigma'}^{\dagger} d_{\sigma} - \sum_{kk'\sigma} B_{kk'} c_{k\sigma}^{\dagger} c_{k'\sigma} - \sum_k A_{kk} \quad (\text{A.25})$$

We have introduced

$$A_{kk'} = V_k^* V_{k'} \frac{1}{\epsilon_k - \epsilon_d}, \quad B_{kk'} = V_k^* V_{k'} \frac{1}{U + \epsilon_d - \epsilon_{k'}} \quad (\text{A.26})$$

In the last line we used  $\sum_{\sigma\sigma'} \delta_{\sigma\sigma'} d_{\sigma'}^{\dagger} d_{\sigma} = \sum_{\sigma} n_{d\sigma} = 1$ .

The impurity is singly occupied, so this is a two level system (either  $\uparrow$  or  $\downarrow$  at the impurity). This means that we can write the impurity as a spin degree of freedom:

$$\vec{S} = d_{\alpha}^{\dagger} \frac{\vec{\sigma}_{\alpha\beta}}{2} d_{\beta}, \quad (\text{A.27})$$

where  $\sigma^i$ 's are the Pauli matrices. Now we use the Pauli matrix identity

$$\vec{\sigma}_{\alpha\beta}\vec{\sigma}_{\gamma\delta} = 2\delta_{\alpha\delta}\delta_{\beta\gamma} - \delta_{\alpha\beta}\delta_{\gamma\delta} \quad (\text{A.28})$$

to write

$$c_{k\alpha}^\dagger \vec{\sigma}_{\alpha\beta} c_{k'\beta} \vec{S} = c_{k\alpha}^\dagger \vec{\sigma}_{\alpha\beta} c_{k'\beta} d_\gamma^\dagger \frac{\vec{\sigma}_{\gamma\delta}}{2} d_\delta = c_{k\sigma}^\dagger c_{k'\sigma'} d_{\sigma'}^\dagger d_\sigma - \frac{1}{2} c_{k\sigma}^\dagger c_{k'\sigma} d_{\sigma'}^\dagger d_{\sigma'} \quad (\text{A.29})$$

Plugging (A.29) into (A.25) gives

$$H_{\text{eff}} = \sum_{k\sigma} \epsilon_k c_{k\sigma}^\dagger c_{k\sigma} + \sum_{kk'} (A_{kk'} + B_{kk'}) c_{k\alpha}^\dagger \vec{\sigma}_{\alpha\beta} c_{k'\beta} \vec{S} + \frac{A_{kk'} - B_{kk'}}{2} c_{k\sigma}^\dagger c_{k'\sigma}, \quad (\text{A.30})$$

where we have dropped the constant terms. If  $V_k = V$  we see that the coupling constants (A.26) do not depend on  $k$  (we use  $|\epsilon_d| \gg \epsilon_k$ ). The first term is now the Kondo coupling, compare to (1.1) and the second term drops out if we assume particle-hole symmetry, i.e.  $2\epsilon_d + U = 0$ .

# Appendix B

## Matsubara

We are going to see how to work out the Matsubara sums using contour integrals. In general a Matsubara sum is

$$\sum_{\omega_n} f(i\omega_n) \quad (\text{B.1})$$

Using l'hôpital we see that the residue of Fermi/Bose distribution function at the Matsubara frequencies is:

$$\lim_{\omega \rightarrow \omega_n} \frac{\omega}{e^{\beta\omega} \pm 1} = \lim_{\omega \rightarrow \omega_n} \frac{1}{\beta e^{\beta\omega}} = \frac{1}{\mp\beta}, \quad (\text{B.2})$$

where the upper sign corresponds to fermions and the lower sign to bosons. Hence by introducing contour integrals the summation in (B.1) corresponds to:

$$\frac{1}{2\pi i} \oint_{\mathcal{C}} d\omega \left[ \mp\beta \frac{1}{e^{\beta\omega} \pm 1} f(\omega) \right], \quad (\text{B.3})$$

where  $\mathcal{C}$  is the contour integral around the imaginary line.

In stead of integrating around the the imaginary line, we can also integrate over the two real half separated by the imaginary line. This gives the following equivalence

$$\sum_{\omega_n} f(i\omega_n) = \pm\beta \sum_{i=1}^l \frac{1}{e^{\beta z_i} \pm 1} \text{Res}_{z_i} f(z) = \pm\beta \sum_{i=1}^l \eta_{F,B}(z_i) \text{Res}_{z_i} f(z) \quad (\text{B.4})$$

where  $f(z)$  has  $l$  poles at  $z_i = z_1, \dots, z_l$ . Note that we pick up an extra minus, because the contour integral needs to be reversed and the contour direction is counter clockwise. Here  $\eta_F$  is the Fermi-Dirac distribution and  $\eta_B$  the Bose-Einstein distribution.



# Appendix C

## Bosonization

Interaction terms can make it extremely difficult to fully solve a quantum mechanical system. Terms up to second order can be solved exactly, but taking into account higher order terms poses new challenges. Bosonization is a technique that can help out in some cases.

Here we are going to describe a bosonization scheme, which is a way to rewrite a fermion operator  $\psi$  in terms of boson operators. It is not straightforward to express bosons in terms of fermions or vice versa. Obviously, the different statistics make a one-to-one connection impossible. Nevertheless, a fermion density operator  $\rho \propto c^\dagger c$  is already more boson-like, since it commutes instead of anti-commutes. This is the first observation of bosonization, since it relates boson operators to fermion densities ( $b \propto c^\dagger c$ ). We already see that this makes quartic fermion interaction terms like  $c^\dagger c \hat{c}^\dagger \hat{c}$ , much simpler in boson language because they become quadratic  $b \hat{b}$ . In this appendix we will introduce the necessary ingredients for bosonization. For a full derivation see [20].

### C.1 Bosonization Conventions

There are several different conventions for setting up the bosonization framework. Here we are going to use the same definitions as [20].

The first remark on bosonization is: it is only applicable in one dimension. In Figure 3.1b we see the one particle spectra for one (Figure 3.1a) and two (Figure 3.1b) dimension. For one dimension we see that if we excite a fermion from just below the Fermi surface ( $k$ ) with small amount of energy ( $\delta$ ) it can only go to one specific momentum ( $k + \delta/v_F$ ), where we assumed linear dispersion close to the Fermi surface. In Figure 3.1b we look at the 2D spectrum from the top. If we excite a fermion from below the Fermi surface ( $\vec{k}$ ) with a finite amount of energy, it can go to any  $\vec{k}'$ , such that  $|\vec{k}'| = |\vec{k}| + \delta/v_F$ , so the momentum is smeared out instead of specifically determined. In fact for  $n$ -dimensions it is smeared out over an  $n - 1$ -sphere ( $S^{n-1}$ ).

For the Kondo problem we can assume that we only have to consider one radial direction after the reduction from three to one dimensions, since there is one impurity in the origin. Hence we can drop  $k < 0$  and consider only the right movers (later on we will see what this means).

Furthermore we need the free energy of the fermion to be linear at the Fermi surface. The linear dispersion is  $\epsilon(k) = v_F k$ , where  $v_F$  is the Fermi velocity.

The fermion fields are defined as

$$\psi_\eta = \left(\frac{2\pi}{L}\right)^{1/2} \sum_k e^{-ikx} c_{k\eta}; \quad (\text{C.1})$$

$$\psi_\eta^\dagger = \left(\frac{2\pi}{L}\right)^{1/2} \sum_k e^{ikx} c_{k\eta}^\dagger. \quad (\text{C.2})$$

where  $\eta$  denotes the different fermion species (e.g. spin,  $\eta = (\uparrow, \downarrow)$ ) and  $L$  is the size of the system. The operators satisfy canonical anti-commutation relations

$$\{c_{k\eta}, c_{k'\eta'}^\dagger\} = \delta_{\eta\eta'} \delta_{kk'}, \quad \{\psi_\eta(x), \psi_{\eta'}^\dagger(x')\} = 2\pi \delta_{\eta\eta'} \delta(x - x'). \quad (\text{C.3})$$

where we have normalized  $\psi$  with a factor of  $2\pi$  which will be useful later. The linearized free energy is then

$$H_0 = \sum_{\eta, k} v_F k :c_{k\eta}^\dagger c_{k\eta}: \quad (\text{C.4})$$

$$= \sum_\eta \int_{-L/2}^{L/2} \frac{dx}{2\pi} : \psi_\eta^\dagger(x) i v_F \partial_x \psi_\eta(x) :, \quad (\text{C.5})$$

The dots  $(:\hat{O}:)$  denote the normal ordered operator. Normal ordering means moving all creation operators to the right and annihilation operators to the left. Alternatively it is defined as  $:\hat{O}: = \hat{O} - \langle 0 | \hat{O} | 0 \rangle$ , where the second term is the expectation value with respect to the ground state.

Before the bosonization can be introduced we have to define the ground state for  $n$  species. Suppose that there are  $N_\eta$  particles of species  $\eta$ , we define the ground state as  $|\vec{N}\rangle_0$ , where  $\vec{N} = (N_1, N_2, \dots, N_n)$  and the subscript 0 means for all species are filled up to the Fermi surface (no excitations). The number operator is therefore

$$\hat{N}_\eta = \sum_k :c_{k\eta}^\dagger c_{k\eta}: = \sum_k \left[ c_{k\eta}^\dagger c_{k\eta} - {}_0\langle \vec{0} | c_{k\eta}^\dagger c_{k\eta} | \vec{0} \rangle_0 \right] \quad (\text{C.6})$$

such that  $\hat{N}_\eta |\vec{N}\rangle = N_\eta |\vec{N}\rangle$ .

### C.1.1 Boson Representation

We will now define the boson operators and the connection the fermion operators, the thorough derivation is in [20]. The boson operators are

$$b_{q\eta} = \frac{-i}{\sqrt{n_q}} \sum_k c_{k-q\eta}^\dagger c_{k\eta} \quad (\text{C.7})$$

$$b_{q\eta}^\dagger = \frac{i}{\sqrt{n_q}} \sum_k c_{k+q\eta}^\dagger c_{k\eta} \quad (\text{C.8})$$

where  $q = \frac{2\pi}{L} n_q > 0$ . These operators indeed satisfy  $[b_{q\eta}, b_{q'\eta'}^\dagger] = \delta_{\eta\eta'} \delta_{qq'}$ , so they are bosonic. If we take a closer look at these boson operators, we note that they both conserve particle number. Furthermore we see that  $b_{q\eta}^\dagger$  raises every particle in site  $k$  to site  $k + q$ , if site  $k$  is occupied and  $k + q$  is empty. Clearly  $b_{q\eta}$  induces the opposite excitation. From this we see that  $b_{q\eta} |\vec{N}\rangle_0 = 0$ , since in  $|(N_1, N_2, \dots)\rangle_0$  no states can be lowered under the Fermi surface. So we have found the ground state



for  $b_{q\eta}$ .

The whole  $\vec{N}$  particle Hilbert space is now spanned by acting with combinations of creation operators on the ground state, i.e. for all  $|\vec{N}\rangle$ , there exists  $f \in \mathbb{R}[x]$  a polynomial such that  $|\vec{N}\rangle = f(b^\dagger) |\vec{N}\rangle_0$ . Note that the particle number is conserved, so  $\vec{N}$  is not changed.

At this point we can also define a boson field:

$$\varphi_\eta(x) = - \sum_{q>0} \frac{1}{\sqrt{n_q}} e^{-iqx} b_{q\eta} e^{-aq/2} \quad (\text{C.9})$$

$$\varphi_\eta^\dagger(x) = - \sum_{q>0} \frac{1}{\sqrt{n_q}} e^{iqx} b_{q\eta}^\dagger e^{-aq/2}. \quad (\text{C.10})$$

And the Hermitian combination

$$\phi_\eta(x) = \varphi_\eta(x) + \varphi_\eta^\dagger(x) = - \sum_{q>0} \frac{1}{\sqrt{n_q}} (e^{-iqx} b_{q\eta} + e^{iqx} b_{q\eta}^\dagger) e^{-aq/2} \quad (\text{C.11})$$

Where  $a > 0$  is often interpreted as the lattice size, but here this infinitesimal parameter is used to regularize the UV divergent sums.

Now we have several useful commutator:

$$[\varphi_\eta(x), \varphi_{\eta'}(x')] = [\varphi_\eta^\dagger(x), \varphi_{\eta'}^\dagger(x')] = 0 \quad (\text{C.12})$$

$$[\varphi_\eta(x), \varphi_{\eta'}^\dagger(x')] = -\delta_{\eta\eta'} \ln \left( 1 - e^{-i\frac{2\pi}{L}(x-x'-ia)} \right) \quad (\text{C.13})$$

$$\stackrel{L \gg (x-x')}{=} -\delta_{\eta\eta'} \ln \left( i\frac{2\pi}{L}(x-x'-ia) \right) \quad (\text{C.14})$$

And

$$[\phi_\eta(x), \phi_{\eta'}(x')] \stackrel{L \gg (x-x')}{=} \stackrel{a \rightarrow 0}{=} -\delta_{\eta\eta'} 2\pi i \sigma(x-x') \quad (\text{C.15})$$

$$[\phi_\eta(x), \partial_x \phi_{\eta'}(x')] \stackrel{L \gg (x-x')}{=} \stackrel{a \rightarrow 0}{=} \delta_{\eta\eta'} 2\pi i \left[ \delta(x-x') - \frac{1}{L} \right] \quad (\text{C.16})$$

Where  $\sigma(x)$  is the sign function, analytically continued in 0 (i.e.  $\sigma(0) = 0$ ).

### C.1.2 Bosonization Identity

Now we want to write the fermion fields in terms of the boson fields. Since the boson fields conserve particle number, we require an additional operator to ensure that  $\psi$  ( $\psi^\dagger$ ) removes (adds) a fermion. This operator is called the Klein factor ( $F_\eta$ ). We can safely assume that  $F_\eta$  commutes with all boson operators and that it acts in the following way  $\vec{N}$ -particle state:

$$F_\eta^\dagger |\vec{N}\rangle = F_\eta^\dagger f(b) |\vec{N}\rangle_0 = f(b) c_{(N_\eta+1)\eta}^\dagger |\vec{N}\rangle_0 \quad (\text{C.17})$$

$$F_\eta |\vec{N}\rangle = F_\eta f(b) |\vec{N}\rangle_0 = f(b) c_{N_\eta\eta} |\vec{N}\rangle_0 \quad (\text{C.18})$$

From this definition it is easy to see that

$$F_\eta F_\eta^\dagger = F_\eta^\dagger F_\eta = 1 \quad (\text{C.19})$$

and

$$\{F_\eta^\dagger, F_{\eta'}\} = 2\delta_{\eta\eta'}, \quad \{F_\eta, F_{\eta'}\} = \{F_\eta^\dagger, F_{\eta'}^\dagger\} = 0, \quad [\hat{N}_\eta, F_{\eta'}^\dagger] = \delta_{\eta\eta'} F_{\eta'}^\dagger, \quad [\hat{N}_\eta, F_{\eta'}] = -\delta_{\eta\eta'} F_{\eta'} \quad (\text{C.20})$$

Combining (C.1) and (C.7) gives  $[b_{q,\eta}, \psi_\eta(x)] = \delta_{\eta\eta'} \frac{i}{\sqrt{n_q}} e^{iqx} \psi_\eta(x)$ , hence:

$$b_{q\eta'} \psi_\eta(x) |\vec{N}\rangle_0 = \delta_{\eta\eta'} \frac{i}{\sqrt{n_q}} e^{iqx} \psi_\eta(x) |\vec{N}\rangle_0 \quad (\text{C.21})$$

Since  $\psi_\eta(x) |\vec{N}\rangle_0$  is an eigenstate of  $b_{q\eta'}$  there is a coherent-state representation of  $\psi_\eta(x)$  in terms of  $b_{q\eta'}^\dagger$ , which turns out to be:

$$\psi_\eta(x) = F_\eta \left( \frac{2\pi}{L} \right)^{1/2} e^{-i \frac{2\pi}{L} (\hat{N}_\eta - \frac{1}{2} \delta_b) x} e^{-i \varphi_\eta^\dagger(x)} e^{-i \varphi_\eta(x)} \quad (\text{C.22})$$

$$= F_\eta a^{-1/2} e^{-i \frac{2\pi}{L} (\hat{N}_\eta - \frac{1}{2} \delta_b) x} e^{-i \phi_\eta(x)} \quad (\text{C.23})$$

Here the Klein factor  $F_\eta$  makes sure the particle number is conserved. The full derivation can be found in (CITE von delft). In the second line we have used (C.36).

## C.2 Free Hamiltonian

The Hamiltonian C.4 can now also be written in terms of the boson operators. We see that

$$[H_{0\eta}, b_{q\eta}^\dagger] = v_F q b_{q\eta}^\dagger \delta_{\eta\eta'}, \quad (\text{C.24})$$

so  $b_{q\eta}^\dagger$  is a raising operator with respect to the free energy  $(H_{0\eta} b_{q\eta} |E\rangle = (E + v_F q) b_{q\eta}^\dagger |E\rangle$ . Therefore we can write the Hamiltonian in terms of the boson operators as

$$H_0 = \sum_\eta \left( \sum_{q>0} v_F q b_{q\eta}^\dagger b_{q\eta} + \frac{2\pi v_F}{L} \frac{1}{2} \hat{N}_\eta (\hat{N}_\eta + 1) \right) \quad (\text{C.25})$$

$$= \sum_\eta \left( \int_{-L/2}^{L/2} \frac{dx}{2\pi} \frac{v_F}{2} :(\partial_x \phi_\eta(x))^2: + \frac{2\pi v_F}{L} \frac{1}{2} \hat{N}_\eta (\hat{N}_\eta + 1) \right) \quad (\text{C.26})$$

where  $\frac{2\pi v_F}{L} \frac{1}{2} \hat{N}_\eta (\hat{N}_\eta + 1)$  is the energy of the ground state. We will assume this to vanish in most cases, since we let  $L$  become large.

### C.2.1 Heisenberg Picture

Since we have the free Hamiltonian, we can derive how the boson and fermion operators behave under time evolutions  $A(\tau) = e^{H_0 \tau} A e^{-H_0 \tau}$ :

$$c_{k\eta}(\tau) = c_{k\eta} e^{-k\tau} \quad (\text{C.27})$$

$$c_{k\eta}^\dagger(\tau) = c_{k\eta}^\dagger e^{k\tau} \quad (\text{C.28})$$

$$b_{q\eta}(\tau) = b_{q\eta} e^{-q\tau} \quad (\text{C.29})$$

$$b_{q\eta}^\dagger(\tau) = b_{q\eta}^\dagger e^{q\tau} \quad (\text{C.30})$$

When we plug this in into the definitions of  $\psi_\eta(x, \tau)$  (C.1) and  $\phi_\eta(x, \tau)$  (C.11), we see that  $x$  and  $\tau$  are only present in the combination  $\tau + ix$ . The spatial and temporal coordinates can be transformed using  $z = \tau + ix$  and  $\bar{z} = \tau - ix$ . Hence the operators only depend on  $z$ , so we can write  $\psi_\eta(x, \tau) = \psi_\eta(z)$  and  $\phi_\eta(x, \tau) = \phi_\eta(z)$ .

We can also derive this more rigorously.

From (C.3) we see that the conjugated momentum of  $\psi_\eta(x, \tau)$  is  $\Pi_\eta(x, \tau) = \frac{i}{2\pi} \psi_\eta^\dagger(x, \tau)$ . So we can write the Hamiltonian density from (C.5) as:

$$\mathcal{H}_{0\eta} =: \Pi_\eta(x, \tau) \partial_x \psi_\eta(x, \tau): \quad (\text{C.31})$$

From the Hamilton equations we derive

$$\partial_\tau \psi_\eta(x, \tau) = -i \partial_t \psi_\eta(x, \tau(t)) = -i \frac{d\mathcal{H}_{0\eta}}{d\Pi_\eta(x, \tau(t))} = -i \partial_x \psi_\eta(x, \tau(t)) \quad (\text{C.32})$$

$$\partial_\tau \psi_\eta(\tau, x) + i \partial_x \psi_\eta(\tau, x) = 0 \quad (\text{C.33})$$

$$\partial_{\bar{z}} \psi_\eta(z, \bar{z}) = 0 \quad (\text{C.34})$$

where we have used  $\partial_{\bar{z}} = \partial_\tau + i \partial_x$ . Consequently  $\psi_\eta$  only depends on  $z$  and only the right movers remain.

## C.3 Some Useful Identities

### C.3.1 Baker-Campbell-Hausdorff

#### Theorem 1. Baker-Campbell-Hausdorff

Let  $\mathfrak{g}$  be the Lie algebra corresponding to the Lie group  $G$ . The linear operator  $\text{ad}_X$  acts on  $\mathfrak{g}$  in the following way:  $\text{ad}_X Y = [X, Y]$  for  $X, Y \in \mathfrak{g}$ . And for  $A \in G$  we can denote  $\text{Ad}_A Y = A Y A^{-1}$ .

For  $X, Y \in \mathfrak{g}$  (hence  $e^X \in G$ ) the following identity is known as the Baker-Campbell-Hausdorff:

$$\text{Ad}_{e^X} Y = e^{\text{ad}_X} Y$$

Or alternatively:

$$e^X Y e^{-X} = Y + [X, Y] + \frac{1}{2!} [X, [X, Y]] + \frac{1}{3!} [X, [X, [X, Y]]] + \dots$$

*Proof.* Consider  $f(s)Y = e^{sX} Y e^{-sX}$ , then  $\frac{d}{ds} f(s)Y = X e^{sX} Y e^{-sX} - e^{sX} Y e^{-sX} X = \text{ad}_X f(s)Y$ .

So we find  $f'(s) = \text{ad}_X f(s)$ . Since  $f(0) = 1$ ,  $f(s) = e^{s \text{ad}_X}$ . If we now set  $s$  to 1, we obtain the desired result.  $\square$

#### Corollary 2. Product of exponents

Now assume  $[X, Y]$  is central, i.e.  $[X, [X, Y]] = [Y, [X, Y]] = 0$ .

Then  $e^X e^Y = e^{X+Y+[X,Y]/2}$ .

*Proof.* We can define  $g(s) = e^{sX} e^{sY}$ .

Therefore  $\frac{d}{ds} g(s) = X e^{sX} e^{sY} + e^{sX} Y e^{sY} = (X + e^{sX} Y e^{-sX}) g(s) = (X + Y + [X, Y]) g(s)$ .

Since  $g(0) = 1$  we now see that  $g(s) = e^{sX+sY+s^2[X,Y]/2}$ . Setting  $s = 1$  gives the desired result.  $\square$

From this we now have set of useful identities. Given that  $[X, [X, Y]] = [Y, [X, Y]] = 0$  the following holds:

$$e^X Y e^{-X} = Y + [X, Y] \quad (\text{C.35})$$

$$e^X e^Y = e^{X+Y+[X,Y]/2} \quad (\text{C.36})$$

$$e^X e^Y = e^Y e^X e^{[X,Y]} \quad (\text{C.37})$$

### C.3.2 Thermal Average of Exponent of Boson Operators

**Theorem 3. Thermal average of exponent of boson operators**

Assume  $H$  is quadratic in boson operators and we can write some boson operators as  $\hat{B} = \sum_j \lambda_j b_j + \bar{\lambda}_j b_j^\dagger$ . Then:

$$\langle e^{\lambda \hat{B}} \rangle = e^{\lambda^2 \langle B^2 \rangle / 2} \quad (\text{C.38})$$

*Proof.* First we expand the exponent:

$$\langle e^{\lambda \hat{B}} \rangle = \sum_{n=0}^{\infty} \frac{\langle (\lambda \hat{B})^n \rangle}{n!} = \sum_{n=0}^{\infty} \frac{\langle (\lambda \hat{B})^{2n} \rangle}{(2n)!} \quad (\text{C.39})$$

The odd terms drop out since  $\langle \hat{B}^{2n+1} \rangle = 0$ .

Now we can apply Wick's theorem to  $\langle \lambda \hat{B}^{2n} \rangle$ . There are  $(2n-1)(2n-3)\dots 1 = \frac{(2n)!}{2^n n!}$  different contractions, so:

$$\langle e^{\lambda \hat{B}} \rangle = \sum_{n=0}^{\infty} \frac{\lambda^{2n} \langle \hat{B}^2 \rangle^n}{(2n)!} \frac{(2n)!}{2^n n!} = \sum_{n=0}^{\infty} \frac{1}{n!} \left( \frac{\lambda^2 \langle \hat{B}^2 \rangle}{2} \right)^n = e^{\lambda^2 \langle B^2 \rangle / 2} \quad (\text{C.40})$$

□

### C.3.3 Normal Ordering of Exponent $\phi$

**Theorem 4. Normal ordering of exponent  $\phi$**

Let  $\phi_\eta(z)$  be as defined in (C.11) then:

$$:e^{i\lambda\phi_\eta(z)}: = \frac{e^{i\lambda\phi_\eta(z)}}{\langle e^{i\lambda\phi_\eta(z)} \rangle} \quad (\text{C.41})$$

*Proof.* Recall that  $\phi_\eta(z) = \varphi_\eta(z) + \varphi_\eta^\dagger(z)$ . therefore:

$$:e^{i\lambda\phi_\eta(z)}: = e^{i\lambda\varphi_\eta^\dagger(z)} e^{i\lambda\varphi_\eta(z)} \quad (\text{C.42})$$

$$= e^{i\lambda(\varphi_\eta^\dagger(z) + \varphi_\eta(z))} e^{-\lambda^2/2[\varphi_\eta^\dagger(z), \varphi_\eta(z)]} \quad \text{using (C.36)} \quad (\text{C.43})$$

$$= e^{i\lambda\phi_\eta(z)} \left( \frac{L}{2\pi a} \right)^{\lambda^2/2} \quad \text{using (C.57)} \quad (\text{C.44})$$

Using (C.38) we see that we can write:

$$\langle e^{i\lambda\phi_\eta(z)} \rangle = e^{-\lambda^2 \langle \phi_\eta(z)^2 \rangle} = \left( \frac{2\pi a}{L} \right)^{\lambda^2/2} \quad \text{using (eq:appthermalaverage) and (C.77)} \quad (\text{C.45})$$

This gives the desired result. □

One can easily check that a similar relation holds for  $e^{i\lambda\phi_\eta(z)} e^{-i\lambda\phi_\eta(z')}$ :

$$:e^{i\lambda\phi_\eta(z)} e^{-i\lambda\phi_\eta(z')} : = \frac{e^{i\lambda\phi_\eta(z)} e^{-i\lambda\phi_\eta(z')}}{\langle e^{i\lambda\phi_\eta(z)} e^{-i\lambda\phi_\eta(z')} \rangle} \quad (\text{C.46})$$

## C.4 Commutation and Anti-Commutation Relations

We shall calculate several commutation relation for the boson operators and field. First of all  $b_{q\eta}$ :

$$[b_{q\eta}, b_{q'\eta'}^\dagger] = \frac{1}{\sqrt{n_q n_{q'}}} \sum_{k, k'} \left( c_{k-q\eta}^\dagger c_{k\eta} c_{k'+q'\eta'}^\dagger c_{k'\eta'} - c_{k'+q'\eta'}^\dagger c_{k'\eta'} c_{k-q\eta}^\dagger c_{k\eta} \right) \quad (\text{C.47})$$

$$= \frac{1}{\sqrt{n_q n_{q'}}} \sum_{k, k'} \left( c_{k-q\eta}^\dagger (\delta_{\eta\eta'} \delta_{kk'+q'} - c_{k'+q'\eta'}^\dagger c_{k\eta}) c_{k'\eta'} - c_{k'+q'\eta'}^\dagger (\delta_{\eta\eta'} \delta_{k'k-q} - c_{k-q\eta}^\dagger c_{k'\eta'}) c_{k\eta} \right) \quad (\text{C.48})$$

$$= \frac{1}{\sqrt{n_q n_{q'}}} \sum_k \left( c_{k+q'-q\eta}^\dagger c_{k\eta'} - c_{k+q'\eta'}^\dagger c_{k+q\eta} \right) \quad (\text{C.49})$$

$$(\text{C.50})$$

If we are not careful here, we might conclude that the commutator vanishes. In fact for  $q \neq q'$  the terms within the sum vanish indeed. For  $q = q'$  the terms are not normal ordered, so they diverge. Now we can use  $c_{k\eta}^\dagger c_{k'\eta'} = :c_{k\eta}^\dagger c_{k'\eta'}: + \langle c_{k\eta}^\dagger c_{k'\eta'} \rangle$  to find:

$$[b_{q\eta}, b_{q'\eta'}^\dagger] = \delta_{\eta\eta'} \delta_{qq'} \frac{1}{n_q} \sum_k \left[ \left( :c_{k\eta}^\dagger c_{k\eta}: - :c_{k+q\eta}^\dagger c_{k+q\eta}: \right) + \left( {}_0\langle \vec{0} | c_{k\eta}^\dagger c_{k\eta} | \vec{0} \rangle_0 - {}_0\langle \vec{0} | c_{k+q\eta}^\dagger c_{k+q\eta} | \vec{0} \rangle_0 \right) \right] \quad (\text{C.51})$$

$$= \delta_{\eta\eta'} \delta_{qq'} \frac{1}{n_q} \sum_k \left( {}_0\langle \vec{0} | c_{k\eta}^\dagger c_{k\eta} | \vec{0} \rangle_0 - {}_0\langle \vec{0} | c_{k+q\eta}^\dagger c_{k+q\eta} | \vec{0} \rangle_0 \right) \quad (\text{C.52})$$

In the normal ordered term we can safely shift  $k \rightarrow k + q$ . For the remaining term we see that:

$$\langle c_{k\eta}^\dagger c_{k\eta} \rangle_0 \equiv {}_0\langle \vec{0} | c_{k\eta}^\dagger c_{k\eta} | \vec{0} \rangle_0 = \begin{cases} 0 & k \leq 0 \\ 1 & k > 0 \end{cases} \quad (\text{C.53})$$

$$\sum_k \left( \langle c_{k\eta}^\dagger c_{k\eta} \rangle - \langle c_{k+q\eta}^\dagger c_{k+q\eta} \rangle \right) = \sum_{0 < k \leq \frac{2\pi}{L} n_q} 1 = n_q \quad (\text{C.54})$$

So indeed  $[b_{q\eta}, b_{q'\eta'}^\dagger] = \delta_{\eta\eta'} \delta_{qq'}$ .  
All other commutators vanish.

Now we are going to take a look at the commutator of  $\varphi_\eta(x)$ :

$$[\varphi_\eta(x), \varphi_{\eta'}^\dagger(x')] = \sum_{q, q' > 0} \frac{1}{\sqrt{n_q n_{q'}}} e^{-i(qx - q'x')} e^{-a(q+q')/2} [b_{q\eta}, b_{q'\eta'}^\dagger] \quad (\text{C.55})$$

$$= \delta_{\eta\eta'} \sum_{q > 0} \frac{1}{n_q} e^{-q(i(x-x') + a)} = \delta_{\eta\eta'} \sum_{n_q > 0} \frac{1}{n_q} e^{-\frac{2\pi}{L} n_q (i(x-x') - ia)} \quad (\text{C.56})$$

$$= -\delta_{\eta\eta'} \ln(1 - e^{-i\frac{2\pi}{L}((x-x') - ia)}) \stackrel{L \gg (x-x')}{\approx} -\delta_{\eta\eta'} \ln \left( i \frac{2\pi}{L} (x - x' - ia) \right) \quad (\text{C.57})$$

In (C.56) we recognized the Taylor series of  $\ln$ .

We can use this to find  $[\phi_\eta(x)\partial_{x'}\phi_{\eta'}(x')]$  first:

$$[\phi_\eta(x), \partial_{x'}\phi_{\eta'}(x')] = \partial_{x'} \left( [\varphi_\eta(x), \varphi_{\eta'}^\dagger(x')] + [\varphi_\eta^\dagger(x), \varphi_{\eta'}(x')] \right) \quad (\text{C.58})$$

$$= i \frac{2\pi}{L} \delta_{\eta\eta'} \left( \frac{1}{e^{i\frac{2\pi}{L}((x-x')-ia)} - 1} + \frac{1}{e^{i\frac{2\pi}{L}((x'-x)-ia)} - 1} \right) \quad (\text{C.59})$$

$$\stackrel{L \gg (x-x')}{=} 2\pi i \left( \frac{a/\pi}{(x-x')^2 - a^2} - \frac{1}{L} \right) \quad (\text{C.60})$$

$$\stackrel{a \rightarrow 0}{=} \delta_{\eta\eta'} 2\pi i [\delta(x-x') - \frac{1}{L}] \quad (\text{C.61})$$

In the last line we used  $\lim_{a \rightarrow \infty} \frac{a/\pi}{x^2 - a^2} = \delta(x)$ . If we now integrate this expression over  $x'$  in de neighbourhood of  $x$  we obtain

$$[\phi_\eta(x), \phi_{\eta'}(x')] = -\delta_{\eta\eta'} 2\pi i \theta(x-x') + C = -\delta_{\eta\eta'} \pi i \sigma(x-x') \quad (\text{C.62})$$

Where we have set  $C = \delta_{\eta\eta'} \pi i$  such that  $[\phi_\eta(x), \phi_\eta(x')] = -[\phi_\eta(x'), \phi_\eta(x)]$  and  $\sigma(x)$  is again the sign function.

## C.5 Useful Correlation Functions

In this appendix we will work out some useful correlation function. We start by calculating the correlation function  $\langle c_{k\eta}^\dagger c_{k'\eta'} \rangle$  and  $\langle b_{q\eta}^\dagger b_{q'\eta'} \rangle$ :

$$\langle c_{k\eta}^\dagger c_{k'\eta'} \rangle = \frac{\text{Tr}(c_{k\eta}^\dagger c_{k'\eta'} e^{-\beta H_0})}{\text{Tr}(e^{-\beta H_0})} \quad (\text{C.63})$$

$$= \delta_{\eta\eta'} \delta_{kk'} \frac{e^{-\beta k}}{1 + e^{-\beta k}} \quad (\text{C.64})$$

$$= \frac{\delta_{\eta\eta'} \delta_{kk'}}{e^{\beta k} + 1} \quad (\text{C.65})$$

Where we have used (C.4)

$$\langle b_{q\eta}^\dagger b_{q'\eta'} \rangle = \frac{\text{Tr}(b_{q\eta}^\dagger b_{q'\eta'} e^{-\beta H_0})}{\text{Tr}(e^{-\beta H_0})} \quad (\text{C.66})$$

$$= \delta_{\eta\eta'} \frac{\sum_{N_\eta=0}^{\infty} \langle N_\eta | b_{q\eta}^\dagger b_{q'\eta'} e^{-\beta H_{0\eta}} | N_\eta \rangle}{\sum_{N_\eta=0}^{\infty} \langle N_\eta | e^{-\beta H_{0\eta}} | N_\eta \rangle} \quad (\text{C.67})$$

$$= \delta_{\eta\eta'} \delta_{qq'} \frac{\sum_{N_\eta=0}^{\infty} N_\eta e^{-\beta q N_\eta}}{\sum_{N_\eta=0}^{\infty} e^{-\beta q N_\eta}} \quad (\text{C.68})$$

$$= -\delta_{\eta\eta'} \delta_{qq'} \frac{1}{\beta} \partial_q \ln \left( \sum_{N_\eta=0}^{\infty} e^{-\beta q N_\eta} \right) \quad (\text{C.69})$$

$$= \delta_{\eta\eta'} \delta_{qq'} \frac{1}{\beta} \partial_q \ln (1 - e^{-\beta q}) \quad (\text{C.70})$$

$$= \frac{\delta_{\eta\eta'} \delta_{qq'}}{e^{\beta q} - 1} \quad (\text{C.71})$$

Where we have used (C.25), simplified  $|\vec{N}\rangle$  to  $|N_\eta\rangle$  and assumed  $L \rightarrow \infty$ .

We assume  $T \rightarrow 0$ , so  $\frac{1}{e^{\beta q} - 1} = -\theta(-q)$  and  $\frac{1}{e^{\beta q} + 1} = \theta(-q)$ . The  $\phi$  two point function becomes

$$\langle \phi_\eta(z) \phi_{\eta'}(0) \rangle = \sum_{q, q' > 0} \frac{e^{-a(q+q')/2}}{\sqrt{n_q n_{q'}}} \left( e^{-qz} \langle b_{q\eta} b_{q'\eta'}^\dagger \rangle + e^{qz} \langle b_{q\eta}^\dagger b_{q'\eta'} \rangle \right) \quad (\text{C.72})$$

$$= \sum_{q, q' > 0} \frac{e^{-a(q+q')/2}}{\sqrt{n_q n_{q'}}} \delta_{\eta\eta'} \delta_{qq'} \left( e^{-qz} (1 - \theta(-q)) + e^{qz} \theta(-q) \right) \quad (\text{C.73})$$

$$= \delta_{\eta\eta'} \sum_{q > 0} \frac{e^{-aq}}{n_q} \left( e^{-qz} \theta(q) + e^{qz} \theta(-q) \right) \quad (\text{C.74})$$

$$= \delta_{\eta\eta'} \sum_{q > 0} \frac{e^{-q(z+a)}}{n_q} = -\delta_{\eta\eta'} \ln(1 - e^{-\frac{2\pi}{L}(z+a)}) \quad (\text{C.75})$$

In (C.74) we see that  $\theta(-q) = 0$ , since  $q > 0$ . Finally in the last step we recognized the Taylor series of  $\ln$ .

We can define the Green's function for the boson operators as

$$\mathcal{G}_{\eta\eta'}(z) = -\langle \mathcal{T} \phi_\eta(z) \phi_{\eta'}(0) \rangle = \theta(\tau) \langle \phi_\eta(z) \phi_{\eta'}(0) \rangle - \theta(-\tau) \langle \phi_{\eta'}(0) \phi_\eta(z) \rangle, \quad (\text{C.76})$$

where  $\mathcal{T}$  is the time ordering operator.

Using (C.75) we see the Green's function can be written as

$$\mathcal{G}_{\eta\eta'}(z) = \delta_{\eta\eta'} \ln(1 - e^{-\frac{2\pi}{L}(-\sigma(\tau)z+a)}) \stackrel{L \gg z}{=} -\ln \left( \frac{2\pi}{L} (\sigma(\tau)z + a) \right), \quad (\text{C.77})$$

with  $\sigma(\tau)$  is the sign function.

Finally, we look at  $\langle h(\tau) h(\tau') \rangle_h$  where  $h$  is confined to  $\Lambda' < k < \Lambda$  and  $\Lambda' = e^{-\delta l} \Lambda$ . We begin at (C.75):

$$\langle h(\tau) h(\tau') \rangle_h = \sum_{\Lambda'/v_f < q < \Lambda/v_f} \frac{e^{-q(|\tau-\tau'|+a)}}{n_q} \quad (\text{C.78})$$

$$= \frac{2\pi}{L} \sum_{\Lambda'/v_f < q < \Lambda/v_f} \frac{e^{-q(|\tau-\tau'|+a)}}{q} \quad (\text{C.79})$$

$$= \int_{\Lambda'/v_f}^{\Lambda/v_f} dq \frac{e^{-q(|\tau-\tau'|+a)}}{q} \quad (\text{C.80})$$

$$= \frac{\Lambda(1 - e^{-\delta l})}{\Lambda} e^{-\Lambda/v_f(|\tau-\tau'|+a)} = e^{-\Lambda/v_f|\tau-\tau'|} \delta l = F(|\tau - \tau'|) \delta l \quad (\text{C.81})$$

where we implicitly assumed that  $\langle h(\tau) h(\tau') \rangle_h$  is time ordered so it only depends on  $|\tau - \tau'|$  and have introduced  $F(|\tau - \tau'|) = e^{-\Lambda/v_f|\tau-\tau'|}$ .

## C.6 Bosonization One-channel Renormalization Group

In Section 3.2 we look at the RG-flow using bosonization. In this appendix we go through the full derivation of the RG-equations.

We can write down a full action from (3.19)

$$S = S_0 + S_\perp \quad (\text{C.82})$$

with

$$S_{\perp} = -\frac{J_{\perp}}{4\pi a} \int d\tau (e^{i(\sqrt{2}-\gamma)\phi(\tau,0)} S^{-}(\tau) + e^{-i(\sqrt{2}-\gamma)\phi(\tau,0)} S^{+}(\tau)) \quad (\text{C.83})$$

To calculate the RG-flow we only have to treat  $J_{\perp}$  perturbatively. In the end this means that we obtain an exact flow equation for  $\gamma$ .

Here  $\phi(\tau, x)$  is the time evolved operator. In fact it only depends on  $\tau + ix$  (see Appendix C.2.1). Now we impose a cut-off on the momentum,  $|k| < \frac{\Lambda}{v_F}$  where  $\Lambda = \Lambda_0 e^l$ . We can then split up  $\phi$ :

$$\begin{aligned} \phi(\tau, x) &= \left( \sum_{0 < q < \Lambda'/v_F} + \sum_{\Lambda'/v_F < q < \Lambda/v_F} \right) \left[ e^{-q(\tau+ix)} \left( \frac{1}{\sqrt{n_q}} e^{-aq/2} b_q \right) + e^{q(\tau+ix)} \left( \frac{1}{\sqrt{n_q}} e^{-aq/2} b_q^{\dagger} \right) \right] \\ &= \phi_{\Lambda'}(\tau, x) + h(\tau, x), \end{aligned} \quad (\text{C.85})$$

with  $\Lambda' = \Lambda_0 e^{l-\delta l}$  ( $\delta l$  small). We assume  $h(\tau, x)$  is small with respect to  $\phi_{\Lambda'}(\tau, x)$ . The partition function then becomes

$$Z = \int d[\phi] e^{-S_0[\phi] - S_{\perp}[\phi]} \quad (\text{C.86})$$

$$= \int d[\phi_{\Lambda'}] d[h] e^{-S_0[\phi_{\Lambda'}] - S_0[h] - S_{\perp}[\phi_{\Lambda'} + h]} \quad (\text{C.87})$$

$$= Z_h \int d[\phi_{\Lambda'}] e^{-S_0[\phi_{\Lambda'}]} \langle e^{-S_{\perp}[\phi_{\Lambda'} + h]} \rangle_h \quad (\text{C.88})$$

Where  $Z_h = \int d[h] e^{-S_0[h]}$  and  $\langle \dots \rangle_h$  is the expectation value with respect to  $S_0[h]$ .

Now we can define an effective action:

$$S_{\text{eff}}[\phi_{\Lambda'}] = S_0[\phi_{\Lambda'}] - \ln \left( \langle e^{-S_{\perp}[\phi_{\Lambda'} + h]} \rangle_h \right) \quad (\text{C.89})$$

$$\stackrel{S_{\perp} \ll 1}{=} S_0[\phi_{\Lambda'}] - \ln \left( 1 - \langle S_{\perp}[\phi_{\Lambda'} + h] \rangle_h + \frac{1}{2} \langle S_{\perp}[\phi_{\Lambda'} + h]^2 \rangle_h \right) \quad (\text{C.90})$$

$$= S_0[\phi_{\Lambda'}] + \langle S_{\perp}[\phi_{\Lambda'} + h] \rangle_h - \frac{1}{2} \left( \langle S_{\perp}[\phi_{\Lambda'} + h]^2 \rangle_h - \langle S_{\perp}[\phi_{\Lambda'} + h] \rangle_h^2 \right) \quad (\text{C.91})$$

### C.6.1 First Order

The first order correction can easily be computed by calculating  $\langle \dots \rangle_h$ :

$$\begin{aligned} \langle S_{\perp}[\phi_{\Lambda'} + h] \rangle_h &= -\frac{J_{\perp}}{4\pi a} \int d\tau (S^{-}(\tau) e^{i(\sqrt{2}-\gamma)\phi_{\Lambda'}(\tau,0)} \langle e^{i(\sqrt{2}-\gamma)h(\tau,0)} \rangle_h \\ &\quad + S^{+}(\tau) e^{-i(\sqrt{2}-\gamma)\phi_{\Lambda'}(\tau,0)} \langle e^{-i(\sqrt{2}-\gamma)h(\tau,0)} \rangle_h) \end{aligned} \quad (\text{C.92})$$

$$= -\frac{J_{\perp}}{4\pi a} \int d\tau \left( S^{-}(\tau) e^{i(\sqrt{2}-\gamma)\phi_{\Lambda'}(\tau,0)} + S^{+}(\tau) e^{-i(\sqrt{2}-\gamma)\phi_{\Lambda'}(\tau,0)} \right) e^{-\frac{(\sqrt{2}-\gamma)^2}{2} \langle h(\tau,0)^2 \rangle_h} \quad (\text{C.93})$$

In the last step we used (C.38). Using (C.81) we see that:

$$\langle h(\tau, 0)^2 \rangle_h = \delta l \quad (\text{C.94})$$

Now we rescale the integral to recover the original cut-off  $\Lambda$ , hence  $\vec{k} \rightarrow \frac{\Lambda'}{\Lambda} \vec{k}$ , but the scalar product  $\vec{k} \cdot \vec{x}$  should be invariant. Therefore  $\tau$  has to be rescaled as well,  $\tau \rightarrow \frac{\Lambda}{\Lambda'} \tau = e^{-\delta l} \tau$ . This gives a factor



$e^{\left(1 - \frac{(\sqrt{2}-\gamma)^2}{2}\right)\delta l} \approx 1 + \left(1 - \frac{(\sqrt{2}-\gamma)^2}{2}\right)\delta l$ . The first order correction now becomes:

$$\langle S_{\perp}[\phi_{\Lambda'} + h] \rangle_h = - \left[ 1 + \left(1 - \frac{(\sqrt{2}-\gamma)^2}{2}\right)\delta l \right] \frac{J_{\perp}}{4\pi a} \int d\tau \left( S^{-}(\tau) e^{i\sqrt{2}\phi_{\Lambda}(\tau,0)} + S^{+}(\tau) e^{-i\sqrt{2}\phi_{\Lambda}(\tau,0)} \right) \quad (\text{C.95})$$

### C.6.2 Second Order

The second order correction is little bit more complicated. To shorten the expression we drop the  $(x=0)$  in the following expressions. We start of with

$$\begin{aligned} \langle S_{\perp}[\phi_{\Lambda'} + h]^2 \rangle_h - \langle S_{\perp}[\phi_{\Lambda'} + h] \rangle_h^2 &= \frac{J_{\perp}^2}{16\pi^2 a^2} \int d\tau d\tau' \\ &S^{-}(\tau) S^{-}(\tau') e^{i(\sqrt{2}-\gamma)\phi_{\Lambda'}(\tau)} e^{i(\sqrt{2}-\gamma)\phi_{\Lambda'}(\tau')} \left[ \langle e^{i(\sqrt{2}-\gamma)h(\tau)} e^{i(\sqrt{2}-\gamma)h(\tau')} \rangle_h - \langle e^{i(\sqrt{2}-\gamma)h(\tau)} \rangle_h^2 \right] \\ &+ S^{+}(\tau) S^{+}(\tau') e^{-i(\sqrt{2}-\gamma)\phi_{\Lambda'}(\tau)} e^{-i(\sqrt{2}-\gamma)\phi_{\Lambda'}(\tau')} \left[ \langle e^{-i(\sqrt{2}-\gamma)h(\tau)} e^{-i(\sqrt{2}-\gamma)h(\tau')} \rangle_h - \langle e^{-i(\sqrt{2}-\gamma)h(\tau)} \rangle_h^2 \right] \\ &+ S^{+}(\tau) S^{-}(\tau') e^{-i(\sqrt{2}-\gamma)\phi_{\Lambda'}(\tau)} e^{i(\sqrt{2}-\gamma)\phi_{\Lambda'}(\tau')} \left[ \langle e^{-i(\sqrt{2}-\gamma)h(\tau)} e^{i(\sqrt{2}-\gamma)h(\tau')} \rangle_h - \langle e^{i(\sqrt{2}-\gamma)h(\tau)} \rangle_h^2 \right] \\ &+ S^{-}(\tau) S^{+}(\tau') e^{i(\sqrt{2}-\gamma)\phi_{\Lambda'}(\tau)} e^{-i(\sqrt{2}-\gamma)\phi_{\Lambda'}(\tau')} \left[ \langle e^{i(\sqrt{2}-\gamma)h(\tau)} e^{-i(\sqrt{2}-\gamma)h(\tau')} \rangle_h - \langle e^{i(\sqrt{2}-\gamma)h(\tau)} \rangle_h^2 \right] \end{aligned} \quad (\text{C.96})$$

Immediately we see that the first two terms vanish, since  $S^{+}S^{+} = S^{-}S^{-} = 0$ . Using (C.38) we can rewrite  $\langle e^{-i(\sqrt{2}-\gamma)h(\tau)} e^{i(\sqrt{2}-\gamma)h(\tau')} \rangle_h = e^{-(\sqrt{2}-\gamma)^2 \langle h(\tau)^2 \rangle_h} e^{(\sqrt{2}-\gamma)^2 \langle h(\tau)h(\tau') \rangle_h}$  and  $\langle e^{i(\sqrt{2}-\gamma)h(\tau)} \rangle_h^2 = e^{-(\sqrt{2}-\gamma)^2 \langle h(\tau)^2 \rangle_h}$ . Using (C.81) to calculate  $\langle h(\tau)^2 \rangle_h = \delta l$  and  $\langle h(\tau)h(\tau') \rangle_h = \delta l F(|\tau - \tau'|) = \delta l e^{-\Lambda|\tau - \tau'|}$  we find

$$\begin{aligned} \langle S_{\perp}[\phi_{\Lambda'} + h]^2 \rangle_h - \langle S_{\perp}[\phi_{\Lambda'} + h] \rangle_h^2 &= (\sqrt{2} - \gamma)^2 \delta l \frac{J_{\perp}^2}{16\pi^2 a^2} \int d\tau d\tau' F(|\tau - \tau'|) \\ &\left[ S^{+}(\tau) S^{-}(\tau') e^{-i(\sqrt{2}-\gamma)\phi_{\Lambda'}(\tau)} e^{i(\sqrt{2}-\gamma)\phi_{\Lambda'}(\tau')} + S^{-}(\tau) S^{+}(\tau') e^{i(\sqrt{2}-\gamma)\phi_{\Lambda'}(\tau)} e^{-i(\sqrt{2}-\gamma)\phi_{\Lambda'}(\tau')} \right] \end{aligned} \quad (\text{C.97})$$

where  $F(|\tau - \tau'|) = e^{-\Lambda/v_F(|\tau - \tau'|)}$ , which is short-ranged, since  $\Lambda \gg 1$ . So we can redefine:

$$\bar{\tau} = \tau - \tau' \quad (\text{C.98})$$

$$T = \frac{\tau + \tau'}{2} \quad (\text{C.99})$$

with  $|\bar{\tau}| \ll |T|$ . For the remaining exponents of (C.97) we get ( $\alpha = \pm$ ):

$$e^{-\alpha i(\sqrt{2}-\gamma)(\phi_{\Lambda'}(\tau) - \phi_{\Lambda'}(\tau'))} = e^{-\alpha i(\sqrt{2}-\gamma)(\phi_{\Lambda'}(T + \frac{\bar{\tau}}{2}) - \phi_{\Lambda'}(T - \frac{\bar{\tau}}{2}))} \quad (\text{C.100})$$

$$= e^{-\alpha i(\sqrt{2}-\gamma)\bar{\tau} \partial_T \phi_{\Lambda'}(T)} \quad (\text{C.101})$$

$$\approx 1 - \alpha i(\sqrt{2} - \gamma)\bar{\tau} \partial_T \phi_{\Lambda'}(T) = -\alpha i(\sqrt{2} - \gamma)\bar{\tau} \partial_T \phi_{\Lambda'}(T) \quad (\text{C.102})$$

Where we used the limit definition of the derivative in (C.101). The 1 in (C.102) can be dropped, because this only gives a renormalization of the free energy. This is not interesting in this case.

From (C.61) we can conclude that the conjugated momentum of  $\phi(x)$  is  $\bar{\Pi}(x) = \frac{1}{2\pi}\partial_x\phi(x)$ . The Hamilton equations using Hamiltonian (C.26) now give:

$$\partial_T\phi(T, x) = -i\partial_t\phi(T(t), x) = -i\frac{d\mathcal{H}_0}{d\bar{\Pi}(T(t), x)} = -i\partial_x\phi(T, x) \quad (\text{C.103})$$

Using (C.102), (C.103) the second order correction (C.97) reads:

$$(\sqrt{2} - \gamma)^3 \delta l \frac{J_\perp^2}{16\pi^2 a^2} \int dT \partial_x \phi_{\Lambda'}(T, 0) [S^+(T)S^-(T) - S^-(T)S^+(T)] \left( \int d\bar{\tau} \bar{\tau} F(\bar{\tau}) \right) \quad (\text{C.104})$$

$$= (\sqrt{2} - \gamma)^3 \delta l \frac{J_\perp^2 v_F^2}{8\pi^2 a^2 \Lambda^2} \int dT \partial_x \phi_{\Lambda'}(T, 0) S^z(T) \quad (\text{C.105})$$

where we used  $[S^+, S^-] = 2S_z$  and  $\int d\bar{\tau} \bar{\tau} F(\bar{\tau}) = \frac{v_F^2}{\Lambda^2}$ .

So now

$$\begin{aligned} S_{\text{eff}}[\phi_\Lambda] &= S_0[\phi_\Lambda] - (\sqrt{2} - \gamma)^3 \frac{J_\perp^2 v_F^2}{16\pi^2 a^2 \Lambda^2} \delta l \int d\tau \partial_x \phi_\Lambda(\tau, 0) S^z(\tau) \\ &\quad - \left[ 1 + \left( 1 - \frac{(\sqrt{2} - \gamma)^2}{2} \right) \delta l \right] \frac{J_\perp}{4\pi a} \int d\tau \left( S^-(\tau) e^{i\sqrt{2}\phi_\Lambda(\tau, 0)} + S^+(\tau) e^{-i\sqrt{2}\phi_\Lambda(\tau, 0)} \right) \end{aligned} \quad (\text{C.106})$$

Since the action does not depend on the cut off, we find

$$\left( \frac{J_z}{2\sqrt{2}\pi} - \gamma \right) (l + \delta l) = \left( \frac{J_z}{2\sqrt{2}\pi} - \gamma \right) (l) + (\sqrt{2} - \gamma)^3 \frac{J_\perp^2 v_F^2}{16\pi^2 a^2 \Lambda^2} \delta l \quad (\text{C.107})$$

$$\frac{J_\perp(l + \delta l)}{4\pi a} = \left[ 1 + \left( 1 - \frac{(\sqrt{2} - \gamma)^2}{2} \right) \delta l \right] \frac{J_\perp}{4\pi a} \quad (\text{C.108})$$

So the RG-equation become

$$\frac{d\gamma(l)}{dl} = -(\sqrt{2} - \gamma)^3 \frac{J_\perp^2 v_F^2}{16\pi^2 a^2 \Lambda^2} \quad (\text{C.109})$$

$$\frac{dJ_\perp(l)}{dl} = \left( 1 - \frac{(\sqrt{2} - \gamma)^2}{2} \right) J_\perp \quad (\text{C.110})$$

## Appendix D

# Symmetries of the Kitaev Chain

In this appendix we are going to use the symmetries of the Kitaev chain to derive identities useful for Section 7.1.

### D.1 Particle-Hole Symmetry

The Kitaev chain is anti-symmetric under the interchange of *particle* and *hole*, meaning the eigenvalues change sign under the transformation. Note that because of particle-hole pairing through the BdG formalism the spectrum is invariant.

Let  $\mathcal{H}$  be the BdG-Hamiltonian of some Kitaev Hamiltonian ( $H$ ) and  $\psi_j$  some eigenstate, with  $E_j > 0$  the eigenvalue then  $\mathcal{H}_{\text{PH}}$  and  $\psi'_j$  are the particle-hole inverted. The Hamiltonian (6.3) transform as follows using:

$$H_{\text{PH}} = -\mu \sum_i \left( c_i c_i^\dagger - \frac{1}{2} \right) - \frac{1}{2} \sum_i \left( t(c_i c_{i+1}^\dagger + c_{i+1} c_i^\dagger) + \Delta(c_i^\dagger c_{i+1}^\dagger + c_{i+1} c_i) \right) \quad (\text{D.1})$$

$$= -\mu \sum_i \left( -c_i^\dagger c_i + 1 - \frac{1}{2} \right) - \frac{1}{2} \sum_i \left( -t(c_{i+1}^\dagger c_i + c_i^\dagger c_{i+1}) - \Delta(c_{i+1}^\dagger c_i^\dagger + c_i c_{i+1}) \right) \quad (\text{D.2})$$

$$= -H. \quad (\text{D.3})$$

Hence also  $\mathcal{H}_{\text{PH}} = -\mathcal{H}$ .

So we can see that:

$$\mathcal{H}_{\text{PH}} \psi'_j = E_j \psi'_j \quad (\text{D.4})$$

$$-\mathcal{H} \psi'_j = E_j \psi'_j \quad (\text{D.5})$$

$$\mathcal{H} \psi'_j = -E_j \psi'_j \quad (\text{D.6})$$

$$(\text{D.7})$$

So  $\psi'_j$  is an eigenstate of  $\mathcal{H}$  and has opposite eigenvalue from  $\psi_j$ . Using (7.7) we see that:

$$\psi_j = \begin{pmatrix} \phi_j \\ \theta_j \end{pmatrix}, \quad \psi'_j = \begin{pmatrix} \theta_j \\ \phi_j \end{pmatrix} \quad (\text{D.8})$$

Suppose we sort the eigenvalues of  $\mathcal{H}$  in increasing order (i.e.  $E_j \leq E_{j+1}$ ), then we can define  $\psi_j$  and  $\psi_{-j}$  to have opposite eigenvalues, respectively  $E_j$  and  $E_{-j}$ . Now we can rewrite (D.8) as:

$$\phi_j = \theta_{-j} \quad (\text{D.9})$$

$$\theta_j = \phi_{-j} \quad (\text{D.10})$$

This discussion does not hold for  $E = 0$  since this state is degenerate, hence the eigen space 2 dimensional. We need two state to span the eigen space, which are  $\psi_1$  and  $\psi_{-1}$ .

## D.2 Inversion + Time Reversal Symmetry

In this section we are going to look at a combination of two transformations. The Kitaev chain turns out to be invariant under simultaneous chain inversion and time reversal. Inversion ( $\mathcal{I}$ ) maps  $c_i$  to  $c_{-i}$  (where we have defined:  $c_{-i} = c_{n+1-i}$  for  $i > 0$ ). Time reversal ( $\mathcal{T}$ ) changes the direction of time. Note that only the superconducting term cares about time direction. Time reversal means  $\Delta \rightarrow -\Delta$ . We can easily see that letting  $c_i \rightarrow ic_i$  and  $c_i^\dagger \rightarrow -ic_i^\dagger$  is equal to time reversal. The Hamiltonian is symmetric under the combination of these operations:

$$H_{\text{ITRS}} = \mathcal{I}\mathcal{P}[H] = \mathcal{I} \left[ -\mu \sum_i \left( c_i^\dagger c_i - \frac{1}{2} \right) - \frac{1}{2} \sum_i \left( t(c_i^\dagger c_{i+1} + c_{i+1}^\dagger c_i) - \Delta(c_i c_{i+1} + c_{i+1}^\dagger c_i^\dagger) \right) \right] \quad (\text{D.11})$$

$$= -\mu \sum_i \left( c_i^\dagger c_i - \frac{1}{2} \right) - \frac{1}{2} \sum_i \left( t(c_i^\dagger c_{i+1} + c_{i+1}^\dagger c_i) + \Delta(c_i c_{i+1} + c_{i+1}^\dagger c_i^\dagger) \right) \quad (\text{D.12})$$

$$= H \quad (\text{D.13})$$

Suppose we have an eigenstate  $\psi$  of  $\mathcal{H}$  with eigenvalue  $E$ . Then  $\mathcal{H}\psi = E\psi$  is invariant under this combined symmetry (inversion and time reversal). so

$$\mathcal{H}\psi_{\text{ITRS}} = \mathcal{H}_{\text{ITRS}}\psi_{\text{ITRS}} = E\psi_{\text{ITRS}} \quad (\text{D.14})$$

Suppose the eigenvalue  $E$  is non degenerate (this only fails for a Majorana edge mode or for a specific parameter  $t = \Delta$  and  $\mu = 0$ ), then the eigenspace belonging to  $E$  is one dimensional. Since both  $\psi$  and  $\psi_{\text{ITRS}}$  are normalized and have the same eigenvalue they are equivalent modulo a phase:

$$\psi = e^{i\alpha} \psi_{\text{ITRS}} \quad (\text{D.15})$$

Again we can split the eigenvector in the particle and the hole part, we then see that (D.15) can be written as:

$$\phi_i = ie^{i\alpha} \phi_{-i} \quad (\text{D.16})$$

$$\theta_i = -ie^{i\alpha} \theta_{-i} \quad (\text{D.17})$$

Note that  $\mathcal{H}$  is a symmetric real matrix. Therefore the eigenvectors  $\psi$  are real (up to an overall complex phase, which we choose to be 0). Hence  $\alpha = \mp\pi/2$  and we see that (D.16) becomes:

$$\phi_i = \pm \phi_{-i} \quad (\text{D.18})$$

$$\theta_i = \mp \theta_{-i} \quad (\text{D.19})$$

### D.3 Condition Majorana Edge Modes

In order to see under what symmetries the Majorana edge modes (MEM) are invariant we will use the transfer Matrix approach.

The word *Majorana* in Majorana edge modes already makes us suspicious that at the edge either  $|\psi_i^{\text{MEM}}\rangle = \phi_i^{\text{MEM}}(c_i + c_i^\dagger)$  or  $|\psi_i^{\text{MEM}}\rangle = \phi_i^{\text{MEM}}(c_i - c_i^\dagger)$ , where  $\phi$  is as in Eq. 7.7. Alternatively one of the following equations holds.

$$\phi_i^{\text{MEM}} = \theta_i^{\text{MEM}} \quad (\text{D.20})$$

$$\phi_i^{\text{MEM}} = -\theta_i^{\text{MEM}} \quad (\text{D.21})$$

Now we will use the transfer matrix approach to show that either (D.20) or (D.21) holds at the edges of the the system.

#### D.3.1 Transfer Matrix

Before we derive the transfer matrix we rewrite the Hamiltonian (6.3) using:

$$c_i = \frac{1}{2}(\gamma_{2i-1} + i\gamma_{2i}), \quad c_i^\dagger = \frac{1}{2}(\gamma_{2i-1} - i\gamma_{2i}). \quad (\text{D.22})$$

The Hamiltonian becomes:

$$H = -\frac{\mu}{2} \sum_{i=1}^n i\gamma_{2i-1}\gamma_{2i} + \frac{i}{4} \sum_{i=1}^{n-1} [(\Delta + t)\gamma_{2i}\gamma_{2i+1} + (\Delta - t)\gamma_{2i-1}\gamma_{2i+2}]. \quad (\text{D.23})$$

Again we can put this into the matrix form

$$H = \Gamma^\top \mathcal{H}_\gamma \Gamma, \quad (\text{D.24})$$

where  $\Gamma = (\gamma_1 \ \gamma_2 \ \dots \ \gamma_{2L-1} \ \gamma_{2L})^\top$  and  $\mathcal{H}_\gamma$  equals

$$\mathcal{H}_\gamma = \begin{pmatrix} \mathcal{H}_0 & \mathcal{H}_+ & 0 & \dots & 0 \\ \mathcal{H}_- & \mathcal{H}_0 & \mathcal{H}_+ & \ddots & \vdots \\ 0 & \mathcal{H}_- & \mathcal{H}_0 & \ddots & 0 \\ \vdots & \ddots & \ddots & \ddots & \mathcal{H}_+ \\ 0 & \dots & 0 & \mathcal{H}_- & \mathcal{H}_0 \end{pmatrix}, \quad (\text{D.25})$$

The block matrices are:

$$\mathcal{H}_0 = \begin{pmatrix} 0 & i\frac{\mu}{4} \\ -i\frac{\mu}{4} & 0 \end{pmatrix} \quad \text{and} \quad \mathcal{H}_\pm = \begin{pmatrix} 0 & i\frac{\pm\Delta-t}{8} \\ i\frac{\pm\Delta+t}{8} & 0 \end{pmatrix}. \quad (\text{D.26})$$

Assume  $|\psi^{\text{MEM}}\rangle = (\alpha_1, \beta_1, \dots, \alpha_L, \beta_L) \cdot \Gamma$  is a MEM localized at site 1. We then have the following equation:

$$\mathcal{H}_\gamma \begin{pmatrix} \alpha_1 \\ \beta_1 \\ \vdots \\ \alpha_n \\ \beta_n \end{pmatrix} = 0. \quad (\text{D.27})$$

Combining (D.25) and (D.27) we find:

$$\mathcal{H}_- \begin{pmatrix} \alpha_{i-1} \\ \beta_{i-1} \end{pmatrix} + \mathcal{H}_0 \begin{pmatrix} \alpha_i \\ \beta_i \end{pmatrix} + \mathcal{H}_+ \begin{pmatrix} \alpha_{i+1} \\ \beta_{i+1} \end{pmatrix} = 0 \quad (\text{D.28})$$

This can be rewritten into the transfer matrix form:

$$\begin{pmatrix} \alpha_i \\ \beta_i \\ \alpha_{i+1} \\ \beta_{i+1} \end{pmatrix} = T \begin{pmatrix} \alpha_{i-1} \\ \beta_{i-1} \\ \alpha_i \\ \beta_i \end{pmatrix}, \quad (\text{D.29})$$

where  $T$  is the transfer matrix:

$$T = \begin{pmatrix} 0 & 0 & 1 & 0 \\ 0 & 0 & 0 & 1 \\ (\mathcal{H}_+)^{-1}\mathcal{H}_- & I_2 & 0 & 0 \\ 0 & 0 & -\frac{2\mu}{\Delta+t} & 0 \end{pmatrix} = \begin{pmatrix} 0 & 0 & 1 & 0 \\ 0 & 0 & 0 & 1 \\ \frac{\Delta-t}{\Delta+t} & 0 & -\frac{2\mu}{\Delta+t} & 0 \\ 0 & -\frac{\Delta+t}{\Delta-t} & 0 & \frac{2\mu}{\Delta-t} \end{pmatrix} \quad (\text{D.30})$$

This matrix has the eigenvalues:

$$\lambda^\pm = \frac{-\mu \pm \sqrt{\mu^2 + t^2 - \Delta^2}}{t + \Delta} \quad (\text{D.31})$$

$$\kappa^\pm = \frac{-\mu \pm \sqrt{\mu^2 + t^2 - \Delta^2}}{t - \Delta} \quad (\text{D.32})$$

With corresponding eigenvectors:

$$|\lambda^\pm\rangle = (1, 0, \lambda^\pm, 0)^\top \quad (\text{D.33})$$

$$|\kappa^\pm\rangle = (0, 1, 0, \kappa^\pm)^\top \quad (\text{D.34})$$

## D.4 Zero Energy Mode in Semi Infinite Chain

We are now going to consider the chain to be semi infinite. This means that the Majoranas localized at both edges are far enough apart, such that they do not feel each other, e.g. the wave function falls off quickly enough.

If we now start at site 1, the MEM should be of the form  $(\alpha_0, \beta_0, \alpha_1, \beta_1)^\top = (0, 0, \alpha_1, \beta_1)^\top$ , because site 0 is not in the chain. We can build this state out of (D.33): an (D.34)

$$(\alpha_0, \beta_0, \alpha_1, \beta_1)^\top = A(|\lambda^+\rangle - |\lambda^-\rangle) + B(|\kappa^+\rangle - |\kappa^-\rangle) \quad (\text{D.35})$$

Here  $A$  and  $B$  are some complex constants. We take the difference between the eigenstate to get  $\alpha_0, \beta_0 = 0$ .

The transfer matrix approach now allows us to find  $(\alpha_i, \beta_i)$  by applying  $T^{i-1}$ :

$$(\alpha_{i-1}, \beta_{i-1}, \alpha_i, \beta_i) = T^{i-1} [A(|\lambda^+\rangle - |\lambda^-\rangle) + B(|\kappa^+\rangle - |\kappa^-\rangle)] \quad (\text{D.36})$$

$$= A((\lambda^+)^{i-1} |\lambda^+\rangle - (\lambda^-)^{i-1} |\lambda^-\rangle) + B((\kappa^+)^{i-1} |\kappa^+\rangle - (\kappa^-)^{i-1} |\kappa^-\rangle) \quad (\text{D.37})$$

Since we want the MEM to be localized  $(\alpha_i, \beta_i)$  should go to zero as  $i$  becomes large. In other words,  $A$  is non zero if  $|\lambda^+|, |\lambda^-| < 1$  and  $B$  is non zero if  $|\kappa^+|, |\kappa^-| < 1$ . Since  $\kappa^\pm = \frac{1}{\lambda^\mp}$  there is a regime in which  $A$  is non zero and a regime where  $B$  is non zero, but they cannot both be finite.

If we assume the system is in the topological sector and  $\Delta > 0$  then  $|\lambda^+|, |\lambda^-| < 1$ , so we  $\beta_i = 0$  and

$\alpha \neq 0$ .

Now we also would like to know the Majorana mode at the other end. The only term in the Hamiltonian (6.3) that concerns direction is the super conductivity. Note that if we let  $\Delta \rightarrow -\Delta$ , the chain is mirrored. Hence we see that at the the other edge (near  $i = n$ )  $\alpha_i = 0$  and  $\beta_i \neq 0$ .

Now we can conclude that at edge near site 1 we have

$$\phi_i^{\text{MEM}} = +\theta_i^{\text{MEM}} \quad \text{near site 1} \quad (\text{D.38})$$

$$\phi_i^{\text{MEM}} = -\theta_i^{\text{MEM}} \quad \text{near site } n \quad (\text{D.39})$$





# References

- [1] W.J. De Haas, J. De Boer, and G.J. Van den Berg. The electrical resistance of gold, copper and lead at low temperatures. *Physica*, 1(7-12):1115–1124, 1934.
- [2] J. Kondo. Resistance minimum in dilute magnetic alloys. *Progress of theoretical physics*, 32(1):37–49, 1964.
- [3] T. Kasuya. A theory of metallic ferro-and antiferromagnetism on zener’s model. *Progress of theoretical physics*, 16(1):45–57, 1956.
- [4] K.G. Wilson. The renormalization group: Critical phenomena and the kondo problem. *Reviews of Modern Physics*, 47(4):773, 1975.
- [5] P.B. Vigman (Wiegmann). Exact solution of sd exchange model at  $t = 0$ . *JETP Lett*, 31(7), 1980.
- [6] N. Andrei. Diagonalization of the kondo hamiltonian. *Physical Review Letters*, 45(5):379, 1980.
- [7] P. Nozieres and A. Blandin. Kondo effect in real metals. *Journal de Physique*, 41(3):193–211, 1980.
- [8] J. Friedel. On some electrical and magnetic properties of metallic solid solutions. *Canadian Journal of Physics*, 34(12A):1190–1211, 1956.
- [9] P.W. Anderson. Localized magnetic states in metals. *Physical Review*, 124(1):41, 1961.
- [10] A.O. Gogolin, A.A. Nersesyan, and A.M. Tsvelik. *Bosonization and strongly correlated systems*. Cambridge university press, 2004.
- [11] L.D. Landau and E.M. Lifshitz. Quantum mechanics: non-relativistic theory, 1977.
- [12] P.W. Anderson. A poor man’s derivation of scaling laws for the kondo problem. *Journal of Physics C: Solid State Physics*, 3(12):2436, 1970.
- [13] K.G. Wilson and J. Kogut. The renormalization group and the  $\varepsilon$  expansion. *Physics Reports*, 12(2):75–199, 1974.
- [14] P. Coleman. New approach to the mixed-valence problem. *Physical Review B*, 29(6):3035, 1984.
- [15] T. Giamarchi. *Quantum physics in one dimension*. Oxford university press, 2004.
- [16] S. Coleman. Quantum sine-gordon equation as the massive thirring model. *Physical Review D*, 11(8):2088, 1975.
- [17] S. Mandelstam. Soliton operators for the quantized sine-gordon equation. *Physical Review D*, 11(10):3026, 1975.
- [18] D.C. Mattis. New wave-operator identity applied to the study of persistent currents in 1d. *Journal of Mathematical Physics*, 15(5):609–612, 1974.
- [19] A. Luther and I. Peschel. Calculation of critical exponents in two dimensions from quantum field theory in one dimension. *Physical Review B*, 12(9):3908, 1975.
- [20] J. Von Delft and H. Schoeller. Bosonization for beginners—refermionization for experts. *arXiv preprint cond-mat/9805275*, 1998.
- [21] G. Toulouse. Infinite-u anderson hamiltonian for dilute alloys. *Physical Review B*, 2(2):270, 1970.
- [22] K. Majumdar, A. Schiller, and S. Hershfield. Nonequilibrium kondo impurity: Perturbation about an exactly solvable point. *Physical Review B*, 57(5):2991, 1998.

- [23] V.J. Emery and S. Kivelson. Mapping of the two-channel kondo problem to a resonant-level model. *Physical Review B*, 46(17):10812, 1992.
- [24] M. Fabrizio and A.O. Gogolin. Toulouse limit for the overscreened four-channel kondo problem. *Physical Review B*, 50(23):17732, 1994.
- [25] N. Cramp   and A. Trombettoni. Quantum spins on star graphs and the kondo model. *Nuclear Physics B*, 871(3):526–538, 2013.
- [26] A.M. Tsvelik. Majorana fermion realization of a two-channel kondo effect in a junction of three quantum ising chains. *Physical review letters*, 110(14):147202, 2013.
- [27] D. Giuliano, P. Sodano, A. Tagliacozzo, and A. Trombettoni. From four-to two-channel kondo effect in junctions of xy spin chains. *Nuclear Physics B*, 909:135–172, 2016.
- [28] M. Fabrizio and G. Zar  nd. Mapping between multichannel exchange models. *Physical Review B*, 54(14):10008, 1996.
- [29] P. Coleman, L.B. Ioffe, and A.M. Tsvelik. Simple formulation of the two-channel kondo model. *Physical Review B*, 52(9):6611, 1995.
- [30] A.Y. Kitaev. Unpaired majorana fermions in quantum wires. *Physics-Uspekhi*, 44(10S):131, 2001.
- [31] P. Fendley. Parafermionic edge zero modes in zn-invariant spin chains. *Journal of Statistical Mechanics: Theory and Experiment*, 2012(11):P11020, 2012.
- [32] J. Alicea and P. Fendley. Topological phases with parafermions: theory and blueprints. *Annual Review of Condensed Matter Physics*, 7:119–139, 2016.
- [33] A.S. Jermyn, R.S.K. Mong, J. Alicea, and P. Fendley. Stability of zero modes in parafermion chains. *Physical Review B*, 90(16):165106, 2014.
- [34] J.C. Budich and M. Heyl. Dynamical topological order parameters far from equilibrium. *Physical Review B*, 93(8):085416, 2016.
- [35] L. Mazza, M. Rizzi, M.D. Lukin, and J.I. Cirac. Robustness of quantum memories based on majorana zero modes. *Physical Review B*, 88(20):205142, 2013.
- [36] S. Hegde, V. Shivamoggi, S. Vishveshwara, and D. Sen. Quench dynamics and parity blocking in majorana wires. *New Journal of Physics*, 17(5):053036, 2015.
- [37] J. Alicea. Majorana fermions in a tunable semiconductor device. *Physical Review B*, 81(12):125318, 2010.
- [38] R.M. Lutchyn, J.D. Sau, and S.D. Sarma. Majorana fermions and a topological phase transition in semiconductor-superconductor heterostructures. *Physical review letters*, 105(7):077001, 2010.
- [39] F. Wegner. Inverse participation ratio in  $2 + \varepsilon$  dimensions. *Zeitschrift f  r Physik B Condensed Matter*, 36(3):209–214, 1980.
- [40] P.W. Anderson. Absence of diffusion in certain random lattices. *Physical review*, 109(5):1492, 1958.

